Title
Aspects of localization in topological insulators

Author
Sathe, Pratik Sunil

Publication Date
2023

Peer reviewed|Thesis/dissertation

UNIVERSITY OF CALIFORNIA

Los Angeles

Aspects of localization in topological insulators

A dissertation submitted in partial satisfaction

of the requirements for the degree

Doctor of Philosophy in Physics

by

Pratik Sathe

2023

ABSTRACT OF THE DISSERTATION

Aspects of localization in topological insulators

by

Pratik Sathe
Doctor of Philosophy in Physics
University of California, Los Angeles, 2023
Professor Rahul Roy, Chair

The topological properties of electronic band structures are closely related to the degree of localization possible for the associated wavefunctions. In this dissertation, we investigate certain aspects of this interplay between topology and localization in the context of static as well as driven (Floquet) topological insulators.

The first part of this dissertation is motivated by Landau levels, the energy levels of electrons in a two dimensional plane that are subject to a perpendicular magnetic field. Landau levels form a key element of theoretical models of the quantum Hall effect, which inspired the study of topological insulators. Each Landau level is highly degenerate or flat, and is topologically non-trivial. Motivated by Landau levels, we study the topological properties of tight-binding Hamiltonians which only have flat energy levels. We find that the spectral projectors of such Hamiltonians are strictly local. In chapters 2 and 3, we show that in one dimension, compact Wannier functions (and their analogs in the absence of lattice translational invariance) can be constructed if and only if the subspace they span is described by a strictly local projector. Using this insight, in Chapter 4, we present and prove a no-go theorem which says that if a strictly local tight-binding Hamiltonian in two dimensions only has flat bands, then each of the bands must have a Chern number of zero. All results are proven without the requirement of lattice translational invariance. The role of an inequality relating the number of energies of the Hamiltonian and the system size is also clarified.

In the second part of this dissertation (Chapter 5), we present some results concerning a delocalization transition that arises in a certain class of Floquet topological insulators. Specifically, we study chiral Floquet topological insulators in one dimension, and show that the localization lengths of eigenstates of the time evolution operator diverge with a universal exponent of two as the time approachs a special point in drive.

The dissertation of Pratik Sathe is approved.

Anshul Kogar

Jens Palsberg

Yaroslav Tserkovnyak

Rahul Roy, Committee Chair

University of California, Los Angeles

2023

To my parents

CONTENTS

LIST OF FIGURES

LIST OF TABLES

ACKNOWLEDGMENTS

First and foremost, I would like to thank my parents Sukhada and Sunil Sathe, and my brother Pushkar. They have been a constant source of support for me, and have provided me with guidance, love and encouragement. I am also indebted to my partner Shreya, who has been kind and supportive throughout. Especially during difficult times, they all listened to me patiently and attentively and kept me on track. This dissertation would not have been possible without their encouragement and help.

I would like to express my heartfelt gratitude for my advisor and committee chair, Prof. Rahul Roy, who has been a teacher, mentor and collaborator throughout my PhD journey. The research presented in this thesis is a culmination of a close collaboration with him that involved many discussions on the white board and even some late-night Zoom sessions on weekends. He taught me how to approach research— asking good questions, acquiring the necessary knowledge to address them effectively, and persistently seeking solutions. Mastering the subject matter thoroughly on the way, and at the end, conveying your discovery in a clear manner makes the process worthwhile. I aspire to hold the high standard and quality of work exemplified by his work.

I would like to extend my gratitude to my colleagues in the research group— Adrian Culver, Fenner Harper, Dominic Reiss, Albert Brown, Xu Liu, David Bauer, Joel Herman and Rithwik Pandey. Beyond being colleagues, they have been great friends on this journey and helped create a supportive work environment. Special thanks to Adrian for a wonderful collaboration. His meticulous attention to detail and the clarity of his writing serve as a source of inspiration for me. I would also like to thank Steven Durr and Ian Powell for their friendship.

I would also like to thank my committee members— Prof. Yaroslav Tserkovnyak, Prof. Jens Palsberg and Prof. Anshul Kogar for their time and their feedback. Special thanks to Prof. Palsberg for his kindness and for the many interesting discussions we had regarding quantum computation and quantum programming.

I have had the good fortune of having made many friends over the duration of the PhD program. I will miss the weekend lunches ('the fattening') with Eric, Kyle, Lukas, Tyler and Eddie. The board games, random discussions and weekend dinners with Akshay, Navjot, Michael, Ha, Siva, Saswat and Sumit were always fun. Having good roommates made my experience much easier; thank you Parthe, Michael, Kush and Qin. Throughout my PhD, and especially during some of the difficult periods, Parthe has been a great friend. I would also like to thank Rachel, Kiki, Isha, Jaydev and Harini for making my weekends and holidays more fun.

I have benefited greatly from the guidance I received from my mentors. Vijay kaka has been a mentor to me since even before my undergraduate years, consistently providing encouragement as well as guidance on career development and networking. During my two internships, Tom Lubinski, Dr. Davide Venturelli and Dr. David Bernal have been excellent mentors. Special thanks to David, who has been an extremely supportive mentor, collaborator, and friend. I am indebted to Shana for providing support through the most difficult times, and for going out of the way to help me on multiple occasions.

I would like to thank Rahul, Adrian and Fenner for fruitful collaborations. Some of the chapters below have been adapted from manuscripts that I co-authored with them. I acknowledge the University of California Laboratory Fees Research Program, UCLA Graduate Division, the Center for Quantum Science and Engineering (CQSE) at UCLA as well as the Bhaumik Institute for Theoretical Physics for financial support.

VITA

2017	Bachelor of Technology (Engineering Physics), Indian Institute of Technology, Bombay
2017	Master of Technology (Engineering Physics), Indian Institute of Technology, Bombay
2018	M.S. (Physics), University of California, Los Angeles
2020	Ph.D. candidate in Physics, University of California, Los Angeles

PUBLICATIONS

Pratik Sathe and Rahul Roy. *Topological Triviality of Flat Hamiltonians.* arxiv preprint arXiv:2309.06487 (2023).

Pratik Sathe and Rahul Roy. *Compact Wannier Functions in One Dimension.* arXiv preprint arXiv:2302.11608 (2023).

Thomas Lubinski, Carleton Coffrin, Catherine McGeoch, Pratik Sathe, Joshua Apanavicius, David E. Bernal Neira. *Optimization applications as quantum performance benchmarks* arXiv preprint arXiv:2302.02278 (2023).

Adrian B. Culver, Pratik Sathe, Rahul Roy. *Scattering Expansion for Localization in One Dimension.* arXiv preprint arXiv:2210.07999 (2023).

Adrian B. Culver, Pratik Sathe, Rahul Roy. *Scattering Expansion for Localization in One*

Dimension: from Disordered Wires to Quantum Walks. arXiv preprint arXiv:2211.13368 (2023).

Pratik Sathe, Fenner Harper, and Rahul Roy. *Compactly supported Wannier functions and strictly local projectors.* Journal of Physics A: Mathematical and Theoretical 54.33 (2021): 335302.

Mattia Serra, Pratik Sathe, Irina Rypina, Anthony Kirincich, Shane D. Ross, Pierre Lermusiaux, Arthur Allen, Thomas Peacock, and George Haller. *Search and rescue at sea aided by hidden flow structures.* Nature communications 11, no. 1 (2020): 1-7.

Mattia Serra, Pratik Sathe, Francisco Beron-Vera, and George Haller. *Uncovering the edge of the polar vortex* Journal of the Atmospheric Sciences 74, no. 11 (2017): 3871-3885.

CHAPTER 1

Introduction

1.1 Overview

Topological phases of matter are a cornerstone of modern condensed matter physics. The prototypical example of a topological phase is the quantum Hall fluid, which spurred rapid theoretical and experiment progress, first to understand the quantum Hall effect(s), and later to generalize, predict and observe topological physics arising in a variety of different contexts. The Hall effect is the phenomenon in which an electric potential develops perpendicular to the direction of the flow of current in a two-dimensional material, when a magnetic field perpendicular to the plane is applied. The quantum Hall effect (QHE) is the remarkable observation that the proportionality constant between the current and the voltage is quantized to some very specific values, which appear as plateaus when one plots this ratio (the transverse conductivity) as a function of the external magnetic field.

The QHE comes in two inter-related varieties, the integer QHE (IQHE) and the fractional QHE (FQHE), which correspond to integer and fractional values for the plateaus of the transverse conductivity divided e^2/h. The theoretical underpinnings of both lie in the study of Landau levels, which describe the spectrum of non-interacting electrons moving in a two-dimensional surface, when subjected to a magnetic field perpendicular to the surface. While IQHE can be understood in this picture (upon incorporating the effects of disorder), the FQHE is more complicated, and arises due to the effects of electron-electron interactions.

A lattice generalization of the IQHE in the absence of a magnetic field is the so-called Chern insulator, in which the effects of the lattice potential cannot be ignored. The spectrum and eigenstates of the Hamiltonian are dictated by Bloch's theorem. Using linear response

theory, it can then be shown that the transverse conductivity is proportional to a topological invariant corresponding to the filled bands called the Chern number. The deep connections between electron wavefunction localization and topology found in the IQHE also manifest themselves in Chern insulators.

Starting from the mid-2000s, there has been a shift towards extending the concept of Chern insulators to other dimensions, while considering symmetries like particle-hole, chiral and time-reversal symmetries. The corresponding systems are broadly called topological insulators and superconductors. Furthermore, various topological effects were also explored in the context of semi-metals, in which bands touch instead of having band gaps. Over the last decade, topological properties in time-periodic, or Floquet systems have also been intensely studied.

The fields of static and Floquet topological insulators are vast, not to mention the progress made in understanding the QHEs. There are some excellent resources that discuss the QHE, such as the book by Yoshioka [1], the lectures notes by Tong [2], and chapters in books by Altland and Simons [3] and by Girvin and Yang [4]. This thesis is primarily concerned with the study of the interplay between topology and wavefunction localization in the context of topological insulators. While the ambition naturally spans all symmetry classes and dimensions, this thesis primarily addresses systems in one and two dimensions.

In this chapter, we focus on some of the basic theory, techniques and concepts that underlie the rest of the chapters. We start with a review of Bloch's theorem and magnetic translation operators in Section 1.2. Next, we review Wannier functions and the tight-binding model, and how Peierls' substitution accounts for the effects of incorporating a magnetic field, in Section 1.3. Next, in Section 1.4, we derive a formula for the transverse conductivity for a filled Bloch in terms of the Chern number and discuss the related topic of the modern theory of polarization. Finally, we discuss twisted boundary conditions which arise when magnetic fluxes are inserted through the torus on which a lattice with periodic boundary conditions is assumed to lie on.

1.2 Bloch's Theorem and Magnetic Translation Operators

Bloch's theorem is concerned with properties of the spectrum and eigenstates of a Hamiltonian describing non-interacting electrons moving in a lattice with no disorder, so that the system is lattice translationally invariant. The discussion here follows the treatment provided in Ref. [4].

1.2.1 Bloch's Theorem

The single particle Hamiltonian for non-interacting electrons in a periodic potential defined on a lattice with primitive vectors $\{\mathbf{a}_j\}$ has the form

$$H = \frac{\mathbf{p}^2}{2m} + U(\mathbf{r}),$$

with $U(\mathbf{r} + \mathbf{a}_j) = U(\mathbf{r})$, and $\mathbf{p} = -i\hbar\nabla$. Bloch's theorem states that the stationary states are labeled by the lattice wave-vector k and band index n, and satisfy:

$$\begin{aligned} \psi_{n\mathbf{k}}(\mathbf{r}) &= e^{i\mathbf{k}.\mathbf{r}} u_{n\mathbf{k}}(r) \\ \text{with } u_{n\mathbf{k}}(\mathbf{r} + \mathbf{a}_j) &= u_{n\mathbf{k}}(\mathbf{r}). \end{aligned} \tag{1.1}$$

Note that the Bloch wavevectors are simultaneous eigenstats of H and the lattice translation operators:

$$\begin{aligned} \hat{T}_{\mathbf{a}_j} \psi_{n,\mathbf{k}}(r) &= e^{i\mathbf{k}.\mathbf{a}_j} \psi_{n,\mathbf{k}} \\ H\psi_{n,\mathbf{k}}(\mathbf{r}) &= \epsilon_{n,\mathbf{k}} \psi_{n,\mathbf{k}}(\mathbf{r}) \end{aligned}$$

Furthermore, one can show [5] using a Fourier expansion that

$$\psi_{n,\mathbf{k}+\mathbf{G}} = \psi_{n,\mathbf{k}} \tag{1.2}$$

$$\text{and } \epsilon_{n,\mathbf{k}+\mathbf{G}} = \epsilon_{n,\mathbf{k}}, \tag{1.3}$$

for any reciprocal lattice vector $\mathbf{G}$. Consequently, we can restrict our attention to the 1^{st} Brillouin Zone (1BZ).

It is straightforward to see from (1.3) that

$$\begin{aligned} h(\mathbf{k})u_{n,\mathbf{k}} &= \epsilon_n(\mathbf{k})u_{n,\mathbf{k}}, \\ \text{where } h(\mathbf{k}) &= \frac{(\mathbf{p}+\hbar\mathbf{k})^2}{2m} + U(\mathbf{r}) \end{aligned} \tag{1.4}$$

1.2.2 Bloch's Theorem in the Presence of a Uniform Magnetic Field

In the presence of a Hamiltonian, (1.1) gets modified to

$$H = \frac{1}{2m}(\mathbf{p} - q\mathbf{A}(r))^2 + U(\mathbf{r}),$$

where $\mathbf{A}(\mathbf{r})$ is the magnetic vector potential, and the magnetic field is $\mathbf{B}(\mathbf{r}) = \nabla \times \mathbf{A}(\mathbf{r})$.

The Hamiltonian no longer commutes with the primitive cell translation vectors $\mathbf{a}_j$ because of the presence of the magnetic vector potential, which does not have the periodicity of the lattice. However, it is possible to define suitably modified variants of translation operators that are mutually commuting and which commute with the Hamiltonian.

First, we note that

$$\begin{aligned} T_{\mathbf{a}_j} H T_{\mathbf{a}_j}^\dagger &= \frac{(\mathbf{p} + e\mathbf{A}(\mathbf{r}+\mathbf{a}_j))^2}{2m} + U(\mathbf{r}) \\ &= H' \text{ (say)}. \end{aligned}$$

Here, we used $U(\mathbf{r}+\mathbf{a}_j) = U(\mathbf{r})$. Clearly $H' \neq H$, since $\mathbf{A}(\mathbf{r})$ does not have lattice periodicity.

However, since the magnetic field is uniform, $\mathbf{B}(\mathbf{r}+\mathbf{a}_j) = \mathbf{B}(\mathbf{r})$. Thus,

$$\begin{aligned} \boldsymbol{\nabla} \times \mathbf{A}(\mathbf{r}) &= \boldsymbol{\nabla} \times \mathbf{A}(\mathbf{r}+\mathbf{a}_j) \\ \text{so that } \mathbf{A}(\mathbf{r}+\mathbf{a}_j) &= \mathbf{A}(\mathbf{r}) + \nabla f_{\mathbf{a}_j}(\mathbf{r}), \end{aligned} \tag{1.5}$$

for some function $f_{\mathbf{a}_j}(\mathbf{r})$.

It is straightforward to verify that

$$e^{i\frac{e}{\hbar}f_{\mathbf{a}_j}(\mathbf{r})} H' e^{-i\frac{e}{\hbar}f_{\mathbf{a}_j}(\mathbf{r})} = H.$$

Thus, we can define the following modified translation operators—

$$\tilde{T}_{\mathbf{a}_j} \coloneqq \exp\left(i\frac{e}{\hbar}f_{\mathbf{a}_j}(\mathbf{r})\right) T_{\mathbf{a}_j}.$$

They commute with H since $\tilde{T}_{\mathbf{a}_j} H \tilde{T}_{\mathbf{a}_j} = H$.

It is straightforward to check that

$$\begin{aligned}\tilde{T}_{\mathbf{a}_1}\tilde{T}_{\mathbf{a}_2}\tilde{T}_{\mathbf{a}_1}^{\dagger} &= \exp\left(\frac{ie}{\hbar}\Phi_{\mathbf{a}_2\times\mathbf{a}_1}\right)\tilde{T}_{\mathbf{a}_2}, \\ &= \exp\left(2\pi i\frac{\Phi_{\mathbf{a}_2\times\mathbf{a}_1}}{\Phi_0}\right)\tilde{T}_{\mathbf{a}_2}\end{aligned}$$

where $\Phi_{\mathbf{a}_2\times\mathbf{a}_1}$ denotes the flux of the magnetic field through the parallelogram $\mathbf{a}_2 \times \mathbf{a}_1$, with the orientation $\mathbf{r} \to \mathbf{r}+\mathbf{a}_2 \to \mathbf{r}+\mathbf{a}_1+\mathbf{a}_2 \to \mathbf{r}+\mathbf{a}_1 \to \mathbf{r}$. $\Phi_0 = \frac{h}{e}$ is the magnetic flux quantum.

Thus, the magnetic translation operators commute if the flux is an integer multiple of the flux quantum:

$$\Phi_{\mathbf{a}_2\times\mathbf{a}_1} = N\Phi_0. \tag{1.6}$$

We will be interested in 2D lattices. Consider a lattice laid in the x-y plane, and a uniform magnetic field along the $\hat{z}$ direction. If the magnetic flux per unit cell in the original lattice is $\frac{p}{q}\Phi_0$ for co-prime integers p and q, then we can choose q of original unit cells to define a magnetic unit cell. For example, we can define a magnetic unit cell defined by primitive vectors $\mathbf{v}_1$ and $\mathbf{v}_2$ given by $\mathbf{v}_1 = q\mathbf{a}_1$ and $\mathbf{v}_2 = \mathbf{a}_2$. We then have

$$[\tilde{T}_{\mathbf{v}_1}, \tilde{T}_{\mathbf{v}_2}] = [\tilde{T}_{\mathbf{v}_i}, H] = 0.$$

We can now obtain simultaneous eigenstates of $\tilde{T}_{\mathbf{v}_1}$, $\tilde{T}_{\mathbf{v}_2}$ and H operators, say $\psi_{n,\mathbf{k}}(\mathbf{r})$, such that

$$\psi_{n,\mathbf{k}}(\mathbf{r}) = e^{i\mathbf{k}.\mathbf{r}}u_{n,\mathbf{k}}(\mathbf{r})$$

$u_{n\mathbf{k}}(\mathbf{r})$ satisfies the slightly different periodicity condition compared to (1.1), as seen below:

$$\begin{aligned}\tilde{T}_{\mathbf{v}_i}\psi_{n,\mathbf{k}}(\mathbf{r}) &= e^{i\mathbf{k}.\mathbf{v}_i}\psi_{n,\mathbf{k}}(\mathbf{r}) \\ \implies e^{i\frac{e}{\hbar}f_{\mathbf{v}_i}(\mathbf{r})}e^{i\mathbf{k}.(\mathbf{r}+\mathbf{v}_i)}u_{n\mathbf{k}}(\mathbf{r}+\mathbf{v}_i) &= e^{i\mathbf{k}.(\mathbf{r}+\mathbf{v}_i)}u_{n\mathbf{k}}(\mathbf{r}) \\ \implies e^{i\frac{e}{\hbar}f_{\mathbf{v}_i}(\mathbf{r})}u_{n\mathbf{k}}(\mathbf{r}+\mathbf{v}_i) &= u_{n\mathbf{k}}(\mathbf{r})\end{aligned}$$

Thus, the periodic function in Bloch's theorem is replaced by a function that is periodic up to a gauge-dependent phase. [Note that the f functions are defined through the relation (1.5), and can be found explicitly for any given gauge choice for the vector potential $\mathbf{A}$.] Note also that while the Bloch wavefunctions are periodic in k space [see (1.2)], the magnetic Bloch wavefunction are periodic only upto a phase factor:

$$\psi_{n,\mathbf{k}+\mathbf{G}}(\mathbf{r})e^{i\theta_n(\mathbf{k}+\mathbf{G})} = \psi_{n,\mathbf{k}}(\mathbf{r})e^{i\theta_n(\mathbf{k})} \tag{1.7}$$

In other words, $e^{i\theta_n(\mathbf{k})}\psi_{n,\mathbf{k}}(\mathbf{r})$ is periodic in lattice reciprocal lattice space for magnetic Bloch wavefunction. In the absence of a magnetic field, $\theta_n(\mathbf{k}) = 0$.

1.2.3 Landau Levels as Magnetic Bloch Bands

In the absence of a periodic ionic potential (i.e. in the absence of a lattice), the electronic spectrum consists of the highly degenerate Landau levels. It is straightforward to apply the results from the previous subsection to this case, with only slight modifications.

Since there is no natural lattice, we can choose any vectors $\mathbf{a}_1$ and $\mathbf{a}_2$ which satisfy (1.6). The smallest magnetic cell corresponds to $N = 1$. The spectrum cannot change depending on the choice of $\mathbf{a}_1$ and $\mathbf{a}_2$, and hence each magnetic Bloch band must be flat. These are exactly the Landau levels which are usually found using alternate routes.

1.3 Peierls' Substitution

Much of the following chapters will concern Wannier functions, and hence we review them here. Closely related is the notion of tight-binding models, which will be used throughout the following chapters. Hence, we first discuss these concepts. Later, in Chapter 4, we will deal with situations wherein an external magnetic field is introduced within a tight-binding model. This can be dealt with by using Peierl's substitution, an approximation which we will review here.

1.3.1 Wannier Functions and the Tight-Binding Approximation

Consider the case wherein the Fermi energy lies in an isolated band (i.e. a band separated by energy gaps from the bands above and below it). Instead of using Bloch wavefunctions, it is often useful to consider an alternate basis of orthogonal wavefunctions called Wannier functions. We will drop the band index that labels the Bloch wavefunctions since we are concerned with a single band here. The Wannier functions $\phi_{\mathbf{R}}(\mathbf{r})$ are defined via

$$\begin{aligned} \phi_{\mathbf{R}}(\mathbf{r}) &= \frac{1}{(2\pi)^3}\int d\mathbf{k} e^{-i\mathbf{R}\cdot\mathbf{k}}\psi_{\mathbf{k}}(\mathbf{r}) \\ \text{and } \psi_{\mathbf{k}}(\mathbf{r}) &= \frac{1}{\sqrt{N}}\sum_{\mathbf{R}}\phi_{\mathbf{R}}(\mathbf{r})e^{i\mathbf{k}\cdot\mathbf{r}}. \end{aligned} \tag{1.8}$$

Essentially, Wannier functions are the inverse Fourier transform of the Bloch wavefunctions, and vice versa.

Let us note some interesting properties of Wannier functions. First, ϕ_R for any lattice vector R is a wavefunction localized at R. All Wannier functions are simply (lattice) translates of each other, and form a complete orthonormal basis for the band. Second, Wannier functions are well localized in space. The larger the band gap, the higher the degree of localization. However, it is impossible to construct exponentially localized Wannier functions if the band is topologically non-trivial.

Since all the relevant dynamics occurs within band n if the Fermi energy is in band n, we can express the Hamiltonian conveniently in the Wannier basis. Specifically, since $|\psi(\mathbf{k})\rangle = \sum_{\mathbf{R}} |\phi_{\mathbf{R}}\rangle e^{i\mathbf{k}\cdot\mathbf{R}}$, we have

$$\begin{aligned} H &= \sum_{\mathbf{k}} \epsilon(\mathbf{k}) |\psi(\mathbf{k})\rangle \langle\psi(\mathbf{k})| \\ &= \sum_{\mathbf{R},\mathbf{R}'} t_{\mathbf{R},\mathbf{R}'} |\phi_{\mathbf{R}}\rangle \langle\phi_{\mathbf{R}'}|, \\ \text{where } t_{\mathbf{R},\mathbf{R}'} &\coloneqq \sum_{\mathbf{k}} e^{i\mathbf{k}\cdot(\mathbf{R}-\mathbf{R}')}\epsilon(\mathbf{k}) \end{aligned}$$

Note also that since $\{|\phi_{\mathbf{R}}\rangle\}$ is an orthonormal basis (within the band), the "hopping elements" t_{ij} can also be represented as

$$t_{\mathbf{R},\mathbf{R}'} = \langle\phi_{\mathbf{R}}| H |\phi_{\mathbf{R}'}\rangle$$

$$= \int \mathrm{d}^n\mathbf{r}\phi^*_{\mathbf{R}}(\mathbf{r})H\phi_{\mathbf{R}'}(\mathbf{r}).$$

In the second quantized notation, if $c_{\mathbf{R}}$ ($c^\dagger_{\mathbf{R}}$) is the annihilation (creation) operator for state $|\phi_R\rangle$, then we can write

$$H = \sum_{\mathbf{R},\mathbf{R}'} t_{\mathbf{R},\mathbf{R}'} c^\dagger_{\mathbf{R}} c_{\mathbf{R}'}. \tag{1.9}$$

This is called the tight-binding representation, and is an exact expression. In real life, the Bloch wavefunctions and Wannier functions are never known exactly. So, an appromixation to the Wannier functions in terms of atomic orbitals is used. This is the so-called linear combination of atomic orbitals (LCAO) approximation. In this approximation, the Hamiltonian is still represented by an equation of form (1.9), but with these LCAO wavefunctions.

1.3.2 Tight-binding Representation in the Presence of a Magnetic Field

So far, we have considered a system with a magnetic field. How does including it affect the tight-binding representation (1.9)? We will follow the treatment in Ref. [6] to answer this question.

First, recall that in the presence of a magnetic field $\mathbf{B}$, the Hamiltonian (1.1) changes to

$$\tilde{H} = \frac{(-i\hbar\nabla - q\mathbf{A})^2}{2m} + U(\mathbf{r}), \tag{1.10}$$

where $\mathbf{A}(\mathbf{r})$ denotes the magnetic vector potential ($\mathbf{B} = \nabla \times \mathbf{A}$).

In order to obtain a representation for (1.10) in terms of tight-binding orbitals, consider an orthogonal basis [6] $\{\tilde{\phi}_{\mathbf{R}}(\mathbf{r})\}$ for the band (in which the Fermi energy lies), obtained from the Wannier basis $\{\phi_{\mathbf{R}}(\mathbf{r})\}$ for the problem without the magnetic field, through the following transformation:

$$\tilde{\phi}_{\mathbf{R}}(\mathbf{r}) = \exp\left(\frac{iq}{\hbar}G(\mathbf{r})\right)\phi_{\mathbf{R}}(\mathbf{r}), \tag{1.11}$$
$$\text{with } G(\mathbf{r}) \coloneqq \int_{\mathbf{R}}^{\mathbf{r}} \mathbf{A}(\mathbf{r}') \cdot \mathrm{d}\mathbf{r}',$$

$$= \int_0^1 (\mathbf{r} - \mathbf{R}) \cdot \mathbf{A}(\mathbf{R} + \lambda(\mathbf{r} - \mathbf{R}))\, \mathrm{d}\lambda. \tag{1.12}$$

(The integral in G is along the straight line connecting $\mathbf{R}$ and $\mathbf{r}$.) We will now obtain the matrix elements of $\tilde{H}$ between various $\{\tilde{\phi}_{\mathbf{R}}(\mathbf{r})\}$ functions. To that end, consider the action of $\tilde{H}$ on $\tilde{\phi}_{\mathbf{R}}(\mathbf{r})$:

$$\tilde{H}\tilde{\phi}_{\mathbf{R}}(\mathbf{r}) = \left[\frac{(-i\hbar\nabla - q\mathbf{A})^2}{2m} + U(\mathbf{r})\right] e^{\frac{ig}{\hbar}G(\mathbf{r})}\phi_{\mathbf{R}}(\mathbf{r}). \tag{1.13}$$

The utility of defining $\tilde{\phi}$ will now become clear. Specifically, we will find that the $q\mathbf{A}$ terms in the equation above will (approximately) cancel with the derivative due to the exponential term we introduced. To that end, let us first calculate the gradient of G:

$$\begin{aligned}\nabla G(\mathbf{r}) &= \nabla \int_0^1 (\mathbf{r} - \mathbf{R}) \cdot \mathbf{A}(\mathbf{R} + \lambda(\mathbf{r} - \mathbf{R}))\, \mathrm{d}\lambda. \\ &= \int_0^1 \nabla \left[(\mathbf{r} - \mathbf{R}) \cdot \mathbf{A}(\mathbf{R} + \lambda(\mathbf{r} - \mathbf{R}))\right] \mathrm{d}\lambda\end{aligned}$$

Recall the formula:

$$\nabla \cdot (\mathbf{C} \cdot \mathbf{D}) = (\mathbf{C} \cdot \nabla)\mathbf{D} + (\mathbf{D} \cdot \nabla)\mathbf{C} + \mathbf{C} \times (\nabla \times \mathbf{D}) + \mathbf{D} \times (\nabla \times \mathbf{C}).$$

Denoting $(\mathbf{r} - \mathbf{R})$ by $\mathbf{C}$ and $\mathbf{A}(\mathbf{R} + \lambda(\mathbf{r} - \mathbf{R}))$ by $\mathbf{D}$, we have

$$\begin{aligned}(\mathbf{C} \cdot \nabla)\mathbf{D} &= ((\mathbf{r} - \mathbf{R}) \cdot \nabla)\mathbf{A}(\mathbf{r}') \\ (\mathbf{D} \cdot \nabla)\mathbf{C} &= \mathbf{A}(\mathbf{r}') \\ \mathbf{C} \times (\nabla \times \mathbf{D}) &= (\mathbf{r} - \mathbf{R}) \times \mathbf{B}(\mathbf{r}') \\ \mathbf{D} \times (\nabla \times \mathbf{C}) &= 0,\end{aligned}$$

wherein $\mathbf{r}' = \mathbf{R} + \lambda(\mathbf{r} - \mathbf{R})$. Summing them up, we get

$$G(\mathbf{r}) = \int_0^1 \mathrm{d}\lambda((\mathbf{r} - \mathbf{R}) \cdot \nabla)\mathbf{A}(\mathbf{r}') + \mathbf{A}(\mathbf{r}') + \mathbf{r}' \times \mathbf{B}(\mathbf{r}')$$

Note however, that $\int_0^1 \mathbf{A}(\mathbf{r}') = \mathbf{A}(\mathbf{r}) - \int_0^1 (\mathbf{r} - \mathbf{R}) \times \mathbf{B}(\mathbf{r}')$. Thus,

$$\nabla G(\mathbf{r}) = \mathbf{A}(\mathbf{r}) + \int_0^1 \mathrm{d}\lambda((\mathbf{r} - \mathbf{R}) \cdot \nabla)\mathbf{A}(\mathbf{r}')$$

Now we will plug this in in order to simplify (1.13). First, note that

$$(-i\hbar\nabla - q\mathbf{A})e^{\frac{iq}{\hbar}G(\mathbf{r})}\phi_{\mathbf{R}}(\mathbf{r}) = e^{\frac{iqG(\mathbf{r})}{\hbar}}\left[-i\hbar\nabla + \int_0^1 \mathrm{d}\lambda((\mathbf{r}-\mathbf{R})\cdot\nabla)\mathbf{A}(\mathbf{r}')\right]\phi_{\mathbf{R}}(\mathbf{r})$$

Approximation 1: We will now argue that the second term is negligible. We invoke the locality of the Wannier functions. Whenever $\mathbf{r}$ is far away from $\mathbf{R}$, $\phi_{\mathbf{R}}(\mathbf{r}) \approx 0$. On the other hand, when $\mathbf{r} \approx \mathbf{R}$, the integral term is almost zero. Hence, we have

$$(-i\hbar\nabla - q\mathbf{A})\tilde{\phi}_{\mathbf{R}} = e^{\frac{iqG(\mathbf{r})}{\hbar}}\left(-i\hbar\nabla\right)\phi_{\mathbf{R}}(\mathbf{r}) \tag{1.14}$$

Thus (1.13) then becomes

$$\tilde{H}\tilde{\phi}_{\mathbf{R}} \approx e^{\frac{iqG(\mathbf{r})}{\hbar}}\left[H\phi_{\mathbf{R}}(\mathbf{r})\right].$$

Thus, we have

$$\begin{aligned}
\left\langle\tilde{\phi}_{\mathbf{R}}\right|\tilde{H}\left|\tilde{\phi}_{\mathbf{R}'}\right\rangle &= \int \mathrm{d}^n\mathbf{r}\tilde{\phi}^*_{\mathbf{R}}(\mathbf{r})\tilde{H}\tilde{\phi}_{\mathbf{R}'}(\mathbf{r}). \\
&= \int \mathrm{d}^n\mathbf{r}\phi^*_{\mathbf{R}}(\mathbf{r})H\phi_{\mathbf{R}'}(\mathbf{r})\exp\left[-\frac{iq}{\hbar}\int_{\mathbf{R}}^{\mathbf{r}}\mathbf{A}\cdot\mathrm{d}\mathbf{r}' + \frac{iq}{\hbar}\int_{\mathbf{R}'}^{\mathbf{r}}\mathbf{A}\cdot\mathrm{d}\mathbf{r}'\right] \\
&= \exp\left(\frac{iq}{\hbar}\int_{\mathbf{R}'}^{\mathbf{R}}\mathbf{A}\cdot\mathrm{d}\mathbf{r}'\right)\int \mathrm{d}^n\mathbf{r}\phi^*_{\mathbf{R}}(\mathbf{r})H\phi_{\mathbf{R}'}(\mathbf{r})\exp\left(-\frac{iq}{\hbar}\int_{\mathbf{R}\to\mathbf{r}\to\mathbf{R}'\to\mathbf{R}}\mathbf{A}\cdot\mathrm{d}\mathbf{r}'\right) \\
&= \exp\left(\frac{iq}{\hbar}\int_{\mathbf{R}}^{\mathbf{R}'}\mathbf{A}\cdot\mathrm{d}\mathbf{r}'\right)\int \mathrm{d}^n\mathbf{r}\phi^*_{\mathbf{R}}(\mathbf{r})H\phi_{\mathbf{R}'}(\mathbf{r})e^{-\frac{iq}{\hbar}\Phi_{\mathbf{R},\mathbf{R}'}(\mathbf{r})},
\end{aligned}$$

where $\Phi_{\mathbf{R},\mathbf{R}'}(\mathbf{r}) = \int_{\mathbf{R}\to\mathbf{r}\to\mathbf{R}'\to\mathbf{R}}\mathbf{A}\cdot\mathrm{d}\mathbf{r}'$ is the flux of the magnetic field through the triangle $\boldsymbol{\Delta}\mathbf{R}\mathbf{r}\mathbf{R}'$.

Approximation 2: The Φ term can be ignored. We use the fact the Wannier functions are well localized at their respective lattice vectors. Let us assume that each Wannier function decays exponentially with a length scale ξ, which is smaller than the lattice constant a. Then, for values of $\mathbf{r}$, for which $|\mathbf{r}-\mathbf{R}|, |\mathbf{r}-\mathbf{R}'| > \xi$, the integrand is negligible. The only significant contribution arises from $\mathbf{r}$ that is in a region close to the line joining $\mathbf{R}$ and $\mathbf{R}'$. Now, if in addition, the length scale over which $\mathbf{A}$ varies in space is much smaller the lattice constant, then for such $\mathbf{r}$, $\Phi_{\mathbf{R},\mathbf{R}'}(\mathbf{r}) \approx \oint_{\mathbf{R}\to\mathbf{r}\to\mathbf{R}'\to\mathbf{R}}\mathbf{A}_0\cdot\mathbf{r}' = \mathbf{A}_0\cdot\oint_{\mathbf{R}\to\mathbf{r}\to\mathbf{R}'\to\mathbf{R}}\mathbf{r}' = 0$. Therefore, we get

$$\tilde{t}_{\mathbf{R},\mathbf{R}'} \coloneqq \left\langle\tilde{\phi}_{\mathbf{R}}\right|\tilde{H}\left|\tilde{\phi}_{\mathbf{R}'}\right\rangle$$

$$= \exp\left(\frac{iq}{\hbar}\int_{\mathbf{R}'}^{\mathbf{R}} \mathbf{A}\cdot \mathrm{d}\mathbf{r}'\right)\int \mathrm{d}^n\mathbf{r}\phi^*_{\mathbf{R}}(\mathbf{r})H\phi_{\mathbf{R}'}(\mathbf{r})$$
$$= \exp\left(\frac{iq}{\hbar}\int_{\mathbf{R}'}^{\mathbf{R}} \mathbf{A}\cdot \mathrm{d}\mathbf{r}'\right)t_{\mathbf{R},\mathbf{R}'}.$$

In other words, in the presence of a slowly varying magnetic field, the Hamiltonian is given by

$$\tilde{H} = \sum_{\mathbf{R},\mathbf{R}'} \tilde{t}_{\mathbf{R},\mathbf{R}'}\tilde{c}^\dagger_{\mathbf{R}}\tilde{c}_{\mathbf{R}'},$$

with $\tilde{c}$ representing the destruction operator for the modified wavefunctions $\tilde{\phi}$. The replacement of the hopping elements, specifically

$$t_{\mathbf{R},\mathbf{R}'} \to t_{\mathbf{R},\mathbf{R}'}e^{\frac{iq}{\hbar}\int_{\mathbf{R}'}^{\mathbf{R}}\mathbf{A}\cdot\mathrm{d}\mathbf{r}'}$$

is called Peierls substitution [7].

1.4 Quantization of Transverse Conductivity

The transverse conductivity of a filled Bloch band is proportional to the Chern number of the band. In this section, we will review a derivation for the corresponding formula. We will closely follow the treatment in Vandertbilt's book [8], starting first with the development of linear response theory at absolute zero.

1.4.0.1 First Order Perturbation Theory

First, let us recall 1^{st} order perturbation theory. Let H be a Hamiltonian parameterized by some parameter λ. Let use denote the eigenvalue equation for the n^{th} energy state by

$$H(\lambda)\left|n(\lambda)\right\rangle = E(\lambda)\left|n(\lambda)\right\rangle.$$

Taylor expanding about each term to first order in $\Delta\lambda$ about some value λ_0, we obtain

$$(H - E_n)\left|\partial_\lambda n\right\rangle = \partial_\lambda(E_n - H)\left|n\right\rangle, \tag{1.15}$$

with $\partial_\lambda \equiv \frac{\partial}{\partial \lambda}$. Note also that E and $|n\rangle$ are functions of λ evaluated at λ_0, but we have dropped this dependence for notational convenience.

Multiplying both sides by $\langle n|$ gives us

$$\partial_\lambda E_n = \langle n| \partial_\lambda H |n\rangle .$$

Plugging this back into (1.15), we get

$$\begin{aligned}(E_n - H)|\partial_\lambda n\rangle &= \underbrace{(1 - |n\rangle \langle n|)}_{Q_n} \partial_\lambda H |n\rangle \\ &= Q_n \partial_\lambda H |n\rangle\end{aligned}$$

Multiplying both sides by $\langle m|$ for $m \neq n$ we get

$$\langle m|\partial_\lambda n\rangle = \frac{\langle m| \partial_\lambda H |n\rangle}{E_n - E_m}.$$

Thus, we have

$$\begin{aligned}Q_n |\partial_\lambda n\rangle &= \underbrace{\left(\sum_{m \neq n} \frac{|m\rangle \langle m|}{E_n - E_m} \right)}_{T_n} \partial_\lambda H |n\rangle \\ &= T_n (\partial_\lambda H) |n\rangle . \end{aligned} \tag{1.16}$$

On the other hand, note that $\langle n|\partial_\lambda n\rangle$ is purely imaginary, since $\partial_\lambda \langle n|n\rangle = 0$. Thus, we can define a purely real quantity, $A_n(\lambda) = i \langle n|\partial_\lambda n\rangle$, so that

$$|\partial_\lambda n\rangle = -iA_n(\lambda) + T_n(\partial_\lambda H)|n\rangle . \tag{1.17}$$

$A_n(\lambda)$ is known as the Berry connection. This solves (1.15). This is basically a compact way of writing down basic results from perturbation theory.

Multiple Independent Electrons: When we have multiple non-interacting electrons in a systems, they occupy distinct energy levels. We can conveniently define

$$Q = \sum_{m}^{\text{unocc.}} |m\rangle \langle m|$$

$$T = \sum_{m}^{\text{unocc.}} \frac{|m\rangle \langle m|}{E_n - E_m}$$

Following the same steps as those in the derivation of (1.16), if we take the sum for m only over unoccupied states instead of $m \neq n$, we get

$$Q \, |\partial_\lambda n\rangle = T(\partial_\lambda H) \, |n\rangle \tag{1.18}$$

Linear response theory is concerned with how (the expectation value of) an observable changes if a perturbation is added to the Hamiltonian describing a system. We see that $\langle O\rangle(\lambda) = \langle n(\lambda)| \, O \, |n(\lambda)\rangle$, so that

$$\partial_\lambda \langle O\rangle = 2 \, \text{Re} \, \langle n| \, O \, |\partial_\lambda n\rangle \tag{1.19}$$

Since $\langle n|\partial_\lambda n\rangle$ is purely imaginary, we can replace O above by OQ_n. Furthermore, in the case of multiple independent (i.e. non-interacting) electrons, the right hand side should contain a sum over all occupied states n, so that

$$\begin{aligned} \partial_\lambda \langle O\rangle &= \sum_{n}^{\text{occ.}} 2 \, \text{Re} \, \langle n| \, OQ_n \, |\partial_\lambda n\rangle \\ &= \sum_{n}^{\text{occ.}} 2 \, \text{Re} \, \langle n| \, OQ \, |\partial_\lambda n\rangle \, , \end{aligned} \tag{1.20}$$

wherein we skipped some straightforward steps that allow us to replace $Q_n \to Q$.

1.4.1 Hall Conductance for a Band Insulator

If we have a set of filled Bloch bands, we can apply the equations in the previous subsections to the Bloch Hamiltonian $H_{\mathbf{k}} = e^{-i\mathbf{k}.\mathbf{r}} H e^{i\mathbf{k}.\mathbf{r}}$. We also replace $|n\rangle \to |u_{n\mathbf{k}}\rangle$. Q is also replaced by $Q_{\mathbf{k}} = \sum_m^{\text{unocc.}} |u_{m\mathbf{k}}\rangle \langle u_{m\mathbf{k}}|$.

Thus, (1.20) in this case becomes

$$\partial_\lambda \langle O\rangle = \sum_{\mathbf{k}} \sum_{n}^{\text{occ.}} 2 \, \text{Re} \, \langle \partial_\lambda u_{n\mathbf{k}}| \, Q_{\mathbf{k}} O \, |u_{n\mathbf{k}}\rangle \, .$$

Using $\sum_{\mathbf{k}} \equiv \frac{V_{\text{cell}}}{(2\pi)^d} \int_{\text{BZ}}$, we thus obtain

$$\partial_\lambda \langle O\rangle = \frac{V_{\text{cell}}}{(2\pi)^d} \sum_{n}^{\text{occ.}} \int_{\text{BZ}} \mathrm{d}\mathbf{k} \; 2 \, \text{Re} \, \langle \partial_\lambda u_{n\mathbf{k}}| \, Q_{\mathbf{k}} O \, |u_{n\mathbf{k}}\rangle \, , \tag{1.21}$$

with d being the dimensionality of the system.

Similarly, (1.18) becomes

$$Q_{\mathbf{k}} \left|\partial_\lambda u_{n\mathbf{k}}\right\rangle = T_{\mathbf{k}}(\partial_\lambda H) \left|u_{n\mathbf{k}}\right\rangle \tag{1.22}$$

(1.21) and (1.22) together imply

$$\partial_\lambda \langle O\rangle = \frac{V_{\text{cell}}}{(2\pi)^d} \sum_n^{\text{occ.}} \int_{\text{BZ}} 2\,\text{Re}\left\langle u_{n\mathbf{k}}\right| (\partial_\lambda H) T_{\mathbf{k}} O \left|u_{n\mathbf{k}}\right\rangle, \tag{1.23}$$

Note: Here, λ should be interpreted as a parameter that characterizes the strength of a perturbing term in the Hamiltonian.

Now consider an external perturbation, in the form of a uniform *weak* electric field $\mathbf{E}$, applied to a 2d crystalline insulator. (If the electric field is strong, higher-order corrections may be required.) With the perturbation, $H_{\mathbf{k}} \to H_{\mathbf{k}} + e\mathbf{E}.\mathbf{r}$. The two components of $\mathbf{E}$ serve as the parameters characterizing the strength of the perturbation. Using the notation $\partial_\mu \equiv \frac{\partial}{\partial E_\mu}$ for $\mu = x, y$, we see that $\partial_\mu H = e r_\mu$ from (1.23), we get

$$\partial_\nu \langle O\rangle = \frac{e A_{\text{cell}}}{(2\pi)^2} \sum_n^{\text{occ.}} \int_{\text{BZ}} 2\,\text{Re}\left\langle u_{n\mathbf{k}}\right| r_\nu T_{\mathbf{k}} O \left|u_{n\mathbf{k}}\right\rangle d^2k, \tag{1.24}$$

We can replace $T_{\mathbf{k}}$ above with $Q_{\mathbf{k}} T_{\mathbf{k}}$ since they are equal.

Note that the conductivity tensor is $\sigma_{\mu\nu} = \partial_\nu \langle -e v_\mu\rangle$. So, we want an expression for $\partial_\nu \langle v\rangle$. To that end, we simplify as follows

$$\begin{aligned}
Q_{\mathbf{k}} \mathbf{r} \left|u_{n\mathbf{k}}\right\rangle &= \sum_m^{\text{unocc.}} \left|u_{m\mathbf{k}}\right\rangle \left\langle u_{m\mathbf{k}}\right| \mathbf{r} \left|u_{n\mathbf{k}}\right\rangle \\
&= i\hbar \sum_m^{\text{unocc.}} \frac{\left|u_{m\mathbf{k}}\right\rangle \left\langle u_{m\mathbf{k}}\right| - \frac{i}{\hbar}[\mathbf{r}, H_{\mathbf{k}}] \left|u_{n\mathbf{k}}\right\rangle}{(E_{n\mathbf{k}} - E_{m\mathbf{k}})} \\
&= i\hbar \sum_m^{\text{unocc.}} \frac{\left|u_{m\mathbf{k}}\right\rangle \left\langle u_{m\mathbf{k}}\right|}{(E_{n\mathbf{k}} - E_{m\mathbf{k}})} \mathbf{v}_{\mathbf{k}} \left|u_{n\mathbf{k}}\right\rangle \\
&= i\hbar T_{\mathbf{k}} \mathbf{v}_{\mathbf{k}} \left|u_{n\mathbf{k}}\right\rangle
\end{aligned}$$

Plugging into (1.24), we get

$$\sigma_{\mu\nu} = -e\partial_\nu \langle v_\mu\rangle / A_{\text{cell}}$$

$$= \frac{-\hbar e^2}{(2\pi)^2} \sum_n^{\text{occ.}} \int_{\text{BZ}} \mathrm{d}^2\mathbf{k}\ 2\,\mathrm{Re}\, i \left\langle u_{n\mathbf{k}} \right| v_\nu T_{\mathbf{k}}^2 v_\mu \left| u_{n\mathbf{k}} \right\rangle$$
$$= \frac{\hbar e^2}{(2\pi)^2} \sum_n^{\text{occ.}} \int_{\text{BZ}} \mathrm{d}^2\mathbf{k}\ 2\,\mathrm{Im} \left\langle u_{n\mathbf{k}} \right| v_\nu T_{\mathbf{k}}^2 v_\mu \left| u_{n\mathbf{k}} \right\rangle$$

When $\mu = \nu$, this is clearly 0, since the term is real. Using (1.22) with $\mathbf{k}$ as the parameter λ, and making use of $\partial_{\mathbf{k}} H_{\mathbf{k}} = \hbar \mathbf{v}_{\mathbf{k}}$[1], we finally obtain

$$\sigma_{yx} = \frac{e^2}{(2\pi)^2 \hbar} \sum_n^{\text{occ.}} \int_{\text{BZ}} \mathrm{d}^2\mathbf{k}\ 2\,\mathrm{Im} \left\langle \partial_y u_{n\mathbf{k}} \right| Q_{\mathbf{k}} \left| \partial_x u_{n\mathbf{k}} \right\rangle$$
$$= \frac{e^2}{(2\pi)^2 \hbar} \sum_n^{\text{occ.}} \int_{\text{BZ}} \mathrm{d}^2\mathbf{k}\ 2\,\mathrm{Im} \left\langle \partial_y u_{n\mathbf{k}} | \partial_x u_{n\mathbf{k}} \right\rangle .$$

To get the second line, we replace $Q_{\mathbf{k}} \to Q_{n\mathbf{k}} = 1 - |u_{n\mathbf{k}}\rangle \langle u_{n\mathbf{k}}|$, and use the fact that $\langle \partial_y u_{n\mathbf{k}} | u_{n\mathbf{k}} \rangle \langle u_{n\mathbf{k}} | \partial_x u_{n\mathbf{k}} \rangle = iA_x(-iA_y)$ is purely real.

Finally, this gives us

$$\sigma_{yx} = \frac{e^2}{\hbar} \sum_n^{\text{occ.}} C_n. \tag{1.25}$$

Note that this approach is partly problematic, since the potential associated with an electric field blows up at large $\mathbf{r}$, and consequently it should not be legal to treat it as a perturbation. A more satisfactory approach involves a time varying magnetic vector potential and no electrostatic potential. However, we will not discuss it here.

1.5 Twisted Boundary Conditions

In Chapter 4, we will deal with twisted boundary conditions, which arise when magnetic fluxes are threaded through the holes of a torus on which a system is assumed to lie one. In this section, we derive the connection between magnetic flux threading and twisted boundary conditions.

[1] which follows from $H_{\mathbf{k}} = e^{-i\mathbf{k}.\mathbf{r}} H e^{i\mathbf{k}.\mathbf{r}} = (\mathbf{p} + \hbar\mathbf{k})^2/2m + U(r)$, $\mathbf{v} = -\frac{i}{\hbar}[\mathbf{r}, H]$ and $\mathbf{v}_{\mathbf{k}} = e^{-i\mathbf{k}.\mathbf{r}} \mathbf{v} e^{i\mathbf{k}.\mathbf{r}}$

1.5.1 Interacting Electrons with Disorder in a Continuum Model

We consider a system of size $x \times y$, with periodic boundary conditions so that the system has a toroidal geometry. Let us assume that there are N electrons that are free to move on a torus, with substrate potential (potential due to a lattice, which may or may not have some disorder) $U(\mathbf{r})$ and electron-electron interactions $V(r)$. Then, the Hamiltonian, without any fluxes inserted is given by

$$H = \sum_{j=1}^{N} \frac{1}{2m_j}(-i\hbar\nabla_j + e\mathbf{A}(\mathbf{r}_j))^2 + \sum_j U(\mathbf{r}_j) + \sum_{j<k} V(|\mathbf{r}_j - \mathbf{r}_k|)$$

Now, consider a flux ϕ_y inserted through a hole, parallel to the $\hat{y}$ direction. The vector potential changes from $\mathbf{A}(\mathbf{r})$ to $\mathbf{A}(\mathbf{r}) + \mathbf{A}'(\mathbf{r})$, with $\mathbf{A}'(\mathbf{r})$ such that $\oint \mathbf{A}'(\mathbf{r})d\mathbf{r} = \phi_y$, for any loop encircling the y axis. The Hamiltonian gets modified to H_ϕ, given by

$$H_\phi = \sum_{j=1}^{N} \frac{1}{2m_j}(-i\hbar\nabla_j + e\mathbf{A}(\mathbf{r}_j) + e\mathbf{A}'(\mathbf{r}_j))^2 + \sum_j U(\mathbf{r}_j) + \sum_{j<k} V(|\mathbf{r}_j - \mathbf{r}_k|)$$

Since $\nabla \times \mathbf{A}'(\mathbf{r}) = 0$, we have $\mathbf{A}'(\mathbf{r}) = \nabla\chi(\mathbf{r})$ for some χ. Note that $\chi(\mathbf{r})$ is not single valued as x goes from 0 to L_x. In fact $\chi(x = L_x) - \chi(x = 0) = \oint \nabla\chi d\mathbf{r} = \oint \mathbf{A}(\mathbf{r}).\mathrm{d}\mathbf{r} = \phi_y$. We will now follow the arguments in Ref. [9].

Let $\psi(\mathbf{r}_1, \ldots, \mathbf{r}_N)$ be an eigenstate of H (the Hamiltonian with the magnetic flux), so that $H\psi = E\psi$. Define a new wavefunctions ψ' as follows:

$$\psi'(\mathbf{r}_1, \ldots, \mathbf{r}_N) = e^{-i\frac{e}{\hbar}\sum_{j=1}^{N}\chi(\mathbf{r}_j)}\psi(\mathbf{r}_1, \ldots, \mathbf{r}_N).$$

Operating H_ϕ on ψ', we see that

$$\begin{aligned} H_\phi\psi' &= e^{-i\frac{e}{\hbar}\sum_{j=1}^{N}\chi(\mathbf{r}_j)}H\psi \\ &= e^{-i\frac{e}{\hbar}\sum_{j=1}^{N}\chi(\mathbf{r}_j)}E\psi \\ &= E\psi' \end{aligned}$$

Thus, ψ' is an eigenstate of H_ϕ. Note however that ψ' must satisfy periodic boundary conditions. Specifically, for any j, $\psi'(x_j = 0) = \psi'(x_j = L_x)$, and similarly for y_j, since the

wavefunction must be single valued. (All the position coordinates not specified as arguments of this function are implied to assume the same values on both sides of an equation.) Therefore, we have

$$\begin{aligned}
\psi'(x_j = L_x) &= \psi'(x_j = 0) \\
\implies \psi(x_j = L_x) e^{-i\frac{e}{\hbar}\sum_{j=1}^{N}\chi(\mathbf{r}_j)} &= \psi'(x_j = 0) e^{-i\frac{e}{\hbar}\sum_{j=1}^{N}\chi(\mathbf{r}_j)} \\
\implies \psi(x_j = L_x) e^{-i\frac{e}{\hbar}\chi(\mathbf{x}_j=0)} &= \psi'(x_j = 0) e^{-i\frac{e}{\hbar}\chi(\mathbf{x}_j=L_x)} \\
\implies \psi(x_j = L_x) &= e^{-i\frac{e}{\hbar}(\chi(\mathbf{x}_j=L_x)-\chi(\mathbf{x}_j=0))}\psi(x_j = 0) \\
\text{so that } \psi(\mathbf{r}_1, \ldots, \mathbf{r}_j = L_x, \ldots, \mathbf{r}_N) &= e^{i2\pi\frac{\phi_y}{\Phi_0}}\psi(\mathbf{r}_1, \ldots, \mathbf{r}_j = 0, \ldots, \mathbf{r}_N).
\end{aligned}$$

Note that this condition will apply to every $j = 1, \ldots, N$, as is also required by anti-symmetry of the wavefunction. These conditions are referred to as *twisted boundary conditions*.

To summarize, the solution to a Hamiltonian with a flux inserted is actually a solution of the flux-free Hamiltonian, but with the requirement that the solution satisfy twisted boundary conditions.

1.5.2 Single-Particle Tight-Binding Hamiltonian without Disorder

We work through this case since it is quite useful in the context of modern theory of polarization, Wannier representability and topological insulators. This is a straightforward exercise and we use a specific gauge.

For a system with lattice translation invariance (LTI) that is defined on a torus, if one inserts magnetic flux along the two holes, the spectrum of the Hamiltonian as well as the eigenstates change in a particular fashion. In this section, we will see precisely how this happens for a single-particle tight-binding Hamiltonian. We will see that the Bloch wavefunctions have the same form as the zero magnetic field case, but the change is in the allowed values of crystal momentum. Additionally, for dispersive bands, all the energy eigenvalues shift slightly, but in the thermodynamic limit, the spectrum remains unchanged.

We will consider a Hamiltonian H with LTI defined on a rectangular lattice of size $L_x \times L_y$ cells, with periodic boundary conditions along both directions. Let H only have

at most nearest-neighbor hopping matrix elements. (Every Hamiltonian can be brought into this form by a unit-cell redefinition, unless the hopping range of the Hamiltonian is of the order of the system size.) We will be considering periodic boundary conditions with $x = 1, \ldots, L_x$ and $y = 1, \ldots, L_y$.

Clearly, $T_{x/y} H T_{x/y}^\dagger = H$, for translation operators $T_x = \sum_{x,y=1}^{L_x} |x+1 \mod L_x, y\rangle \langle x, y|$ and T_y defined similarly. To find the eigenvalues and eigenvectors, we define $H(k_x, k_y) = \langle k_x, k_y | H | k_x, k_y \rangle$ and diagonalize it. Here, $|k_x\rangle = \frac{1}{\sqrt{L_x}} \sum_{x=1}^{L_x} e^{-ik_x x} |x\rangle$ and similarly for $|k_y\rangle$. Clearly, $T_{x/y} \left|k_{x/y}\right\rangle = e^{ik_{x/y}} \left|k_{x/y}\right\rangle$ but with the restriction that $k_{x/y} = \frac{2\pi}{L_{x/y}} n$, with $n = 0, \ldots, L_{x/y} - 1$.

We will only add flux ϕ parallel to the $\hat{y}$ direction in the following discussion. (The consequences of adding flux along both the $\hat{x}$ and $\hat{y}$ directions can be inferred straightforwardly.) Let the Hamiltonian after flux insertion be denoted by $H(\phi)$. We can use a gauge in which only those bonds that connect locations (L_x, y) and $(1, y')$ for any y, y' get an addition phase through Peierls' substitution. Specifically,

$$\langle 1, y' | H(\phi) | L_x, y \rangle = e^{-i2\pi \frac{\phi}{\Phi_0}} \langle 1, y' | H(\phi = 0) | L_x, y \rangle ,$$

where $\Phi_0 = e/h$ is the magnetic flux quantum. Clearly, $T_x H(\phi) T_x^\dagger = H(\phi)$, but only if ϕ is an integer multiple of Φ_0. To make progress in diagonalizing $H(\phi)$, we define a 'twisted' translation operator:

$$T_x(\phi) = \left(\sum_{x=1}^{L_x - 1} |x+1\rangle \langle x| \right) + e^{-i2\pi \frac{\Phi}{\Phi_0}} |1\rangle \langle L_x| .$$

(We have suppressed the y index here.) It is straightforward to check that

$$[T_x(\phi), H(\phi)] = 0,$$
$$\text{and } [T_y, H(\phi)] = 0$$

for all values of ϕ.

Furthermore, eigen-equations for $T_x(\phi)$ are of the form:

$$T_x(\phi) |k_x\rangle = e^{ik_x} |k_x\rangle$$

$$\text{where } |k_x\rangle = \frac{1}{\sqrt{L_x}} \sum_{x=1}^{L_x} e^{-ik_x x} |x\rangle$$
$$\text{and } k_x = \frac{2\pi}{L_x}\left(n - \frac{\phi}{\Phi_0}\right)$$

Defining $H_\phi(k_x) \coloneqq \langle k_x| H(\phi) |k_x\rangle$, we then have

$$H_\phi(k_x) = H_{\phi=0}(k_x)$$
$$\text{but with } k_x = \frac{2\pi}{L_x}(n - \frac{\phi}{\Phi_0})$$

Now, if one inserts fluxes ϕ_x and ϕ_y along both the directions, if we denote the modified Hamiltonian by $H_{\phi_x,\phi_y}(k_x, k_y)$, we see that

$$H_{\phi_x,\phi_y}(k_x, k_y) = H_{0,0}(k_x, k_y)$$
$$\text{but with } k_x = \frac{2\pi}{L_x}(n_x - \frac{\phi_x}{\Phi_0})$$
$$\text{and } k_y = \frac{2\pi}{L_y}(n_y - \frac{\phi_y}{\Phi_0})$$

Clearly, the spectrum is unchanged if the ϕ_x and ϕ_y are integer multiples of Φ_0 (and the eigenvectors are the same as well, but now they correspond to shifted energies). However, for other values of the fluxes, the spectrum undergoes a change. Additionally, the crystal momentum k_x drifts as ϕ_x is increased: $k_x \to k_x - \frac{2\pi}{L_x}\frac{\phi_x}{\Phi_0}$, and similarly for k_y.

Such an analysis is useful in numerically confirming the topological character of a model. In a cylindrical geometry, for example when periodic boundary condition is imposed only along the $\hat{x}$ direction, we get 'edge modes' that go from one band to another. The insertion of a flux along the $\hat{y}$ direction then results in what is known as 'spectral flow', a signature of topological non-triviality in an open system.

1.6 Outline of this Thesis

The connections between localization properties of Wannier functions and projection operators that are strictly local are explored in Chapters 2 and 3. Specifically, in Chapter 2,

we show that if the projection operator onto a subspace of the single-particle Hilbert space is strictly-local hopping on a 1d lattice, then it must follow that there exists an orthogonal basis of compactly supported wavefunctions spanning the subspace. This is phrased in terms of Wannier functions, and their generalization in the absence of lattice translational invariance. Generalization to higher dimensional systems is proposed, and it is shown that if an orthogonal basis of compact wavefunctions spans a subspace, then the corresponding projection operator must be Chern trivial, by virtue of having a vanishing topological index.

In Chapter 3, we sharpen these results and show that in one dimensional systems, strict locality of projection operators is equivalent to the existence of compactly-supported Wannier functions. Connections to a variant, called compactly-supported Wannier-type functions and to maximally-localized Wannier functions are presented.

In Chapter 4, the results from the two preceding chapters are used in order to show that if a Hamiltonian only has flat bands, then all its bands must be topologically trivial. Specifically, we show that the Chern number of each band must be zero.

In Chapter 5, which can be read independently of the rest of the chapters, we present preliminary results pertaining to a universal delocalization transition in chiral Floquet topological insulators.

CHAPTER 2

Compactly Supported Wannier functions and Strictly Local Projectors

---

This chapter was originally published as Ref. [10][1]:

Pratik Sathe, Fenner Harper, and Rahul Roy. "Compactly supported Wannier functions and strictly local projectors" Journal of Physics A: Mathematical and Theoretical 54.33 (2021): 335302.

2.1 Abstract

Wannier functions that are maximally localized help in understanding many properties of crystalline materials. In the absence of topological obstructions, they are at least exponentially localized. In some cases such as flat-band Hamiltonians, it is possible to construct Wannier functions that are even more localized, so that they are compactly supported thus having zero support outside their corresponding locations. Under what general conditions is it possible to construct compactly supported Wannier functions? We answer this question in this paper. Specifically, we show that in 1d non-interacting tight-binding models, strict locality of the projection operator is a necessary and sufficient condition for a subspace to be spanned by a compactly supported orthogonal basis, independent of lattice translation symmetry. For any strictly local projector, we provide a procedure for obtaining such a

[1]The following acknowledgement appeared in the original manuscript: We thank A. Culver, D. Reiss, X. Liu, A. Brown and L. Lindwasser for useful discussions and comments. P.S., F.H., and R.R. acknowledge support from the NSF under CAREER Grant No. DMR-1455368, and from the Mani L. Bhaumik Institute for Theoretical Physics.

basis. For higher dimensional systems, we discuss some additional conditions under which an occupied subspace is spanned by a compactly supported orthogonal basis, and show that the corresponding projectors are topologically trivial in many cases. We also show that a projector in arbitrary dimensions is strictly local if and only if for any chosen axis, its image is spanned by hybrid Wannier functions that are compactly supported along that axis.

2.2 Introduction

Extended Bloch wavefunctions and localized Wannier functions [11] are two common choices of basis vectors for a Bloch band. Localized Wannier functions have applications in a number of fields, including the modern theory of polarization [12], orbital magnetization [13], quantum transport [14] and tight binding interpolation [5, 15]. Consequently, conditions required for the existence of localized Wannier functions have been investigated extensively. Isolated bands of 1d inversion symmetric systems are always spanned by exponentially localized Wannier functions as shown by Kohn [16]. The localization properties of Wannier functions can often be inferred from the localization properties of the associated band projector. For instance, band projectors often possess real space matrix elements which decay exponentially [17], leading to generalizations [18, 19] of Kohn's result.

Because of the importance of obtaining localized Wannier functions, there has been significant interest in obtaining Wannier functions that are as localized as possible. A popular variational approach seeks localized Wannier functions by numerically minimizing the second moment of the Wannier functions around their centers [20]. It has been shown that maximally localized Wannier functions decay exponentially (or faster) in 1d systems, with extensions proved for higher dimensional systems in the absence of topological obstructions [21].

A related, and sometimes more extreme form of wavefunction localization is compact support or strict localization in lattice models, wherein a wavefunction has non-zero support only over a finite set of orbitals of the lattice. Wavefunctions that are linear combinations of a finite set of orbitals bear a close analogy to Boys orbitals [22] which are studied in chemistry in

the context of chemical bonding and other applications. The wavefunctions of Bloch electrons deep under the Fermi level are also expected to correspond to compactly supported (CS) Wannier functions. Additionally, in some applications, it is useful to approximate highly localized Wannier functions by CS wavefunctions [23, 24, 25, 26].

Non-orthogonal bases consisting of CS wavefunctions, also known as CS Wannier-type functions have also received significant attention [27, 28, 29]. CS Wannier-type functions exist most commonly in strictly local (SL) flat-band Hamiltonians [30] in the context of which they are also known as compact localized states (CLSs). Such bases help in understanding a number of many-body quantum phenomena (see [31] for a review), including novel superconducting phases in multi-layer twisted graphene [32, 33]. CLSs have been used to classify and construct flat-band Hamiltonians [34, 35, 36]. Models so constructed are often made interacting, in order to study interesting many-body quantum phenomena arising in such contexts. For example, orthogonal CLSs have been used to construct models with many-body localized states [37] and quantum scar states [38] in flat-band systems. Orthogonal CLSs that span an entire flat band are precisely CS Wannier functions of the flat band. Indeed, the conditions associated with the existence of orthogonal CLSs spanning flat bands and of CS Wannier functions in systems without flat bands are closely related.

Yet another variant of Wannier functions are hybrid Wannier functions [39], that are localized and Wannier-like along one direction, and Bloch wave-like along the other directions. Localized hybrid Wannier functions have a number of applications, including the study of twisted bilayer graphene [40], and characterization of static [41, 42, 43] and Floquet topological insulators [44]. Similar to CS Wannier functions, a set of hybrid Wannier functions that are CS along one of the axes can span a band in some cases. We refer to such functions as CS hybrid Wannier functions.

While conditions associated with the existence of exponentially localized Wannier functions, and of CLSs have been studied, those required for the existence of CS Wannier functions and CS hybrid Wannier functions remain unexplored. These considerations motivate us to pose the following questions: In a tight-binding lattice model, given an arbitrary set

of occupied states, is there a way of determining whether their span possesses a CS Wannier basis? Analogously, in the absence of lattice translational invariance, under what conditions can the occupied subspace be spanned by an orthogonal basis of CS wavefunctions? We call such a basis a compactly supported orthogonal basis or a CSOB in short. We show that the localization properties of the associated projector has a direct bearing on these questions. For 1d systems, we answer this question completely, showing an equivalence between strict locality of an orthogonal basis and strict locality of the associated orthogonal projector. For higher dimensional systems, we obtain necessary and sufficient conditions for the existence of such a basis, as well as for CS hybrid Wannier functions. Our main results are summarized below.

Main Result. *For an arbitrary subspace spanned by single particle states in a non-interacting tight-binding model, independent of translational invariance, the following statements are true.*

(1) In 1d systems, an orthogonal basis consisting of compactly supported wavefunctions (i.e. a CSOB) spanning the subspace exists iff. the associated orthogonal projector is strictly local.

(2) For a lattice in d dimensions, compactly supported hybrid Wannier functions localized along an axis exist for any choice (out of d possible choices) of the localization axis if and only if the associated band projector is strictly local.

(3) For arbitrary dimensional lattices, if the space is spanned by a CSOB, then the projector onto it is strictly local. If a projector is of a nearest neighbor form (or reducible to this form via a change of primitive vectors, or unit cell enlargement), its span possesses a CSOB.

Localization properties of Wannier functions are closely related to the associated bands' topology [45, 46, 47, 48]. Indeed, for many classes of Hamiltonians, exponentially localized Wannier functions exist iff. the band is topologically trivial. Hence, in addition to the Main

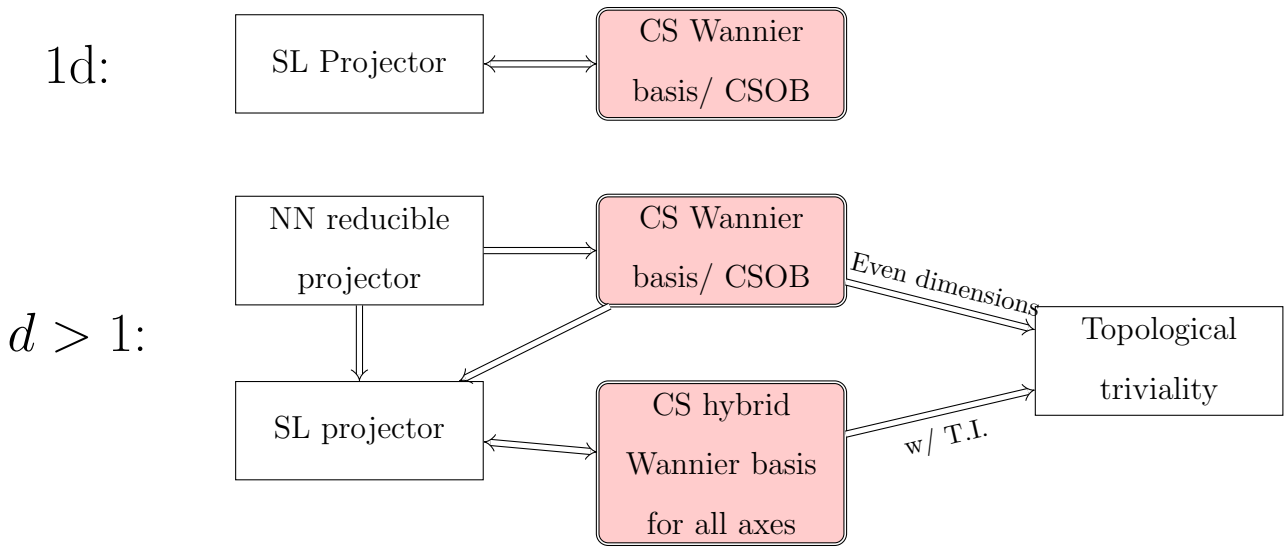

Figure 2.1: Summary of the main results of this paper. All the statements hold true independent of whether the the system is translationally invariant (TI), except for the statement connecting the existence of CS hybrid Wannier basis for all axes to topological triviality.

Result, we also discuss topological properties of projectors associated with CSOBs and CS hybrid Wannier functions. In particular, using existing results from the literature, we show that all translationally invariant SL projectors in $d > 1$ are topologically trivial. Moreover, for even dimensional systems, we show that if a space is spanned by a CSOB, then it is necessarily Chern trivial, irrespective of translational invariance. We also show that if CS hybrid Wannier functions exist for any choice of the localization axis, the corresponding projector is *necessarily* topologically trivial for a translationally invariant system. This contrasts with exponentially localized hybrid Wannier functions, which can be constructed for any band regardless of its topological properties [20, 49]. We summarize the Main Results as well as these extra results in figure 2.1.

We note that each of the three parts of the Main Result consists of a necessary condition and a sufficient condition for the existence of a CSOB (or a CS hybrid Wannier functions). The necessary condition in all cases is that the projector should be SL, and is straightforward to prove. Proving the sufficient condition is harder, and hence a significant portion of this paper deals with this aspect. Since the sufficient conditions are different for 1d and higher

dimensions, these two cases are discussed separately. In section 2.3, we discuss the notation and definitions used in this paper, and prove the necessary direction from the Main Result. In addition, we also discuss the relationship between CLSs and CS Wanner-type functions, and show how to obtain non-orthogonal CLSs corresponding to any SL projector. In section 2.4, we prove by construction for 1d systems, that the image of any SL projector is spanned by a CSOB (or a CS Wannier basis if translationally invariant). Similarly, in section 2.5, we prove the sufficient part of points (2) and (3) of the Main Result. In addition we prove the extra results pertaining to topological triviality mentioned above. We conclude the paper with section 2.6.

2.3 Preliminary discussion

In this section, we discuss some basic definitions and notation used in this paper as well as the connections between compact localized states that arise in flat-band systems, and compactly supported Wannier-functions associated with strictly local projectors. We also prove the sufficient part of the Main Result. At the end of this section, we provide a simple method for constructing strictly local projectors in 1d and 2d.

2.3.1 Notation

We consider d dimensional tight-binding models, with any (single particle) operator being represented by a matrix with rows and columns labeled by pairs of indices $(\vec{r}, i)$, with $\vec{r} \in \mathbb{Z}^d$ denoting a Bravais lattice site position, and $i \in \{1, \ldots, n_{\vec{r}}\}$ denoting the orbital index (which subsumes all quantum numbers, including spin quantum numbers if present). Our conclusions remain valid for finite lattices as well, for which we replace $\mathbb{Z}^d$ by an appropriate set of integer tuples. We denote a position basis vector by $|\vec{r}, i\rangle$, and refer to it as orbital i at site $\vec{r}$.

Henceforth, we use the terms site and cell interchangeably. Specifically, a cell at location $\vec{r}$ will mean the same as the site at location $\vec{r}$. By a supercell representation of the lattice,

we mean a labelling scheme in which multiple sites in the original lattice representation are grouped together to form a new site. This reversible transformation involves relabeling of quantum numbers, as described in section 2.4.3.

We denote the Hilbert space associated with all the orbitals at cell $\vec{r}$ by $\mathcal{H}^{\vec{r}}$, and the total Hilbert space by $\mathcal{H}_{total}$. We note that

$$\mathcal{H}_{total} = \bigoplus_{\vec{r} \in \mathbb{Z}^d} \mathcal{H}^{\vec{r}}, \tag{2.1}$$

with $\oplus$ denoting a direct sum. In general, the number of orbitals at cell $\vec{r}$, denoted by $n_{\vec{r}}$, may be different for different cells, and our conclusions do not depend on them being equal. For notational simplicity, we assume without loss of generality that $n_{\vec{r}} = n$ is independent of the location. For systems with translational invariance, this condition is automatically satisfied. Additionally we find it convenient to rewrite $\mathcal{H}_{total}$ as,

$$\mathcal{H}_{total} = \mathbb{Z}^{\otimes d} \otimes \mathcal{H}, \tag{2.2}$$

where $\mathcal{H}$ denotes the n-dimensional orbital space. We refer to any orthonormal basis vectors of $\mathcal{H}$ as orbitals.

In this paper, we consider orthogonal projection operators, i.e. operators $P : \mathcal{H}_{total} \to \mathcal{H}_{total}$, that satisfy $P^2 = P^\dagger = P$, with $(.)^\dagger$ denoting the matrix conjugate transposition operation. We define a strictly local (SL) projection operator to be one which has a finite upper bound on the extent of its hopping elements:

Definition 1. *An orthogonal projection operator $P : \mathcal{H}_{total} \to \mathcal{H}_{total}$ is said to be strictly local if there exists a finite integer b such that $\langle \vec{r}, i| P |\vec{r}\,', j\rangle = 0 \; \forall \; |\vec{r} - \vec{r}\,'| > b$ and $i, j \in \{1, \ldots, n\}$. The maximum hopping distance of P is the smallest integer b which satisfies this condition.*

A wavefunction which has non-zero support only on a finite number of sites is said to be compactly supported. Specifically,

Definition 2. *A wavefunction is compactly supported iff. there exists a finite integer r, such that it has zero support outside a ball of radius r. The smallest integer value of r is called*

the size of the wavefunction. A basis is said to be a compactly supported orthogonal basis (CSOB) of (a finite) size R iff. every constituent wavefunction is compactly supported and has a size of at most R.

In the context of finite sized lattices, a basis is considered to be compactly supported only if R is smaller than the size of the lattice. Similarly, only those projection operators that have a maximum hopping distance smaller than the size of the lattice will be considered to be strictly local.

For an SL projector P, the following notation will be used in the paper:

1. Let $\Pi^P_{\vec{r}}$ denote the set of vectors obtained by operating P on all the orbitals at cell $\vec{r}$. That is,

$$\Pi^P_{\vec{r}} \coloneqq \{P\,|\vec{r}, i\rangle : i \in 1, \ldots, n\}. \tag{2.3}$$

   The choice of which orbital basis is chosen while calculating $\Pi^P_{\vec{r}}$ will be specified, or will be clear from the context.

2. Let $\mathcal{H}^P_{\vec{r}} \subset \mathcal{H}_{total}$ denote the space spanned by $\Pi^P_{\vec{r}}$.

3. Let $\mathcal{H}^P \equiv \cup_{\vec{r}\in\mathbb{Z}^d}\mathcal{H}^P_{\vec{r}}$ denote the image of P.

4. Let $\widetilde{\Pi}^P_{\vec{r}}$ denote an orthonormal basis of $\mathcal{H}^P_{\vec{r}}$. ($\widetilde{\Pi}^P_{\vec{r}}$ can be obtained by applying the Gram-Schmidt orthogonalization procedure on $\Pi^P_{\vec{r}}$). We note that since P is SL, all wavefunctions in the sets $\widetilde{\Pi}^P_{\vec{r}}$ and $\Pi^P_{\vec{r}}$ are compactly supported.

5. Let $P_{\vec{r}}$ denote the orthogonal projection operator onto $\mathcal{H}^P_{\vec{r}}$. $P_{\vec{r}}$ can be expressed as

$$P_{\vec{r}} = \sum_{|\chi\rangle\in\widetilde{\Pi}^P_{\vec{r}}} |\chi\rangle\langle\chi|\,. \tag{2.4}$$

2.3.2 Compactly Supported Wannier functions and Compact Localized States

While the primary object of interest of this paper is compactly supported (CS) Wannier functions, a closely related type of basis consists of CS Wannier-type functions, which exist prominently in flat-band Hamiltonians. As we will show later, CS Wannier functions'

existence is related to the strict localization of the associated projector. While flat-band projectors need not be SL projectors and vice versa, both their images are spanned by CS Wannier-type functions and in some cases CS Wannier functions as well. In this section, we will discuss these two types of bases for flat-band Hamiltonians and SL projectors.

Let us first discuss Wannier-type functions, which are in a sense a generalization of Wannier functions. Similar to Wannier functions, Wannier-type functions consist of a set of wavefunctions localized at a cell, and all their lattice translates, and span a band or a set of bands. However, unlike Wannier functions which are by definition orthogonal, Wannier-type functions can be non-orthogonal, or even linearly dependent. Consequently, a set of m bands may be spanned by $l \geq m$ *flavors* of Wannier-type functions, whereas exactly m flavors of Wannier functions span m bands. Wannier-type functions that are CS [28, 29] are desirable in certain applications [24]. Importantly, the existence of non-orthogonal CS Wannier-type functions does not in general imply the existence of CS Wannier functions.

CS Wannier-type functions exist most notably as bases spanning flat bands in flat-band Hamiltonians [30, 31]. Such functions corresponding to a flat band are also Hamiltonian eigenstates, and are also referred to as compact localized states (CLSs). In most flat-band Hamiltonians, the CLSs are not mutually orthogonal, and can even by linearly dependent. Indeed, in the presence of band touching, CLSs may not even span the entire flat band [50]. However, it is always possible to modify such models so that they have orthogonal CLSs spanning a flat band in an enlarged unit cell. This can be done by choosing a subset of CLSs, comprising regularly spaced CLSs with no physical overlap on the lattice [37, 38]. While such a set does not span a full band in a primitive cell representation, they always span an entire flat band in an appropriately enlarged unit cell. Hence, they can also be referred to as CS Wannier functions. In some cases, flat-band Hamiltonians possess orthogonal CLSs naturally, without needing unit cell enlargement. Some popular examples from the literature with such bases are discussed in sections 2.4 and 2.5. It is possible to create many more examples of flat-band Hamiltonians with orthogonal CLSs, by constructing nearest neighbor projectors as done in section 2.3.4.

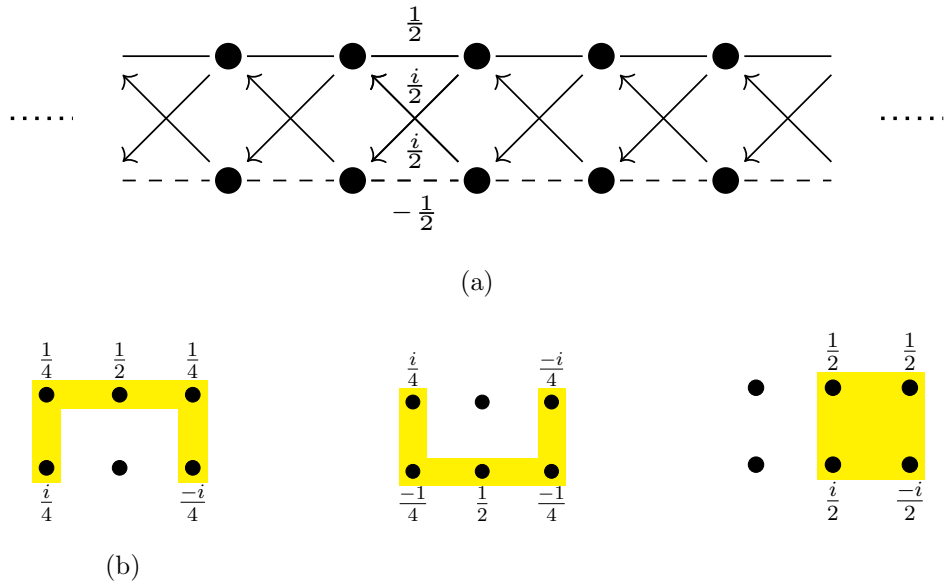

Figure 2.2: The real space connectivity of the projector from equation (2.5) is shown in (a). The upper and lower array of dots represents the two sublattices A and B respectively. An on-site potential of $\frac{1}{2}$ is present for each orbital. Two flavors of non-orthogonal CLSs, i.e. CS Wannier-type functions spanning the image of the projector are shown in (b) and (c). An orthogonal CLS, i.e. a CS Wannier function is shown in (d).

While the term CLSs is commonly used only in the context of flat-band Hamiltonians, the distinction between orthogonal CLSs and CS Wannier functions is unnecessary for our purpose. Indeed, it is always possible to deform a band's energy without changing the subspace corresponding to it. Expressing a Hamiltonian as $H(\vec{k}) = \sum_i E_i(\vec{k})P_i(\vec{k})$, where P_i's are the band projectors, one can modify a band's energy function to 'flatten' the corresponding band [51] without modifying the band projectors, and vice versa. Such an operation does not affect the Wannier and Wannier-type functions spanning that band, since they are associated with the band subspace, and have no dependence on the band dispersion. Thus, (non-)orthogonal CLSs are a special type of CS Wannier(-type) functions. As a result, the conditions associated with the existence of orthogonal CLSs spanning a flat band, and those associated with the existence of CS Wannier functions for any band which may or may not be flat, are equivalent to each other.

These arguments also highlight that the properties of the band projector are connected to the existence of CS Wannier functions or orthogonal CLSs spanning a band. Indeed, as we will show later in the paper, the existence of CS Wannier functions is tied to the band projector being SL. Like SL flat-band Hamiltonians, SL projectors also possess CS Wannier-type functions. In 1d, they have the additional property that their images are spanned by CS Wannier functions. Regardless of the dimension, non-orthogonal CLSs can be constructed straightforwardly for any SL projector. To that end, we first note that for any lattice vector $|\vec{r}, \alpha\rangle$, since $P^2 = P$,

$$P(P\,|\vec{r}, \alpha\rangle) = (P\,|\vec{r}, \alpha\rangle).$$

Thus, if $P\,|\vec{r}, \alpha\rangle \neq 0$, it is an eigenvector of P with eigenvalue 1. Since P is strictly local, $P\,|\vec{r}, \alpha\rangle$ is compactly supported. Additionally, if P is translationally invariant, then the set $\{P\,|\vec{r}, \alpha\rangle\,|\vec{r} \in \mathbb{Z}^n\}$ is one flavor of CLS. If there are l number of α's for which $P\,|\vec{x}, \alpha\rangle \neq 0$, we obtain l number of CLSs which together span the band(s) corresponding to P. In general, without further processing, none of these wavefunctions are guaranteed to be mutually orthogonal. Moreover, it is possible for two wavefunctions within the same flavor of CLSs to be non-orthogonal to each other.

The existence of CS Wannier-type functions for SL projectors can be understood as a destructive interference phenomenon, similar to CLS in flat-band Hamiltonians. This is based on the rather simple observation that any SL projector can also be regarded as a flat-band Hamiltonian with two flat bands. The CLSs for the band with energy 1 are exactly the CS Wannier-type functions spanning the SL projector's image. Although gapped flat-bands are always spanned by a set of CLSs, they need not be orthogonal CLSs. Indeed, it is impossible to find orthogonal CLSs spanning a flat-band for many flat-band Hamiltonians. Hence, interpreting an SL projector as a flat-band Hamiltonian does not directly help us to conclude that CS Wannier functions spanning it exist. Especially in 1d, this is a reflection of the fact that SL projectors are a subset of flat-band projectors. For some explicit examples of flat-band projectors that are not SL, see section 3 in reference [30].

We illustrate many of these points using a simple example of a 1d projector [see fig-

ure 2.2(a)], given by

$$P(k) = \frac{1}{2}\begin{pmatrix} 1+\cos k & \sin k \\ \sin k & 1-\cos k \end{pmatrix}. \tag{2.5}$$

We can construct two sets of CLSs by operating the projector on each A and B sublattice orbital [figures 2.2(b) and 2.2(c) show one CLS each from these two sets]. Each set of CLS is not only non-orthogonal, but also linearly dependent, so that neither of the two sets span the image of the projector individually. However, both sets of CLSs considered together span the image of the projector, and hence form two flavors of CS Wannier-type functions. As we will show in the next section, one can always find CS Wannier functions spanning the image of any 1d SL projector. For the example under consideration, this consists of the CLS shown in figure 2.2(d), and all its lattice translates. It can be easily verified that this set is orthogonal, and hence spans the image of P. While it is possible to also obtain these orthogonal CLSs using only destructive interference-based observations, it does not follow immediately that this can be done for projectors with more complicated connectivity, higher number of dimensions (for example, see (2.24)) or in the absence of lattice translation symmetry.

Thus, while it is clear that for any SL projector, one can construct non-orthogonal CLSs, it is far less obvious (and possibly untrue for $d > 1$) that one can construct orthogonal CLSs. One of the objectives of this paper is to present a systematic procedure for the construction of such orthogonal CLSs/CS Wannier functions, and the identification of conditions required for the existence of such functions.

Before proceeding, we note that for non-translationally invariant SL projectors, although CLSs as defined above don't exist, we may define an analogous basis. Specifically, the set $\{P\,|\vec{r},\alpha\rangle\,|\vec{r} \in \mathbb{Z}^d, \alpha = 1,\ldots,n\}$ is a non-orthogonal basis of the image of P, and consists of CS wavefunctions.

2.3.3 Compact Basis and Strictly Local Projectors

The primary focus of this paper is the identification of necessary and sufficient conditions for the existence of a compactly supported orthogonal basis (CSOB) corresponding to a subspace. In this section, we prove the necessary condition for all dimensions: the strict locality of the associated orthogonal projector.

Proving that the span of a CSOB always corresponds to an SL projector is straightforward. Let a set S be a CSOB of size R on a d-dimensional lattice. Let P be the orthogonal projector onto the space spanned by S. Then for any two locations $z, z' \in \mathbb{Z}^d$ such that $|z - z'| > R$, and orbitals α, β, we note that

$$\begin{aligned} \langle z, \alpha | \, P \, | z', \beta \rangle &= \sum_{|\chi\rangle \in S} \langle z, \alpha | \chi \rangle \, \langle \chi | z', \beta \rangle \\ &= 0. \end{aligned}$$

In other words, the maximum hopping distance of P is at most R. By definition, P is then an SL projector.

Following a similar reasoning, we can easily show that if an orthogonal basis consists of wavefunctions each of which are compactly supported along only one axis, then the corresponding projector is strictly local along that axis. This implies that if CS hybrid Wannier functions exist for all choices of the localized axis, then the projector is SL (along all directions). This proves the necessary part of point (2) of the Main Result.

2.3.4 A Simple Method for Constructing SL Projectors

In this section, we present a simple method for constructing translationally invariant SL projectors in one and two dimensions. We note that while one may use the equivalence that we have proven for 1d and construct SL projectors from a compactly supported translationally invariant orthogonal basis, such a method is not entirely straightforward to implement since one first needs to construct a translationally invariant orthogonal basis which is compactly supported and of an appropriate size. A much simpler alternative inspired by Clifford alge-

bras can however be used, wherein an NN projector can be constructed by first obtaining what we call an NN *flat* Hamiltonian. Such a flat Hamiltonian is an example of a flat-band Hamiltonian with all bands being flat and with energies ± 1. We obtain the projector P onto the -1 eigenspace of H, and note that the since $H = \mathbb{1} - 2P$, P is guaranteed to be a nearest neighbor projector. We start by constructing an example of a 1d NN flat-band Hamiltonian in subsection 2.3.4.1, followed by a construction of a 2d NN flat band Hamiltonian in subsection 2.3.4.2. While we explicitly describe the procedure only for strictly local projectors in 1 and 2 dimensional lattices, this method can be straightforwardly generalized to higher dimensions, and larger hopping distances. Although there exist SL projectors that cannot be generated using this method, it can still be used to create many interesting examples of SL projectors.

2.3.4.1 1d Strictly Local Projectors

It is convenient to utilize the Fourier space representation since we only consider translationally invariant projectors. First, we construct a flat NN Hamiltonian H, from which we will extract the desired NN projector. For H to be an NN Hamiltonian, its Fourier space representation must be of the form:

$$H(k) = C_+ e^{ik} + C_0 + C_- e^{-ik},$$

with C_+, C_- and C_0 being $n \times n$ matrices which are constrained by the equations $H(k)^\dagger = H(k)$, and $H(k)^2 = 1$. For simplicity, we choose H to possesses two bands. Consequently, $H(k)$ can be expressed in terms of the identity matrix $1_{2\times 2}$ and the two-dimensional Pauli matrices $\{\sigma_i\}$ as

$$H(k) = a_0(k) 1_{2\times 2} + \sum_{i=1}^{3} a_i(k)\sigma_i.$$

Since $\{\sigma_i, \sigma_j\} = 2\delta_{ij}$, the condition that $H(k)$ is flat translates to $\sum_{\mu=0}^{3} a_\mu^2(k) = 1$ and $a_i a_0 = 0$. In order to obtain interesting solutions, we choose $a_0 = 0$. Together with $H^\dagger = H$,

this implies that

$$\begin{aligned} a_1(k)^2 + a_2(k)^2 + a_3(k)^2 = 1; \\ a_i(k)^* = a_i(k). \end{aligned} \tag{2.6}$$

Since the Hamiltonian is of an NN form, each $a_i(k)$ is expressible as

$$a_i(k) = c_i X + c_i^* X^{-1} + d_i,$$

with complex c_i's, real d_i's, and $X \coloneqq e^{ik}$. Conditions (2.6) imply that

$$\begin{aligned} \sum_i c_i^2 = 0 \\ \sum_i c_i d_i = 0 \\ \sum_i 2|c_i|^2 + d_i^2 = 1. \end{aligned} \tag{2.7}$$

Solutions to these equations can be used to construct various flat Hamiltonians and projectors. A trivial example is one with $c_i = 0$, and $d_1 = 0$, $d_2 = 0$ and $d_3 = 1$, which corresponds to

$$H(k) \equiv \begin{pmatrix} 1 & 0 \\ 0 & -1 \end{pmatrix},$$
$$\text{and } P(k) = \frac{1_{2\times 2} - H(k)}{2} \equiv \begin{pmatrix} 0 & 0 \\ 0 & 1 \end{pmatrix}.$$

Less trivial solutions of constraints (2.7) can be used to construct more interesting projectors. For example, consider the following parameters:

$$c_1 = \frac{1}{3},\ c_2 = \frac{1}{3}e^{\frac{2\pi}{3}i},\ c_3 = \frac{1}{3}e^{\frac{4\pi}{3}i},\ d_i = \frac{1}{3}.$$

The corresponding Hamiltonian is given by

$$H(k) = \frac{1}{3}\begin{pmatrix} (1 + 2\cos\big(k + \frac{4\pi}{3}\big)) & (1 + 2\cos k) - i(1 + 2\cos\big(k + \frac{2\pi}{3}\big)) \\ (1 + 2\cos k) + i(1 + 2\cos\big(k + \frac{2\pi}{3}\big)) & -(1 + 2\cos\big(k + \frac{4\pi}{3}\big)) \end{pmatrix}. \tag{2.8}$$

The projector $P(k)$ onto the -1 eigenspace can be obained by using the equation $P(k) = (1_{2\times 2} - H(k))/2$. Since $P(k)$ has matrix elements which are Laurent polynomials in e^{ik}, it is an SL projector.

Having obtained an SL projector, one can use it to construct Hamiltonians which have CS Wannier functions, with any choice of the band energy (flat, or otherwise). For example one may construct a strictly local flat-band Hamiltonian, with the flat band possessing CS Wannier functions, i.e. orthogonal compact localized states (CLSs). To that end, if $P(k)$ is an SL projector obtained using the method above, we can choose it to correspond to some constant energy, say E. The band associated with the remaining subspace, i.e. the image of $1 - P(k)$, can be chosen to have a dispersion $E(k)$, which should be chosen to be a real function expressible as a Laurent polynomial in e^{ik}. We can also add more bands to our Hamiltonian by constructing another Hermitian matrix $H'(k)$ with entries which are Laurent polynomials in e^{ik}. Arbitrary examples of $H'(k)$ and $E(k)$ satisfying the constraints mentioned above can be easily constructed. Putting it all together, we obtain a strictly local flat band Hamiltonian $\mathbb{H}(k)$ using

$$\mathbb{H}(k) = H'(k) \oplus [E(k)(1 - P(k)) + EP(k)]. \tag{2.9}$$

In order to construct an SL flat band Hamiltonian with a larger number of flat bands, one can use the method above to create multiple SL $P(k)$'s and assign a constant energy to each projector. Specifically, we may construct multiple flat band Hamiltonians using (2.9), and take their direct sum to construct a flat-band Hamiltonian with a larger number of flat bands. Alternatively, one may use the higher dimensional Dirac (or gamma) matrices for an analogous construction. To illustrate the latter procedure, we show how this can be used to construct nearest-neighbor projectors on 2d lattices in the next subsection.

2.3.4.2 2d Strictly Local Projectors

Similar to the previous subsection, we start with the construction of a flat Hamiltonian H. Here, we choose H to have four bands in order to demonstrate the use of higher dimensional

generators of the Clifford algebra. Hence, we express the flat Hamiltonian in terms of Dirac matrices Γ^μ, instead of Pauli matrices, as follows:

$$H(\vec{k}) = \sum_{\mu=0}^{3} a_\mu(\vec{k})\Gamma^\mu;$$

$$\text{with } \Gamma^0 = \gamma^0 = \begin{pmatrix} \mathbb{1}_2 & 0 \\ 0 & -\mathbb{1}_2 \end{pmatrix},$$

$$\Gamma^1 = i\gamma^1 = i \begin{pmatrix} 0 & \sigma^x \\ -\sigma^x & 0 \end{pmatrix},$$

$$\Gamma^2 = i\gamma^2 = i \begin{pmatrix} 0 & \sigma^y \\ -\sigma^y & 0 \end{pmatrix},$$

$$\text{and } \Gamma^3 = i\gamma^3 = i \begin{pmatrix} 0 & \sigma^z \\ -\sigma^z & 0 \end{pmatrix}.$$

The Dirac matrices satisfy the anti-commutation relations $\{\Gamma^\mu, \Gamma^\nu\} = 2\delta^{\mu\nu}$ and $\Gamma^{\mu\dagger} = \Gamma^\mu$. For $H(\vec{k})$ to be a nearest-neighbor Hamiltonian, the parameters $a_i(\vec{k})$ must be of the form

$$\begin{aligned} a_i(\vec{k}) = {} & c_{ix}X + c_{ix}^* X^{-1} + c_{iy}Y + c_{iy}^* Y^{-1} \\ & + c_{ixy}XY + c_{ixy}^* X^{-1}Y^{-1} \\ & + c_{-ixy}XY^{-1} + c_{-ixy}^* X^{-1}Y \\ & + d_i, \end{aligned} \tag{2.10}$$

with complex c's, real d's, and $X = e^{ik_x}$, $Y = e^{ik_y}$. $H(\vec{k})^2 = \mathbb{1}$ leads to the condition:

$$\sum_i a_i^2 = 1. \tag{2.11}$$

Equating the coefficients of all products of all powers of X and Y gives us the following conditions:

$$\sum 2(|c_{ix}|^2 + |c_{iy}|^2 + |c_{ixy}|^2 + |c_{-ixy}|^2) + d_i^2 = 1$$

$$\sum c_{iy}c_{-ixy} + c_{iy}^* c_{ixy} + c_{ix}d_i = 0$$

$$\sum c_{ix}c^*_{-ixy} + c^*_{ix}c_{ixy} + c_{iy}d_i = 0$$
$$\sum c^2_{ix} + 2c_{ixy}c_{-ixy} = 0$$
$$\sum c^2_{iy} + 2c_{ixy}c^*_{-ixy} = 0$$
$$\sum c_{ix}c_{iy} + c_{ixy}d_i = 0$$
$$\sum c_{ix}c^*_{iy} + c_{-ixy}d_i = 0$$
$$\sum c_{ix}c_{ixy} = 0$$
$$\sum c_{ix}c_{-ixy} = 0$$
$$\sum c_{iy}c_{ixy} = 0$$
$$\sum c_{iy}c^*_{-ixy} = 0$$
$$\sum c^2_{ixy} = 0$$
$$\sum c^2_{-ixy} = 0.$$

Any solution of these set of equations can used to create a projector. For example, choosing $c_{ixy} = c_{-ixy} = d_i = 0$, the following choice satisfies all the conditions:

μ	0	1	2	3
$c_{\mu x}$	0	0	$\frac{1}{2\sqrt{2}}$	$\frac{i}{2\sqrt{2}}$
$c_{\mu y}$	$\frac{1}{2\sqrt{2}}$	$\frac{i}{2\sqrt{2}}$	0	0

This corresponds to the Hamiltonian:

$$H(\vec{k}) = \frac{1}{2\sqrt{2}} \begin{pmatrix} Y + Y^{-1} & 0 & -(X - X^{-1}) & -(Y - Y^{-1}) + (X + X^{-1}) \\ 0 & Y + Y^{-1} & -(Y - Y^{-1}) - (X + X^{-1}) & (X - X^{-1}) \\ X - X^{-1} & (Y - Y^{-1}) - (X + X^{-1}) & -(Y + Y^{-1}) & 0 \\ (Y - Y^{-1}) & -(X - X^{-1}) & 0 & -(Y + Y^{-1}) \end{pmatrix}.$$

We obtain $P(\vec{k})$ by using $P(\vec{k}) = \frac{1_{4\times4} - H(\vec{k})}{2}$.

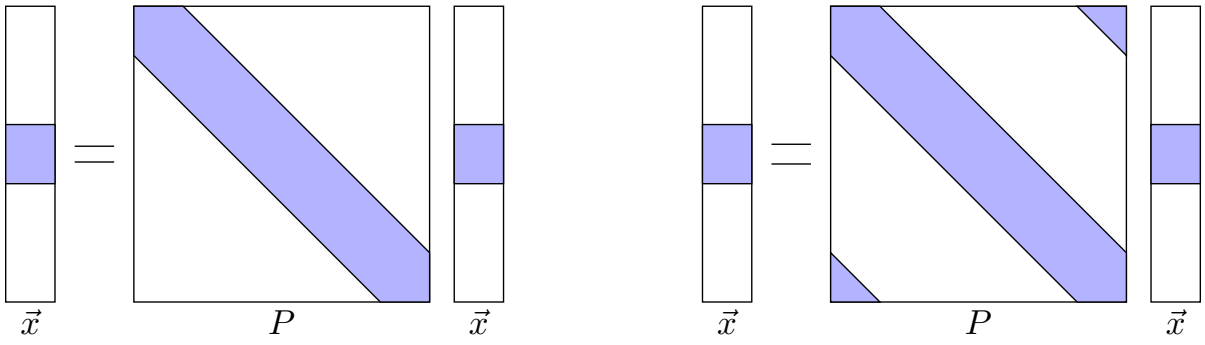

(a) (b)

Figure 2.3: (a) SL projectors on 1d lattices are represented by band diagonal projection matrices, and CS wavefunctions are represented by sparse vectors which have non-zero components only within a finite patch (shown in blue). The main result for 1d projectors implies an orthogonal projection operator is band diagonal if and only if it possess a CS orthogonal eigenbasis. (b) 1d SL projectors on finite periodic lattices are band diagonal, with appropriate modifications at the corners. In theorem 1, a relation between the band width of the projector and the number of non-zero elements of the basis vectors is provided.

2.4 Compactly Supported Orthogonal Basis: 1d lattices

As shown in section 2.3.3, it is straightforward to show that if a compactly supported orthogonal basis (CSOB) or a CS Wannier basis exists, then the corresponding projector is necessarily SL. In this section, we prove the converse, i.e. if a 1d projector is SL, then there exists a CSOB spanning its image, thereby completing the proof of part (1) of the Main Result. Specifically, we will show that

Theorem 1. *In 1d systems, the span of a set of occupied states possesses a compactly supported orthogonal basis (CSOB) if and only if the orthogonal projector onto the span is strictly local. Additionally:*

(1) If the maximum hopping distance of an SL projector is b, then there exists such a basis consisting of wavefunctions of a maximum size of $3b$ cells, irrespective of the presence of translational invariance.

(2) If the projector is translationally invariant, its image is spanned by a compactly supported Wannier basis in a size $2b$ supercell representation of the lattice.

We prove these statements through algorithmic constructions of CSOBs and CS Wannier functions, and provide bounds on their sizes on the way.

Let us briefly discuss some properties of SL projectors and outline the approach we will use in this section. We note that 1d SL projectors are band-diagonal matrices when expressed in the orbital basis (see figure 2.3). For example, every 1d nearest neighbor (NN) projector can be represented by a block tridiagonal matrix, with the block size being equal to the number of orbitals per cell. Although it is straightforward to obtain a CSOB for a block size of one, the corresponding statement is not obvious for larger block sizes. However, using the Gram-Schmidt orthogonalization procedure with an appropriate orthogonalization sequence, we show that it is always possible to obtain such an eigenbasis for any block size (see section 2.4.1). If the projector is also translationally invariant, i.e. with repeating blocks in the matrix representation, the basis can be chosen to be a Wannier basis in a supercell representation (see section 2.4.2). We then extend these results to all 1d SL projectors, since they can be represented as NN projectors using supercell representations (see section 2.4.3). In terms of matrices, this is equivalent to expressing any band diagonal matrix as a block-tridiagonal matrix by grouping together the original blocks into appropriate larger blocks. In this sense, the problem of obtaining a CSOB for any SL projector is equivalent to the problem of obtaining one for an NN projector.

While a number of model Hamiltonian systems possessing CS Wannier functions and orthogonal CLSs have been studied in the literature, to our knowledge, this is the first time that the connection of such systems with the strict localization of the corresponding projection operator has been explicitly established. Most examples from the literature with CS Wannier functions involve flat-band Hamiltonians defined on the Creutz ladder [52], the sawtooth lattice [37, 38] and the diamond lattice [53]. Here, we briefly discuss the Creutz lattice, which has been extensively studied both theoretically [54, 55, 56] and experimentally [57, 58]. As noted in [56], for one choice of parameters (see figure 2.4), the Creutz

ladder has two exactly flat bands of energies $\pm 2t$, each of which is spanned by CS Wannier functions. The corresponding Hamiltonian in k-space is given by:

$$H(k) = 2t \begin{pmatrix} \sin k & \cos k \\ \cos k & -\sin k \end{pmatrix}. \tag{2.12}$$

As mentioned in section 2.3.2, SL flat-band Hamiltonians possess some destructive interference properties, which constrain the movement of initially localized particles. For example, in the system under consideration, a particle initially localized on an A orbital cannot diffuse to a B orbital located more than a hop away (see figure 2 and related discussion in reference [56]). Based on this observation, one can obtain orthogonal CLSs, or equivalently, CS Wannier functions for the two bands of this Hamiltonian. The Wannier functions (labeled by $\pm$ for the two bands) localized at cell z are given by:

$$|W_\pm\rangle = \frac{1}{2}\left(\pm i\,|z, A\rangle \pm |z, B\rangle + |z+1, A\rangle + i\,|z+1, B\rangle\right).$$

In accordance with the predictions of our paper, the band projectors onto the two bands are SL, and are given by

$$P_\pm(k) = \frac{1}{2} \begin{pmatrix} 1 \pm \sin k & \pm \cos k \\ \pm \cos k & 1 \mp \sin k \end{pmatrix}. \tag{2.13}$$

Indeed, using the techniques developed in the next subsection, one can obtain these CS Wannier functions from the expressions for the projectors $P_\pm(k)$.

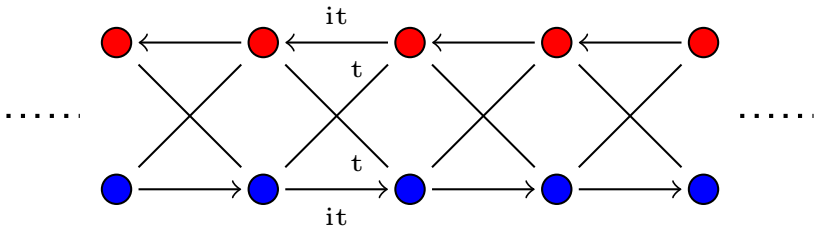

Figure 2.4: Example of a popular model with CS Wannier functions: the Creutz ladder. The hopping amplitudes result in two flat bands and CS Wannier functions. The A (B) orbitals are shown in red (blue). The hopping amplitudes are shown next to the arrows.

While most popular flat-band Hamiltonians do not possess CS Wannier functions, i.e. a set of orthogonal CLSs spanning the flat band, as discussed in section 2.3.2, it is possible to construct models with orthogonal CLSs by enlargement of the unit cell of any known flat-band model. This was done for example in [37] and [38] to obtain CS Wannier functions spanning a flat band in the sawtooth lattice.

Although most of the examples from the literature involve flat bands, CS Wannier functions and SL projectors can correspond to dispersive bands. Such an example is provided in Appendix 2.A, along with a discussion of the CS Wannier functions obtained using the algorithm from the next subsection.

2.4.1 Nearest Neighbor Projectors

In this section, we present an algorithm for obtaining a CSOB corresponding to any nearest neighbor (NN) projector. The algorithm is based on the Gram-Schmidt orthogonalization procedure, and produces a CSOB with each basis vector having a maximum spatial extent of 3 consecutive lattice cells. The methods in this section are applicable even if the projector is not translationally invariant.

The basic idea underlying our procedure is to obtain the set $\widetilde{\Pi}_z^P$ defined in section 2.3.1, corresponding to the localized eigenstates of P_z for some lattice site z, and to 'reduce' P to $P-P_z$ as required by the Gram-Schmidt procedure. Then, we operate this reduced projector $P - P_z$ on another cell z', and iterate along a sequence of cell locations which includes all the integers. The union of all the $\widetilde{\Pi}_z^P$ sets will form an orthonormal basis for the image of P. While at the first step, $\widetilde{\Pi}_z^P$ is guaranteed to have compactly supported wavefunctions, it is not obvious that the size of the corresponding wavefunctions stays bounded for subsequent steps. With the help of the following lemma, we can show that the size of each vector at any step will be at most three consecutive cells.

Lemma 1. *For any $z \in \mathbb{Z}$, orbital indices $i, j \in \{1, \ldots, n\}$, and integers $\delta, \delta' > 0$,*

$$\langle z - \delta, i | \, (P - P_z) \, | z + \delta', j \rangle = 0. \tag{2.14}$$

Additionally,

$$(P - P_z)\,|z, j\rangle = 0. \tag{2.15}$$

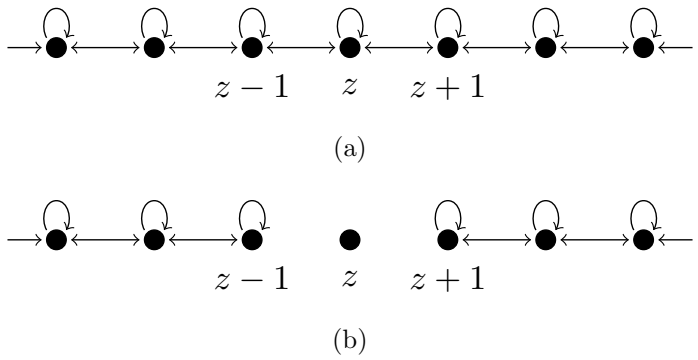

Figure 2.5: Change in the connectivity of an NN projector after a Gram-Schmidt step. Each dot represents a cell, with arrows indicating possible non-zero matrix elements of P. (a) Connectivity of an NN projector P. (b) Connectivity of the reduced projector $P - P_z$. Missing arrows indicate that the corresponding matrix elements are zero.

Proof. For any cell z, let $P_{zz} : \mathcal{H}^z \to \mathcal{H}^z$ denote the $n \times n$ matrix corresponding to the matrix elements of P between different orbitals at cell z, i.e.

$$(P_{zz})_{ij} = \langle z, i|\, P\, |z, j\rangle\,.$$

Since P is Hermitian, P_{zz} is also Hermitian. Hence, there exists a unitary matrix U_z, such that $D_z = U_z^\dagger P_{zz} U_z$ is a real diagonal matrix. Let d_z denote the vector of diagonal elements of the matrix D_z. The unitary U_z defines a new basis at z:

$$|z, i\rangle' \coloneqq \sum_j (U_z)_{ji}\, |z, j\rangle\,. \tag{2.16}$$

We call the orbital basis $\{|z, \alpha\rangle' \,|\alpha = 1, \ldots, n\}$ a diagonal basis at z. Since $\langle z, i|'\, P\, |z, j\rangle' = d_i \delta_{ij}$, we can significantly reduce the intra-cell connectivity of P, by performing the unitary transformation at every cell separately. Equivalently, we use the global unitary transformation

$$U \coloneqq \bigoplus_{z \in \mathbb{Z}} U_z. \tag{2.17}$$

Hereafter, for notational convenience, we drop the prime outside the vectors, and assume that we have already rotated the basis to a diagonal one. Thus, $\langle z,\alpha|\, P\,|z,\beta\rangle = 0$ whenever $\alpha \neq \beta$.

Now we obtain a few important identities using the fact that P is an orthogonal NN projector, and using appropriate insertions of resolution of identity:

1. Since P is positive-semidefinite, for any cell z and orbital α, we have

$$\langle z,\alpha|\, P\,|z,\alpha\rangle \geq 0. \tag{2.18}$$

2. For any two neighboring cells z and $z+1$ and orbitals α,β, we have

$$\langle z,\alpha|\, P\,|z,\alpha\rangle + \langle z+1,\beta|\, P\,|z+1,\beta\rangle = 1, \quad \text{whenever } \langle z,\alpha|\, P\,|z+1,\beta\rangle \neq 0. \tag{2.19}$$

   This follows from

$$\begin{aligned}
\langle z,\alpha|\, P\,|z+1,\beta\rangle &= \langle z,\alpha|\, P^2\,|z+1,\beta\rangle \\
&= \langle z,\alpha|\, P\,|z,\alpha\rangle\, \langle z,\alpha|\, P\,|z+1,\beta\rangle + \langle z,\alpha|\, P\,|z+1,\beta\rangle\, \langle z+1,\beta|\, P\,|z+1,\beta\rangle \\
&= \langle z,\alpha|\, P\,|z+1,\beta\rangle \left(\langle z,\alpha|\, P\,|z,\alpha\rangle + \langle z+1,\beta|\, P\,|z+1,\beta\rangle\right).
\end{aligned}$$

3. Similarly, for any two cells z and $z+2$ separated by two hops, since P is an NN operator,

$$\sum_{\gamma} \langle z,\alpha|\, P\,|z+1,\gamma\rangle\, \langle z+1,\gamma|\, P\,|z+2,\beta\rangle = 0. \tag{2.20}$$

Now we obtain the projector P_z by orthogonalizing Π_z (using the diagonal basis orbitals of P_{zz} in expression 2.3). Since $\langle z,\alpha|\, P\,|z,\beta\rangle = 0$ whenever $\alpha \neq \beta$, Π_z is already orthogonal, so we only need to normalize the vectors in it in order to obtain an orthonormal set. Whenever $P\,|z,\alpha\rangle \neq 0$, we denote the corresponding normalized vector by

$$|P,z,\alpha\rangle := \frac{P\,|z,\alpha\rangle}{\sqrt{\langle z,\alpha|\, P\,|z,\alpha\rangle}}.$$

Thus, we obtain P_z by adding the projector onto each orthonormal vector:

$$P_z \equiv \sum_{\alpha}^{(d_z)_\alpha \neq 0} |P,z,\alpha\rangle\, \langle P,z,\alpha| = \sum_{\alpha}^{(d_z)_\alpha \neq 0} P \frac{|z,\alpha\rangle\, \langle z,\alpha|}{\langle z,\alpha|\, P\,|z,\alpha\rangle} P.$$

Since Π_z consists of wavefunctions with non-zero support only on cells z and $z \pm 1$, equation (2.14) is already satisfied, whenever $\delta > 1$ or $\delta' > 1$. Thus, we only need to verify that (2.14) is satisfied for $\delta = \delta' = 1$, for which, we get

$$\langle z-1, \alpha | \, P_z \, | z+1, \beta \rangle = \sum_{\gamma}^{(d_z)_\gamma \neq 0} \frac{\langle z-1, \alpha | \, P \, | z, \gamma \rangle \, \langle z, \gamma | \, P \, | z+1, \beta \rangle}{\langle z, \gamma | \, P \, | z, \gamma \rangle}.$$

Any non-zero term in the summation will have $\langle z-1, \alpha | \, P \, | z, \gamma \rangle \neq 0$. From condition (2.19), all such orbitals γ at cell z possess the same self-hop:

$$\langle z, \gamma | \, P \, | z, \gamma \rangle = 1 - \langle z-1, \alpha | \, P \, | z-1, \alpha \rangle \neq 0.$$

Thus, we get

$$\begin{aligned} \langle z-1, \alpha | \, P_z \, | z+1, \beta \rangle &= \frac{1}{1 - \langle z-1, \alpha | \, P \, | z-1, \alpha \rangle} \sum_{\gamma} \langle z-1, \alpha | \, P \, | z, \gamma \rangle \, \langle z, \gamma | \, P \, | z+1, \beta \rangle \\ &= 0, \end{aligned} \tag{2.21}$$

where we have used condition (2.20). Since P has vanishing matrix elements between orbitals lying on opposite sides of z, this proves equation (2.14).

We note that $P \, | z, \alpha \rangle = P_z \, | z, \alpha \rangle$ and hence $(P - P_z) \, | z, \alpha \rangle = 0$. This leads to equation (2.15). The connectivity of the reduced projector is shown in figure 2.5. □

Based on this lemma, we present a method for obtaining a CSOB for the image of an NN projector, as described in Procedure 1.

Lemma 2. *The set $\widetilde{\Pi}$ obtained from the Gram-Schmidt algorithm 1 is an orthonormal basis of the image of the NN projector $\mathcal{P}$. Furthermore, every element of $\widetilde{\Pi}$ is compactly supported, with a spatial extent of no more than three consecutive cells.*

Proof. The set $\cup_z \Pi_z^P$ spans the image of $\mathcal{P}$. Hence, procedure 1, which is the application of the Gram-Schimidt procedure on it, creates an orthonormal basis of the image of $\mathcal{P}$. Lemma 1 implies that the reduced projector $P - P_z$ obtained at any iteration in the procedure is also an NN projector. Thus, every vector belonging to $\widetilde{\Pi}_z^P$ for any z is guaranteed to be compactly supported, with a maximum spatial extent of 3 consecutive cells. □

Procedure 1: Procedure for Constructing a CSOB for the Image of any 1d NN Projector

Input : An NN projector $\mathcal{P}$ acting on a 1d lattice.

Procedure: Define a non-repeating sequence $S \equiv z_0, z_1, \ldots$ of integers, s.t. it contains all the integers. Set $P \leftarrow \mathcal{P}$. Initialize $k = 0$, and do:

1. Set $z \leftarrow z_k$.
2. Obtain Π_z^P (as defined in eq. (2.3)).
3. Orthonormalize the set Π_z^P to obtain $\widetilde{\Pi}_z^P$.
4. Obtain P_z from $\widetilde{\Pi}_z^P$ using (2.4).
5. Update $P \leftarrow P - P_z$, increment k, and go back to step (1).

Output: The set $\widetilde{\Pi} := \cup_{z\in\mathbb{Z}} \widetilde{\Pi}_z^P$ of compactly supported wavefunctions, which is an orthonormal basis of the image of the projector $\mathcal{P}$.

It is possible to choose a sequence S so that at most n of the created basis vectors have a spatial extent of 3 cells, with all the remaining vectors having a spatial extent of at most 2 consecutive cells. For an example, see figure 2.6.

2.4.2 Translationally Invariant Nearest Neighbor Projectors

Although Procedure 1 from the previous section also works for translationally invariant projectors, in general, the obtained basis may not consist of Wannier functions. In this section, we will show that it is possible to obtain a Wannier basis consisting of compactly supported functions for the image of P, in a size 2 supercell lattice representation. By a size 2 supercell representation of the lattice, we mean relabelling the cells so that the lattice is regarded as consisting of "supercells" which are each twice the size of the original cell. In this representation, the unit cell is the supercell which consists of two primitive unit cells. We also use a supercell representation for the conversion of an SL projector to an NN projector,

as will be discussed in the next subsection. To that end, we first divide the lattice into two subsets, A, and B, consisting of alternating cells. For concreteness, we choose A to consist of even locations ($2\mathbb{Z}$), and B to be the odd locations ($2\mathbb{Z}+1$).

We define the set Π_A^P as being

$$\Pi_A^P = \bigcup_{i \in A} \Pi_i^P.$$

We also define $\mathcal{H}_A^P$ to be the span of Π_A^P, and P_A to be the orthogonal projection onto $\mathcal{H}_A^P$. From lemma 1, we note that $P - P_A$ has a significantly reduced connectivity, as shown in figure 2.7. Specifically, the only non-zero matrix elements of $P - P_A$ between any two orbitals, are those between any two orbitals located at the same cell belonging to set B.

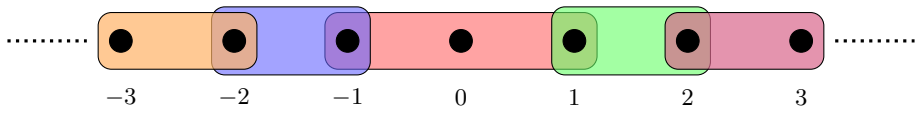

Figure 2.6: If we use the sequence $S = 0, -1, 1, -2, 2, \ldots$ in procedure 1, then all sets $\widetilde{\Pi}_z^P$ except for $\widetilde{\Pi}_0^P$ consist of wavefunctions of a maximum size of 2. Each colored rectangle represents the maximum spatial extent of the wavefunctions in $\widetilde{\Pi}_z^P$ obtained during one iteration of the procedure. Each unit cell is represented by a black dot.

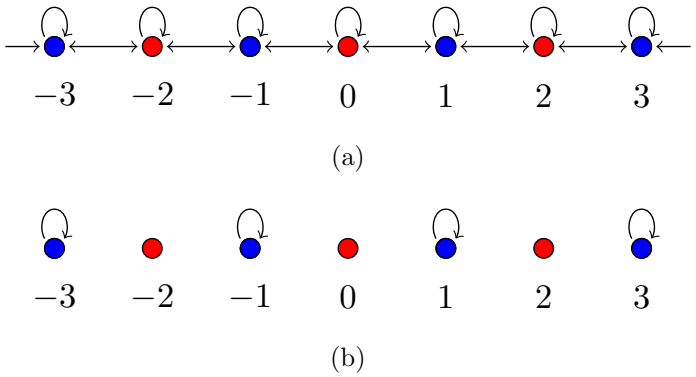

Figure 2.7: Sets A and B are shown in red and blue respectively. (a) Connectivity of an NN projector P. (b) Connectivity of $P - P_A$. Missing arrows indicate vanishing matrix elements.

Since P is translationally invariant, it is useful to define a translation operator $\widehat{\mathcal{T}}$, which

Procedure 2: Compactly Supported Wannier Basis for 1d translationally invariant NN projectors

Input : A 1d translationally invariant NN projection operator P.

Procedure:

1. Obtain Π_0^P, and orthogonalize it to obtain the set $\widetilde{\Pi}_0^P$.
2. Obtain the orthogonal projection operator P_0 onto the span of Π_0^P.
3. Obtain a reduced projection operator $P' \coloneqq P - P_0 - \widehat{\mathcal{T}}^2 P_0 \widehat{\mathcal{T}}^{\dagger 2}$.
4. Obtain and orthogonalize $\Pi_1^{P'}$ to obtain the set $\widetilde{\Pi}_1^{P'}$.
5. Obtain the set $\tilde{\Pi}$, defined as

$$\widetilde{\Pi} = \left(\bigcup_{z \in \mathbb{Z}} \{ \widehat{\mathcal{T}}^{2z} |\chi\rangle : |\chi\rangle \in \widetilde{\Pi}_0^P \} \right) \cup \left(\bigcup_{z \in \mathbb{Z}} \{ \widehat{\mathcal{T}}^{2z} |\chi\rangle : |\chi\rangle \in \widetilde{\Pi}_1^{P'} \} \right). \tag{2.22}$$

Output: The set $\tilde{\Pi}$ consisting of compactly supported Wannier functions spanning the image of P, corresponding to a size 2 supercell representation.

satisfies

$$\widehat{\mathcal{T}} |z, i\rangle = |z+1, i\rangle ,$$

for all $z \in \mathbb{Z}$ and $i \in \{1, \ldots, n\}$. Since P is translationally invariant, $P = \widehat{\mathcal{T}}^\dagger P \widehat{\mathcal{T}}$.

The algorithm for obtaining a CSOB is summarized in Procedure 2.

Lemma 3. *The output obtained using Procedure 2 is a compactly supported Wannier basis spanning the image of P corresponding to a size 2 supercell representation.*

Proof. The output of Procedure 2 is the set $\widetilde{\Pi}$, which is a union of two disjoint sets (see equation (2.22)). The first set is a union of the set $\widetilde{\Pi}_0^P$, and all its even unit cell translates. We will now show that this set is an orthogonal basis of $\mathcal{H}_A^P$.

First, we note that the the set $\{\widehat{\mathcal{T}}^{2z} |\chi\rangle : |\chi\rangle \in \widetilde{\Pi}_0^P\}$ is an orthogonal basis of $\mathcal{H}_{2z}^P$, since P is translationally invariant. Moreover, for any $z \neq 0$, this set is also orthogonal to the

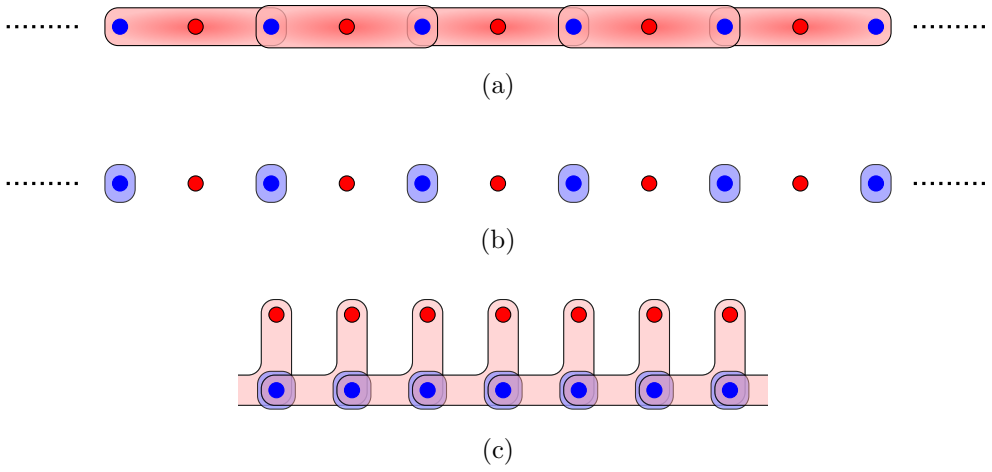

Figure 2.8: The red and blue dots denote the lattice sites belonging to sets A and B respectively. (a) Wavefunctions in $\widetilde{\Pi}_z^P$ centered at cell $z \in A$ are chosen to be the wavefunctions in $\widetilde{\Pi}_0^P$ translated by z cells. Each red rectangle centered at z denotes the maximum spatial extent of wavefunctions belonging to $\widetilde{\Pi}_z^P$. (b) Each blue bubble denotes the maximum spatial extent of the wavefunctions in the set $\widetilde{\Pi}_1^{P-P_A}$, and its translates by an even number of cells. (c) The two sets of functions together form a Wannier basis in a size 2 supercell representation, with each supercell consisting of one cell each from A and B.

set $\widetilde{\Pi}_0^P$. To see this, we show that *any* orthonormal bases $\widetilde{\Pi}_{z_1}^P$ and $\widetilde{\Pi}_{z_2}^P$ for distinct locations $z_1, z_2 \in A$ are mutually orthogonal. Let $|\Psi\rangle \in \mathcal{H}_{z_1}^P$ and $|\Phi\rangle \in \mathcal{H}_{z_2}^P$ be two vectors. There exist vectors $|\psi\rangle \in \mathcal{H}^{z_1}$ and $|\phi\rangle \in \mathcal{H}^{z_2}$ such that $|\Psi\rangle = P|\psi\rangle$ and $|\Phi\rangle = P|\phi\rangle$. Taking the inner product of $|\Psi\rangle$ and $|\Phi\rangle$, we obtain

$$\begin{aligned}\langle\Phi|\Psi\rangle &= \langle\phi| P^\dagger P |\psi\rangle \\ &= \langle\phi| P |\psi\rangle \\ &= 0,\end{aligned}$$

since z_1 and z_2 are located at least two hops away, which is larger than the maximum hopping distance of P. Thus, $\mathcal{H}_{z_1}^P$ and $\mathcal{H}_{z_2}^P$ are mutually orthogonal for distinct $z_1, z_2 \in A$. Thus, the set $\bigcup_{z\in\mathbb{Z}}\{\widehat{\mathcal{T}}^{2z}|\chi\rangle : |\chi\rangle \in \widetilde{\Pi}_0^P\}$ is an orthogonal basis of $\mathcal{H}_A^P$. Additionally, since P is NN hopping, it consists of compactly supported wavefunctions with a maximum spatial extent of 3 cells, as shown in figure 2.8(a).

The second set in equation (2.22) is an orthonormal basis of $\mathcal{H}^P \setminus \mathcal{H}^P_A$. To prove this, we first note that

$$\begin{aligned} P' \left|1, i\right\rangle &= (P - P_0 - \widehat{\mathcal{T}}^2 P_0 \widehat{\mathcal{T}}^{\dagger 2}) \left|1, i\right\rangle \\ &= \left[P - \left(\sum_{z\in\mathbb{Z}} \widehat{\mathcal{T}}^{2z} P_0 \widehat{\mathcal{T}}^{\dagger 2z}\right)\right] \left|1, i\right\rangle \\ &= (P - P_A) \left|1, i\right\rangle . \end{aligned}$$

Hence, the set $\widetilde{\Pi}_1^{P'}$ is an orthonormal basis of $\mathcal{H}_1^{P-P_A}$. $P - P_A$ remains invariant under translations by an even number of cells. Since $P - P_A$ is also a nearest neighbor projector (using lemma 1), using the same arguments as for the first set, we conclude that $\bigcup_{z\in\mathbb{Z}}\{\widehat{\mathcal{T}}^{2z} \left|\chi\right\rangle : \left|\chi\right\rangle \in \widetilde{\Pi}_1^{P'}\}$ is an orthogonal basis of $\mathcal{H}^P \setminus \mathcal{H}^P_A$. Additionally, using lemma 1, we infer that every wavefunction it contains is compactly supported, with non-zero support on only one cell [see figure 2.8(b)].

Thus, $\widetilde{\Pi}$ is a compactly supported orthogonal basis of $\mathcal{H}^P$. By construction,

$$\widehat{\mathcal{T}}^{2z} \left|\chi\right\rangle \in \Pi \text{ if } \left|\chi\right\rangle \in \widetilde{\Pi},$$

for any $z \in \mathbb{Z}$. Thus, $\widetilde{\Pi}$ consists of compactly supported Wannier basis, within a size 2 supercell representation [figure 2.8(c)]. □

2.4.3 Supercell Representation and Strictly Local Projectors

As discussed at the beginning of this section, an SL operator on a 1d lattice with a maximum hopping distance b can be expressed as an operator with only nearest neighbor hopping terms

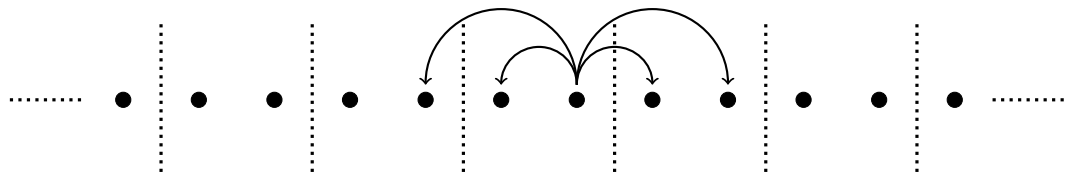

Figure 2.9: An example of conversion of a 1d SL operator to an NN operator using a supercell representation. If an operator has a maximum hopping distance of 2, then grouping the sites in pairs converts the operator to an NN operator in the 'supercell' representation.

using a supercell representation with each supercell consisting of b number of primitive cells (for an illustrative example, see figure 2.9). The range of the operator is reduced, at the cost of an increase in the number of orbitals per cell ($n \to nb$). This transformation enables us to apply the techniques and results for NN projectors ($b = 1$) to SL projectors ($b \geq 1$).

In particular, if we choose the supercell located at the origin to consist of primitive cells $0, 1, \ldots, b-1$, the position and orbital indices in the two representations have the following correspondence:

$$\begin{aligned} &\text{Primitive cell} \longleftrightarrow \text{Supercell} \\ &|z, i\rangle \;\equiv\; |z \setminus b, n \times (z \bmod b) + i\rangle_s \,, \end{aligned} \tag{2.23}$$

with the subscript s denoting a vector in the supercell representation, and $\setminus$ denoting the quotient upon division.

Putting together the results from the previous subsections and the conversion of an SL projector to an NN projector using the supercell representation, we arrive at the following results for arbitrary range SL projectors.

Corollary 1. *The image of an SL projector on a 1d lattice with a maximum hopping distance b possess a CSOB consisting of wavefunctions of a maximum spatial extent of $3b$ consecutive cells.*

We first create a size b supercell representation where P is a NN projector. Using Procedure 1, we obtain a CSOB in this supercell representation. We revert back to the original, or primitive cell representation using the correspondence (2.23). This process is summarized in the following sequence:

$$\begin{array}{lllll} \text{Primitive cell} \longrightarrow & & \text{Supercell representation} & & \longrightarrow \text{Primitive cell} \\ \text{representation} & & & & \text{representation} \\ \text{SL Projector} \longrightarrow & \text{NN Projector} & \xrightarrow{\text{Procedure 1}} & \text{CSOB} & \longrightarrow \text{CSOB} \\ (b \geq 1) & (b = 1) & & (\text{max size } 3) & (\text{max size } 3b) \end{array}$$

Similarly, we can use Procedure 2 for obtaining a Wannier basis for arbitrary range translationally invariant SL projectors.

Corollary 2. *The image of a translationally invariant strictly local projector with a maximum hopping distance b on a 1d lattice is spanned by a compactly supported Wannier basis within a size* 2*b supercell lattice representation.*

The procedure for obtaining such a basis is summarized in the following sequence:

Primitive cell	$\xrightarrow{\text{Size b}}$	Size b supercell	$\xrightarrow{\text{Size 2}}$	Size $2b$ supercell
representation		representation		representation
SL Projector ($b \geq 1$)	$\longrightarrow$	NN Projector ($b = 1$)	$\xrightarrow{\text{Procedure 2}}$	CS Wannier basis.

To summarize, we have shown that the image of a strictly local projector in 1d is always spanned by a compactly supported orthogonal basis (or a compactly supported Wannier basis if the projector has lattice translational invariance). This completes our proof of theorem 1.

Having presented a technique for the construction of CS Wannier functions for 1d SL projectors, we apply this technique to an example Hamiltonian with a band associated with an SL projector in Appendix 2.A. Furthermore, we discuss why the Gram-Schmidt orthogonalization procedure in our algorithm is easier to use instead of the symmetric orthogonalization procedure [59]. We also compare our results with those obtained using the maximally localized Wannier functions procedure [20].

In the next section we will study how these results can be extended to higher dimensional lattices which have a larger coordination number. We close this section with some comments on the Bethe lattice which is sometimes regarded as an infinite dimensional lattice. For an NN projector on the Bethe lattice with an arbitrary coordination number, using the methods of Lemma 1, we can show that projecting out a site results in a reduced connectivity for the projector. Consequently, analogous to Lemma 3 and Procedure 1, using an arbitrary sequence of site locations guarantees the creation of an orthonormal basis which is compactly supported.

2.5 Higher dimensional lattices

In 1d, we were able to show that for an arbitrary basis of wavefunctions, the existence of a compactly supported orthogonal basis (CSOB) equals the strict locality of the associated projector. However, the results for the 1d case do not all carry over to higher dimensional lattices. While strict locality of the projector is a necessary condition for the existence of a CSOB even in higher dimensions (see section 2.3.3), the methods we have employed so far for the 1d case do not prove that it is a sufficient one. Our proof for the existence of a CSOB given any 1d SL projector relied on the fact that any 1d SL projector can be represented as a nearest-neighbor (NN) projector in a supercell representation, or equivalently, a block tridiagonal matrix in the orbital basis. In higher dimensions, such a simple matrix representation for even the simplest non-trivial SL projector, i.e. an NN projector is lacking. Generic SL or NN projectors in $d > 1$ cannot be represented by block tridiagonal matrices, or even band diagonal matrices. This makes the task of identifying the properties of a projector that are equivalent to the existence of a CSOB difficult.

Consequently, we identify a condition more stringent than strict locality of the projector as a sufficient condition for the existence of a CSOB. While NN projectors in $d > 1$ cannot in general be represented as block tridiagonal matrices, it is still possible to show that the image of any NN projector is spanned by a CSOB. However, unlike in 1d, higher dimensional SL projectors cannot in general be expressed as NN projectors using a supercell transformation. Consequently, we can extend the results for NN projectors only to those SL projectors that can be brought to an NN form using a supercell representation. We call such projectors NN-reducible projectors. (For a discussion of the condition of being NN-reducible, we refer the reader to section 2.5.4.) Due to these considerations, unlike in 1d, we obtain separate necessary and sufficient conditions for the existence of a CSOB spanning a subspace. Since the necessary condition has already been proved in section 2.3.3, in this section, we focus on proving the sufficient condition, which is that a projector should be NN hopping, or NN-reducible.

Additionally, as mentioned in the introduction, in higher dimensional lattices it is pos-

sible to construct 'hybrid Wannier functions' that are compactly supported along just one dimension. We show that their existence hinges on the the strict locality of projectors just like the existence of compactly supported wavefunctions in one dimension.

For all these cases, we provide algorithms for obtaining CSOBs and CS hybrid Wannier functions, and provide upper bounds on their sizes. In summary, we will prove the following statements.

Theorem 2. *Let P be a strictly local projector with a maximum hopping distance b, acting on a $d > 1$ dimensional tight binding lattice.*

(1) If P is NN reducible, there exists a compactly supported orthonormal basis spanning its image, with each basis vector having a size of at most $3b \times \ldots \times 3b$ cells.

(2) If P is translationally invariant and NN reducible, there exists a compactly supported Wannier basis spanning its image, in a size $2b \times \ldots \times 2b$ supercell lattice representation.

(3) If P is translationally invariant, its image is spanned by hybrid Wannier functions which have compact support along the localized (i.e. Wannier-like) dimension, in a size $2b$ supercell representation of the lattice. The supercell transformation is required only along the localized dimension, which may be chosen to be any of the d dimensions. Moreover, if P is strictly local along any one direction with a maximum hopping distance b, (with no restrictions on the localization along the other directions), then strictly local hybrid Wannier functions corresponding to a size $2b$ supercell which are localized along that direction can be formed.

In addition, we will discuss the topological properties of such projectors in this section.

Before proving these statements, we first discuss some model Hamiltonians with CS Wannier functions. In figure 2.10, we show two examples from the literature of 2d flat-band Hamiltonians, that have flat bands spanned by orthogonal CLSs, i.e. flat-band CS Wannier functions. These Hamiltonians are based on the square kagome lattice [60, 54] with six sites per unit cell and the frustrated bilayer [61, 62] with two sites per unit cell. In both

cases the natural choices of the primitive cells are such that each CLS lies entirely within a unit cell. While CS Wannier functions can be easily constructed for the flat bands in these examples, for many flat-band Hamiltonians, orthogonal CLSs spanning a flat band do not exist. However, as discussed in section 2.3.2, it is possible to modify such Hamiltonians by enlargement of the unit cell, so that orthogonal CLSs span an entire flat band. This approach was used for example in reference [54], to construct two Hamiltonians on the kagome lattice wherein a flat band is spanned by CS Wannier functions. One can apply the same technique to other flat-band models from the literature, such as the decorated square lattice [63] and the dice lattice [64].

In all of these examples, the CS Wannier functions are associated with flat bands, and are localized within one cell each. Consequently, the corresponding band projector is on-site hopping, and hence is independent of k in a k-space representation. One can simply diagonalize the projector in order to obtain CS Wannier functions in such cases. However, there are many Hamiltonians with a band spanned by CS Wannier functions that are spread across multiple cells, and with band projectors that are strictly local, but not on-site hopping. While one can diagonalize a translationally invariant NN projector expressed in k-space, in general a Fourier transform of the obtained Bloch wavefunction results in exponentially localized Wannier functions as opposed to CS Wannier functions (for an example, see Appendix 2.A). Similarly, as discussed in section 2.3.2, it may be possible to construct CS Wannier functions using destructive interference arguments for translationally invariant NN projectors if they have a simple form. However, it is not straightforward to do so for a more complicated projector, such the following 2d NN projector:

$$P(k) = \frac{1}{12}\begin{pmatrix} e^{-iky}\sqrt{3}+e^{iky}\sqrt{3}+6 & -e^{-iky}\sqrt{3}+e^{iky}\sqrt{3}+2e^{ikx}-2 & e^{-iky}\sqrt{3}+2e^{ikx}+1 & -e^{iky}\sqrt{3}+2e^{ikx}+1 \\ e^{-iky}\sqrt{3}-e^{iky}\sqrt{3}+2e^{-ikx}-2 & -e^{-iky}\sqrt{3}-e^{iky}\sqrt{3}+6 & e^{-iky}\sqrt{3}-2e^{-ikx}-1 & e^{iky}\sqrt{3}+2e^{-ikx}+1 \\ e^{iky}\sqrt{3}+2e^{-ikx}+1 & e^{iky}\sqrt{3}-2e^{ikx}-1 & 7-2e^{-ikx}-2e^{ikx} & e^{-ikx}\left(-e^{i(k_x+k_y)}\sqrt{3}-2e^{2ikx}+2\right) \\ -e^{-iky}\sqrt{3}+2e^{-ikx}+1 & e^{-iky}\sqrt{3}+2e^{ikx}+1 & -e^{-iky}\sqrt{3}-2e^{-ikx}+2e^{ikx} & 5+2e^{-ikx}+2e^{ikx} \end{pmatrix}. \tag{2.24}$$

In contrast, the method presented in this section enables us to construct CS Wannier functions since this projector is NN hopping. The Wannier functions (centered at (x, y)) so obtained are $|W_1\rangle = \frac{1}{\sqrt{6}}|x, y\rangle \otimes (|B\rangle + |C\rangle + |D\rangle) + \frac{1}{\sqrt{6}}|x+1, y\rangle \otimes (|A\rangle - |C\rangle + |D\rangle)$ and $|W_2\rangle = \frac{1}{2}|x, y\rangle \otimes (|A\rangle - |B\rangle + |C\rangle) + \frac{1}{2\sqrt{3}}|x, y-1\rangle \otimes (|A\rangle + |B\rangle - |D\rangle)$, where the orbitals

are labelled by letters A to D.

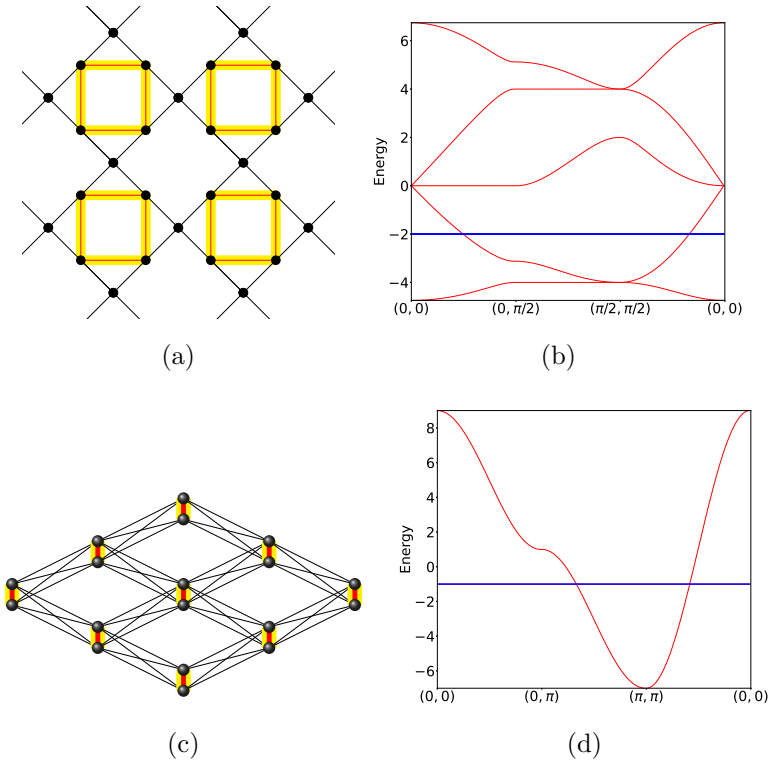

Figure 2.10: (a) The square kagome lattice and (c) the frustrated bilayer lattice. In both cases, the black and red segments denote hopping elements with values t_1 and t_2 respectively. The flat band CLSs, i.e. CS Wannier functions are highlighted in yellow. In the case of the square kagome lattice, each CLS has support on four sites and an amplitude of $\frac{1}{2}$ with alternating signs on the four sites. For the frustrated bilayer lattice, each CLSs has an amplitude of $+1$ and -1 on the two sites where it is located. The band structures of the square kagome lattice with $(t_1, t_2) = (2, 1)$, and of the frustrated bilayer with $(t_1, t_2) = (0, 1)$ are shown in figures (b) and (d). The flat band is colored blue.

Having discussed some examples, we proceed to the proof of theorem 2, which we split across the following subsections. Since the problem of finding hybrid Wannier functions can be reduced to a one dimensional problem, we start with the proof of point (3) of Theorem 2 in subsection 2.5.1. In subsections 2.5.2 and 2.5.3 we present procedures for obtaining CSOBs for NN projectors. In subsection 2.5.4, we discuss how to determine whether a projector is NN-reducible, and show how a supercell representation can be used to extend the results

for NN projectors to the more general class of NN-reducible projectors. In subsection 2.5.5, we discuss the topological properties of SL projectors as well as projectors associated with CSOBs and CS hybrid Wannier functions.

2.5.1 Hybrid Wannier Functions for Strictly Local Projectors

Procedure 3: Compactly Supported Hybrid Wannier functions for Strictly Local Projectors

---

Input : A translationally invariant SL projection operator P operating on a d dimensional lattice

Procedure: To obtain hybrid Wannier functions which are Wannier-like along the d^{th} dimension, for every value of $\vec{k}_\perp$ in the $d-1$ dimensional B.Z.:

1. Obtain the 1d projector $P(\vec{k}_\perp)$ using expression (2.26).
2. Use a size b supercell representation to express $P(\vec{k}_\perp)$ as a 1d NN projector.
3. Following Procedure 2, obtain a CW basis for the image of $P(\vec{k}_\perp)$. Let $\widetilde{\Pi}_\perp^{\vec{k}_\perp}$ denote this basis.
4. Obtain the set $\widetilde{\Pi}^{\vec{k}_\perp} \coloneqq \{\vec{k}_\perp \otimes |\psi\rangle : |\psi\rangle \in \widetilde{\Pi}_\perp^{\vec{k}_\perp}\}$.

Obtain the set

$$\widetilde{\Pi} \coloneqq \bigcup_{\vec{k}_\perp}^{B.Z._{d-1}} \widetilde{\Pi}^{\vec{k}_\perp}.$$

Output: The set $\widetilde{\Pi}$ consisting of hybrid Wannier functions within a size $1 \times \ldots \times 1 \times 2b$ supercell representation, which are compactly supported and Wannier-like along the d^{th} dimension.

As discussed in the introduction, hybrid Wannier functions are a variant of Wannier functions for $d > 1$ dimensional translationally-invariant systems. Hybrid Wannier functions can be obtained by taking the inverse Fourier transform of the Bloch wavefunctions along

exactly one dimension. Such wavefunctions can be chosen to be localized and Wannier-like along one dimension, and Bloch wave-like and delocalized along the other dimensions. Starting with a real space representation of a translationally invariant SL projector, we outline a procedure for obtaining such a basis, so that it is compact localized along the localized dimension. We will use the convention (2.2) of expressing the Hilbert space as a tensor product, $\mathbb{Z}^{\otimes d} \otimes \mathcal{H}$, throughout this section, where $\mathcal{H}$ represents the space of orbitals and spin.

First, we revisit the k-space, or Fourier space representation for a projector. As is customary, we consider finite periodic lattices of size $L_1 \times \ldots \times L_d$, so that the number of sites $N = L_1 \ldots L_d$. For infinite lattices, we take the limit of the lengths going to infinity. Without loss of generality, we choose the direct lattice to be a hyper-cube so that the Brillouin Zone (B.Z.) consists of reciprocal lattice vectors $\vec{k}$ satisfying $\vec{k}.\vec{R} \in 2\pi\mathbb{Z}$ for any $\vec{R} \in \mathbb{Z}^d$ such that $k_i \in (-\pi, \pi] \ \forall \ i \in \{1, \ldots, d\}$. An orthogonal band projection operator P can be expressed as

$$
\begin{aligned}
P &= \sum_{\vec{k} \in B.Z.} |\vec{k}\rangle \langle \vec{k}| \otimes P(\vec{k}), \\
\text{where } |\vec{k}\rangle &\coloneqq \frac{1}{\sqrt{N}} \sum_{\vec{r} \in \mathbb{Z}^d} e^{-i\vec{k}.\vec{r}} |\vec{r}\rangle , \\
\text{and } P(\vec{k}) &\coloneqq \langle \vec{k}| P |\vec{k}\rangle .
\end{aligned}
$$

We have suppressed all orbital quantum numbers in the expressions above to aid readability. Each $P(\vec{k})$ is an $n \times n$ matrix function of $\vec{k}$. Since P is idempotent, $P(\vec{k})P(\vec{k'}) = \delta_{\vec{k},\vec{k'}} P(\vec{k})$, i.e. all the $P(\vec{k})$'s for distinct $\vec{k}$'s are mutually orthogonal projection operators.

In order to obtain hybrid Wannier functions which are localized along the m^{th} dimension, we express P in the Fourier space corresponding to all spatial dimensions, except for the m^{th} dimension. Here, we only discuss the case with $m = d$; the rest can be obtained by simple modifications. Let $B.Z._{d-1}$ denote the Brillouin zone in $d-1$ dimensions. Denoting the spatial position along the d^{th} dimension by z, we obtain

$$
P = \sum_{\vec{k}_\perp \in B.Z._{d-1}} |\vec{k}_\perp\rangle \langle \vec{k}_\perp| \otimes P(\vec{k}_\perp), \tag{2.25}
$$

with $\vec{k}_\perp \equiv (k_1, \ldots, k_{d-1})$, and $P(\vec{k}_\perp)$ being an orthogonal projection operator given by

$$P(\vec{k}_\perp) \coloneqq \sum_{z,z' \in \mathbb{Z}} |z\rangle \langle z'| \otimes \langle \vec{k}_\perp, z| P |\vec{k}_\perp, z'\rangle . \tag{2.26}$$

Since $P(\vec{k}_\perp)P(\vec{k}'_\perp) = \delta_{\vec{k}_\perp, \vec{k}'_\perp} P(\vec{k}_\perp)$, equation (2.25) implies that the task of obtaining an orthogonal basis for the image of P can be split into the task of obtaining orthogonal bases for each $P(\vec{k}_\perp)$ individually. Since P is strictly local, each $P(\vec{k}_\perp)$ can be thought of as being a one dimensional strictly local projector acting on a lattice with positions $z \in \mathbb{Z}$. Corollary 2 guarantees that each $P(\vec{k}_\perp)$ must have a compactly supported Wannier basis in a size $2b$ supercell representation. This leads us to a procedure of obtaining hybrid Wannier functions which are compact localized along any chosen dimension (see procedure 3).

While in our considerations so far, we have considered an SL projector, if we were to consider a projector that was strictly local along any one direction without the requirement that it be strictly local along any of the other directions, it follows from the arguments above that hybrid Wannier functions which are localized in one direction can still be constructed. This completes our proof for part one of Theorem 2.

2.5.2 Nearest Neighbor Projectors

We now construct a CSOB for nearest-neighbour projectors in d dimensions. Similar to the 1d case, the Gram-Schmidt orthogonalization must be carried out in a sequence which guarantees that after any step, the reduced projector remains NN hopping or on-site hopping, if the original projector is NN hopping. We observe that unlike in the 1d case, this puts restrictions on the orthogonalization sequence in higher dimensions. Although there are multiple possible types of sequences which ensure this condition is satisfied, for concreteness, here, we present a specific one (in Procedure 4), which also be used to obtain a CW basis for translationally invariant NN projectors as well.

This procedure relies on dividing the lattice into two sets, A and B consisting of alternating cells similar to what was done in section 2.4.2. For concreteness, we choose A and B

to be given by

$$\begin{aligned} A &= \{\vec{r} : \vec{r} \in \mathbb{Z}^d; \sum_{i=1}^{d} r_i \in 2\mathbb{Z}\}; \\ B &= \{\vec{r} : \vec{r} \in \mathbb{Z}^d; \sum_{i=1}^{d} r_i \in 2\mathbb{Z}+1\}. \end{aligned} \tag{2.27}$$

Since any two distinct cells $\vec{r}_1, \vec{r}_2 \in A$ are separated by at least two hops, $P_{\vec{r}_1} P_{\vec{r}_2} = 0$, and hence $P_A \coloneqq \sum_{\vec{r} \in A} P_{\vec{r}}$ is an orthogonal projector.

Lemma 4. *The orthogonal projector $P - P_A$ satisfies $\langle \vec{r}_1, i| (P - P_A) |\vec{r}_2, j\rangle = 0$ for all $i, j \in \{1, \ldots, n\}$, unless $\vec{r}_1 = \vec{r}_2 \in B$.*

Proof. Let $\hat{\delta}_i$ denote the unit vector along dimension i. Similar to the proof for 1d projectors (Lemma 1), we introduce the diagonal basis (cf (2.17)), with the primes dropped for notational convenience. As before, we denote the diagonal of the $P_{\vec{r}\vec{r}}$ matrix in this representation by $d_{\vec{r}}$, so that $\langle \vec{r}, \alpha| P |\vec{r}, \beta\rangle = (d_{\vec{r}})_\beta \delta_{\alpha\beta}$.

Since $P |\vec{r}, \alpha\rangle = P_A |\vec{r}, \alpha\rangle$ whenever $\vec{r} \in A$, both $\vec{r}_1$ and $\vec{r}_2$ must belong to B for the corresponding matrix element to be non-zero. If $\vec{r}_1, \vec{r}_2 \in B$ and are distinct, we get

$$\begin{aligned} \langle \vec{r}_1, \alpha| P - P_A |\vec{r}_2, \beta\rangle &= - \langle \vec{r}_1, \alpha| P_A |\vec{r}_2, \beta\rangle \\ &= - \langle \vec{r}_1, \alpha| \sum_{s=\pm 1} \sum_{m=1}^{d} P_{\vec{r}_2 + s\hat{\delta}_m} |\vec{r}_2, \beta\rangle , \end{aligned} \tag{2.28}$$

since $P_{\vec{r}} |\vec{r}_2, \beta\rangle = 0$ unless $\vec{r}$ is a nearest neighbor of $\vec{r}_2$. Since P only has NN hopping terms, this is zero, unless $\vec{r}_1$ and $\vec{r}_2$ are equal to each other, or are two hops away from each other, i.e. only if $\vec{r}_2$ is of the form $\vec{r}_1 \pm \hat{\delta}_p \pm \hat{\delta}_q$ for some $p, q \in \{1, \ldots, d\}$. In order to show that the matrix element is zero for the case with two hops, we will require the higher dimensional analogs of equations (2.18), (2.19) and (2.20), which are

$$\langle \vec{r}, \alpha| P |\vec{r}, \alpha\rangle \geq 0, \tag{2.29}$$

$$\langle \vec{r}, \alpha| P |\vec{r}, \alpha\rangle + \langle \vec{r} + \hat{\delta}_p, \beta| P |\vec{r} + \hat{\delta}_p, \beta\rangle = 1 \ \forall p \in \{1, \ldots, n\}, \text{ whenever } \langle \vec{r}, \alpha| P |\vec{r} + \hat{\delta}_p, \beta\rangle \neq 0, \tag{2.30}$$

Procedure 4: Construction of a CSOB for any NN projector in arbitrary dimensions

Input : A nearest neighbor projector P acting on a $d \geq 1$ dimensional lattice

Procedure: Divide the lattice into two sets A and B consisting of alternating cells, according to (2.27).

1. Obtain $\widetilde{\Pi}^{P}_{\vec{r}}$ and hence $P_{\vec{r}}$, for every $\vec{r} \in A$.
2. Obtain the orthogonal projector $P - P_A \coloneqq P - \sum_{\vec{r}\in A} P_{\vec{r}}$.
3. Obtain $\widetilde{\Pi}^{P-P_A}_{\vec{r}}$ for every $\vec{r} \in B$.

Output: The set $\tilde{\Pi} \coloneqq \left(\bigcup_{\vec{r}\in A} \widetilde{\Pi}^{P}_{\vec{r}}\right) \cup \left(\bigcup_{\vec{r}\in B} \widetilde{\Pi}^{P-P_A}_{\vec{r}}\right)$ which is a CSOB spanning the image of P.

and $$\sum_{\gamma} \sum_{\vec{v}}^{\text{c.n.}} \langle \vec{r}, \alpha | \, P \, | \vec{v}, \gamma \rangle \, \langle \vec{v}, \gamma | \, P \, | \vec{w}, \beta \rangle = 0 \tag{2.31}$$

respectively. The summation in (2.31), with a superscript 'c.n.' (for common neighbors) is over those vectors $\vec{v}$ which are nearest neighbors of both $\vec{r}$ and $\vec{w}$.

For the case where $\vec{r}_2$ is two hops away from $\vec{r}_1$, expression (2.28) simplifies to zero as follows:

$$\begin{aligned} \langle \vec{r}_1, \alpha | \sum_{m=1}^{d} P_{\vec{r}_2 + \hat{\delta}_m} \, | \vec{r}_2, \beta \rangle &= \langle \vec{r}_1, \alpha | \sum_{\vec{w}}^{\text{c.n.}} P_{\vec{w}} \, | \vec{r}_2, \beta \rangle \\ &= \sum_{\vec{w}}^{\text{c.n.}} \sum_{\gamma}^{(d_{\vec{w}})_\gamma \neq 0} \frac{\langle \vec{r}_1, \alpha | \, P \, | \vec{w}, \gamma \rangle \, \langle \vec{w}, \gamma | \, P \, | \vec{r}_2, \beta \rangle}{\langle \vec{w}, \vec{\gamma} | \, P \, | \vec{w}, \gamma \rangle}. \end{aligned}$$

If $\langle \vec{r}_1, \alpha | \, P \, | \vec{r}_1, \alpha \rangle = 1$, then every term in the summation is zero. Otherwise, we get

$$\begin{aligned} \ldots &= \frac{(\delta_{\vec{r}_1})_\alpha}{1 - \langle \vec{r}_1, \alpha | \, P \, | \vec{r}_1, \alpha \rangle} \sum_{\vec{w}}^{\text{c.n.}} \sum_{\gamma} \langle \vec{r}_1, \alpha | \, P \, | \vec{w}, \gamma \rangle \, \langle \vec{w}, \gamma | \, P \, | \vec{r}_2, \beta \rangle && \text{from (2.30),} \\ &= 0, && \text{from (2.31).} \end{aligned}$$

Thus, matrix elements of $P - P_A$ can be non-vanishing only if $\vec{r}_1 = \vec{r}_2 \in B$. □

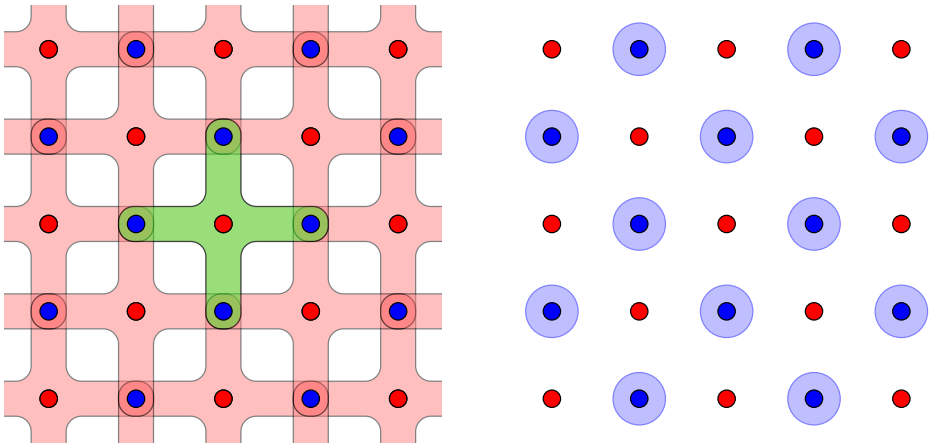

(a) (b)

Figure 2.11: *Procedure 4 for a 2d NN projector*: Cells belonging to sets A and B are represented by red and blue dots respectively. (a) In order to obtain P_A, we operate P on each cell belonging to A, and orthogonalize the vectors. Each colored shape centered at location $\vec{r}$ denotes the maximum spatial extent of the wavefunctions in $\widetilde{\Pi}^{P}_{\vec{r}}$. (We show one shape in green, in order to highlight the 'plus' shape of each of these sets). (b) Since $P - P_A$ is on-site hopping, operating it on any cell in set B creates wavefunctions which are localized at exactly that cell. Each blue circle centered at $\vec{r} \in B$ represents the maximum extent of vectors in $\widetilde{\Pi}^{P-P_A}_{\vec{r}}$.

The basis vectors obtained using Procedure 4 consist of wavefunctions which have a maximum spatial extent (volume) of at most $3 \times \ldots \times 3$ cells. As shown in figure 2.11, they are in fact significantly smaller in extent than this upper bound.

2.5.3 Translationally Invariant Nearest Neighbor Projectors

Let $\widehat{\mathcal{T}}_i$ denote the unit translation operator along the i^{th} dimension. For $\vec{r} \in \mathbb{Z}^d$, let $\widehat{\mathcal{T}}_{\vec{r}}$ denote a translation by an amount $\vec{r}$.

Although Procedure 4 can also be used to generate a compactly supported orthonormal basis from translationally invariant projectors, in general the resulting basis will not be a Wannier basis. However, the wavefunctions can be chosen to have translational invariance

properties if each $\widetilde{\Pi}^{P}_{\vec{r}}$ ($\widetilde{\Pi}^{P-P_A}_{\vec{r}}$) for $\vec{r} \in A$ ($\vec{r} \in B$) is chosen to be a translation of $\widetilde{\Pi}^{P}_{\vec{0}}$ ($\widetilde{\Pi}^{P-P_A}_{\hat{\delta}_1}$) by $\vec{r}$ ($\vec{r}-\hat{\delta}_1$) cells. Based on this principle, we propose a method (Procedure 5) for obtaining a CS Wannier basis spanning the image of P within a supercell representation. For $d = 1$, this procedure is equivalent to Procedure 2.

Procedure 5: Compactly Supported Wannier Basis for d dimensional NN Projectors

---

Input : A translationally invariant NN projection operator P on a d dimensional lattice

Procedure:

1. Obtain Π^{P}_{0}, and orthogonalize it to obtain the set $\widetilde{\Pi}^{P}_{0}$.

2. Obtain the orthogonal projection operator P_0 onto the span of Π^{P}_{0}.

3. Obtain a reduced projection operator (which removes all the nearest neighbors of the site $\hat{\delta_1}$)

$$P' \coloneqq P - \sum_{i=1}^{d} \widehat{\mathcal{T}}_i \widehat{\mathcal{T}}_1 P_0 \widehat{\mathcal{T}}_1^{\dagger} \widehat{\mathcal{T}}_i^{\dagger} - \sum_{i=1}^{d} \widehat{\mathcal{T}}_i^{\dagger} \widehat{\mathcal{T}}_1 P_0 \widehat{\mathcal{T}}_1^{\dagger} \widehat{\mathcal{T}}_i.$$

4. Obtain and orthogonalize $\Pi^{P'}_{\hat{\delta}_1}$ to obtain the set $\widetilde{\Pi}^{P'}_{\hat{\delta}_1}$.

5. Obtain the set Π, defined as

$$\Pi = \left(\bigcup_{\vec{r} \in A} \{ \widehat{\mathcal{T}}_{\vec{r}} \, |\chi\rangle : |\chi\rangle \in \widetilde{\Pi}^{P}_{0} \} \right) \cup \left(\bigcup_{\vec{r} \in B} \{ \widehat{\mathcal{T}}_{\vec{r}-\hat{\delta}_1} \, |\chi\rangle : |\chi\rangle \in \widetilde{\Pi}^{P'}_{\hat{\delta}_1} \} \right) \tag{2.32}$$

Output: The set Π consisting of compactly supported Wannier functions spanning the image of P, within a size $2 \times \ldots \times 2$ supercell representation.

Using steps similar to those used for proving theorem 3, we can show that Procedure 5 outputs a CW basis as claimed.

2.5.4 Supercell representation and Nearest Neighbor Reducible Projectors

We now discuss how to extend the results and methods for NN projectors to SL projectors with larger hopping distances. To that end, we use a supercell representation analogous to the one used for 1d in section 2.4.3. Unlike in 1d where every SL projector is an NN projector in some supercell representation, in general, an SL projector in $d > 1$ becomes a *next*-nearest-neighbor (NNN) hopping projector instead of an NN projector using this transformation. Specifically, if the maximum hopping distance of an SL projector is b, then the projector has at most NNN hopping terms within a size $b \times \ldots \times b$ supercell representation (see figure 2.12). This reversible transformation is associated with the correspondence:

Primitive cell representation $\longleftrightarrow$ Supercell representation

$$|r_1, \ldots, r_d, i\rangle \;\equiv\; \Big|r_1 \setminus b, \ldots, r_d \setminus b, i + \sum_{m=1}^{d} n^m (r_m \bmod b)\Big\rangle_s , \tag{2.33}$$

Since the methods developed in sections 2.5.2 and 2.5.3 are applicable only to NN projectors (and not general NNN projectors), even after using a supercell representation, these techniques cannot be applied to a general SL projector operator for $d > 1$.

Hence, we look for projectors that have an NN-hopping form using suitable transformations. We call such projectors NN-reducible. Which SL projectors are NN-reducible? While SL projectors with various types of connectivity are NN-reducible, here we highlight some particularly simple cases. It is easy to see that SL projectors that satisfy $\langle \vec{r}, i| \, P \, |\vec{r}\,', j\rangle = 0$, whenever $\vec{r} - \vec{r}\,'$ is not along any of the primitive cell directions become NN hopping within a supercell representation of the type described above. For example, an SL projector on a square lattice that has non-zero hoppings only along the $\pm\hat{x}$ and $\pm\hat{y}$ directions, but no other direction is NN-reducible. This is in contrast with the NNN-reducible projectors of the type shown in figure 2.12(b). For some SL projector that appear to be of an NNN form after the transformation (2.33), it may still be possible to apply the results from the previous sections to obtain CS Wannier functions. For example, if an SL projector on a square lattice in a supercell representation only connects neighboring cells along the $\hat{x}$ and $\hat{x} + \hat{y}$ directions, the projector is NN-hopping if we regard these two vectors as being the lattice vectors. We

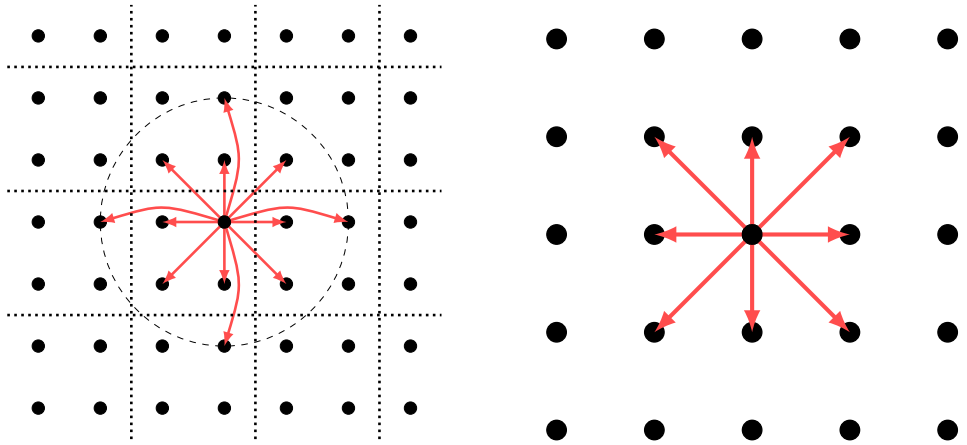

(a) (b)

Figure 2.12: Each black dot represents a lattice cell (which may consist of multiple orbitals). The dashed circle denotes the maximum hopping distance from that cell. (a) The connectivity of a generic SL operator with a maximum hopping distance of $b = 2$. Hopping elements from an arbitrary cell are shown in red.Grouping all the sites within each cell of a 2×2 grid, we obtain a supercell representation. (b) The operator becomes an NNN hopping operator in the supercell representation. Here, the operator connects neighboring cell along the $\hat{x}$, $\hat{y}$, as well as the $\hat{x} \pm \hat{y}$ directions, with $\hat{x}$ and $\hat{y}$ denoting the two axes.

consider all such SL projectors that can be brought to an NN form using change of primitive cell vectors and supercell transformations as NN-reducible. Without loss of generality, we only consider NN-reducible projectors that have hopping elements only along the primitive cell directions below.

For such projectors, we obtain the following results:

Corollary 3. *If an SL projector with a maximum hopping distance b is NN reducible, its image is spanned by a CSOB consisting of wavefunctions of a maximum spatial extent of $3b \times \ldots \times 3b$ cells.*

The procedure for obtaining such a basis is summarized in the following table:

Primitive cell	$\xrightarrow[b\times\ldots\times b]{\text{Size}}$	Supercell representation			$\longrightarrow$	Primitive cell
representation						representation
SL Projector	$\longrightarrow$	NN Projector	$\xrightarrow{\text{Procedure 4}}$	CSOB	$\longrightarrow$	CSOB
$(b \geq 1)$		$(b = 1)$		(max size 3)		(max size $3b$).

Corollary 4. *If a translationally invariant SL projector with a maximum hopping distance b is NN reducible, its image is spanned by a CS Wannier basis within a size $2b \times \ldots \times 2b$ supercell representation.*

The procedure for obtaining such a basis is summarized in the following table:

Primitive cell	$\xrightarrow{\text{Size b}}$	Size b supercell	$\xrightarrow{\text{Size 2}}$	Size $2b$ supercell
representation		representation		representation
SL Projector $(b \geq 1)$	$\longrightarrow$	NN Projector $(b = 1)$	$\xrightarrow{\text{Procedure 5}}$	CS Wannier basis.

This completes our proof for theorem 2.

2.5.5 Topological Triviality and Compact Bases

So far, we have investigated the conditions under which is it possible for a band to be spanned by compactly supported orthogonal bases (CSOBs) or by compactly supported hybrid Wannier functions. Specifically, we identified localization properties of associated projection operators that are necessary or sufficient for the existence of such bases. Similar questions regarding the existence of localized Wannier functions have a long history, as noted in the introduction. The existence of exponentially localized Wannier functions has a bearing on the topological properties of the corresponding bands, with non-trivial band topology restricting the degree of localization possible for Wannier functions. This motivates us to investigate the topological properties of bands possessing CSOBs.

We start with a brief overview of known results. Thouless [45] showed that well localized magnetic Wannier functions can be constructed in 2d if and only if the Chern number is zero. For $d \leq 3$, it was later shown that in the presence of time-reversal symmetry and translational invariance, exponentially localized Wannier functions corresponding to an

isolated band or a set of isolated bands always exist [16, 18, 19, 65]. For systems with other symmetry properties, the existence of such localized Wannier functions is not guaranteed, or even impossible, when the bands are topologically non-trvial. For instance, bands with non-zero Chern numbers do not possess exponentially localized Wannier functions [48]. More generally, there exists a localization dichotomy [46] which says that either exponentially localized Wannier functions exist and the Chern numbers are zero, or all Wannier functions are delocalized (with diverging second moment of the position operator) and the Chern numbers are non-zero. Recently, this result was partially extended to disordered systems [66], with a proof for the vanishing of the Chern marker for 2d insulators possessing exponentially localized generalized Wannier functions.

Since compactly supported Wannier functions (in R^n) are even more localized than generic exponentially local Wannier functions, one may expect topological triviality to follow immediately from these results. While we find this to be true (as discussed below), care is needed while drawing such a conclusion. In all the works discussed above, the wavefunction localization is described in terms of decay of wavefunction amplitude in real space, i.e. R^n. We note that this notion of localization may not in general be the same as localization in tight-binding models which we consider in this paper. Specifically, orbitals on the lattice ($\mathbb{Z}^n$) which are used as the basis in tightbinding descriptions may themselves not be compactly supported, or even exponentially localized in space (R^n). Thus the wavefunctions which are linear combinations of a finite set of such tightbinding orbitals do not in general vanish outside a certain bounded region in space as one might otherwise assume from the use of the term "compact support" in describing these wavefunctions.

A number of results relating compact support localization of Wannier functions in tight-binding models and topological triviality of associated bands are relevant to the cases considered in this paper. Specifically, it was proved that flat bands in 2d flat-bands Hamiltonians which are strictly local in a tight-binding sense always have a Chern number of zero [30]. This property can be viewed as arising due to the fact that the flat bands in such models are spanned by compactly supported Wannier-type functions or CLSs. More recently, this

result was generalized to all symmetry classes and arbitrary dimensions greater than one, by proving that the vector bundle associated with band(s) which are spanned by CS Wannier-type functions are topologically trivial [29]. As discussed in section 2.3.2, CS Wannier-type functions are in general non-orthogonal, and consequently the orthogonal Wannier functions we consider in this paper are a special type of CS Wannier-type functions. Similarly, the set of SL projectors is a subset of the set of projectors that have their images spanned by CS Wannier-type functions. Thus, it follows directly from the results in [29] that:

Theorem 3. *For translationally invariant tight-binding models in $d > 1$, a set of bands that is spanned by compactly supported Wannier functions is topologically trivial. More generally, bands associated with strictly local projectors are topologically trivial.*

It follows that translationally invariant NN and NN-reducible projectors are topologically trivial, since they are SL.

While a topological obstruction exists for constructing localized Wannier functions, no such obstruction exists for localized hybrid Wannier functions. Since hybrid Wannier functions can be treated as 1d Wannier functions (see section 2.5.1), using the arguments in [20], it follows that for any number of dimensions, hybrid Wannier functions that are exponentially localized along the localized axis exist, independent of the topological properties of the associated band(s). For example, as can be seen using the Coulomb gauge, quantum Hall systems admit localized hybrid Wannier-like solutions that are exponentially decaying along one direction, despite the Chern number being non-zero [1]. Similarly, anomalous quantum Hall systems possess maximally localized hybrid Wannier functions that are exponentially localized [49] despite a non-vanishing Chern number. These statements do no preclude the possibility of a topologically non-trivial band being spanned by compactly supported hybrid Wannier function. An interesting consequence of the theorem above, and the equivalence of strict localization of a projector, and the existence of CS hybrid Wannier functions along all axes, we find that such bands are *necessarily* topologically trivial. Specifically:

Theorem 4. *For a $d > 1$ dimensional system, if a set of bands is such that for any of*

the d orthogonal axes, there exist hybrid Wannier functions (spanning the bands) that are compactly supported along the chosen axis, then the band(s) are topologically trivial.

In this section, we have so far only considered systems which are translationally invariant. It would be interesting to study the topological properties of similar systems without translational invariance. For example, an analog of compactly supported hybrid Wannier functions could be a set of wavefunctions not related by lattice translations that are each compactly supported along one direction, but possibly delocalized along the other directions. We leave the question of topological triviality of such cases for future work.

Based on physical ground we anticipate that even non-translationally invariant SL projectors as well as bands associated with CSOBs should be topologically trivial. Using simple arguments applied to recent results from the literature, we will now show that the latter statement is indeed true. Specifically, we consider projectors that have no symmetries except possibly lattice translation symmetry, i.e. class A systems from the Altland-Zirnbauer classification scheme [67]. The topological classification of systems across all dimensions is organized in the form of a periodic table [68, 69]. As can be seen from the table, odd dimensional class A projectors are always K-theoretically trivial. However, in $2n$ dimensions, they are characterized by the integer valued n^{th} Chern number [70].

Using simple arguments, we will now show that the topological Chern invariant for class A projectors that are associated with CSOBs is zero.

Theorem 5. *In all dimensions, if a projector without symmetries (except possibly lattice translation symmetry) is such that its image is spanned by a compactly supported orthogonal basis, then it is Chern trivial.*

We only need to show that such projectors in even dimensions are Chern trivial. To that end, we use the real space expression from [70], for the integer valued Chern number, which for a $2n$ dimensional system is given by

$$\text{Ind } P = -\frac{(2\pi i)^n}{n!} \sum_{\sigma} (-1)^{\sigma} \operatorname{Tr} P[\theta_{\sigma_1}, P] \dots [\theta_{\sigma_n}, P], \tag{2.34}$$

where Tr denotes the trace operation, the summation is over all permutations σ, and θ_i denotes the projection operator onto the positive half plane along the i^{th} direction, i.e. $\theta_i = \sum_\alpha \sum_{r_i>0} |\vec{r},\alpha\rangle \langle\vec{r},\alpha|$. Our arguments are based on the following properties of the index: (i) the additivity of the index for mutually orthogonal projectors, (ii) the independence of the index from the choice of the origin, or axes, and (iii) the local computability of the index. Physically, since the $2d$ case is of the most interest, we demonstrate our arguments by applying them to the 2d case. These arguments and the conclusion are valid for higher dimensional cases as well.

First, we note that for 2d, the index is the same as the Chern marker expression [71, 72], which is the real space analog of the k-space expression for Chern number used for periodic systems. The Chern marker for a projector P is given by

$$\mathrm{Ch}\, P = -2\pi i \,\mathrm{Tr}\, P[[\theta_x, P], [\theta_y, P]]. \tag{2.35}$$

As shown explicitly in [71], the Chern marker is additive, i.e. Chern marker of the sum of two mutually orthogonal projectors is the sum of the Chern markers of the two projectors.

Consider a CSOB of size R, consisting of wavefunctions $|\psi_i\rangle$. Let P be the orthogonal projector onto the span of the CSOB. Clearly, P is SL, and is the sum of the orthogonal projection operators P_i projecting onto states $|\psi\rangle_i$'s:

$$\begin{aligned} P &= \sum_{i=1} P_i; \\ \text{with } P_i &= |\psi_i\rangle \langle\psi_i|, \\ P_i P_j &= \delta_{ij} P_i. \end{aligned} \tag{2.36}$$

By definition, each wavefunction $|\psi_i\rangle$ has non-zero support only within a circle B_i centered at some location $\vec{c}_i$ of radius R. (The $\vec{c}_i$'s are not unique; however, the conclusions that follow do not depend on the choice.) Thus, each projector P_i has non-zero hopping terms only within B_i.

From (2.35), we note that $\mathrm{Ch}\, P_i \neq 0$ only if $|\psi_i\rangle$ straddles both the axes, i.e. if $|\vec{c}_i| \leq R$, and is zero otherwise. For example, if B_i lies entirely in the right half plane, then the

operator θ_x can be replaced by the identity operator in equation (2.35), resulting in a zero Chern marker (and similarly for other cases). Using this, and the additivity of the Chern marker, we obtain

$$\mathrm{Ch}\, P = \mathrm{Ch}\, (\underbrace{\sum_{|\vec{c}_i| \leq R} P_i}_{\tilde{P}}) + \mathrm{Ch}(\sum_{|\vec{c}_i| > R} P_i) = \mathrm{Ch}\, \tilde{P}.$$

(For a cartoon picture see figure 2.13.) Since the Chern number is independent of the choice of the origin, we may shift the origin and reevaluate the Chern number without affecting its value. Consider moving the origin by a distance of at least $2R$ in any direction. For example, let the new location of the origin be $(-3R, -3R)$. Since none of the constituent wavefunctions of $\tilde{P}$ straddle both of the new axes, $\mathrm{Ch}\, \tilde{P} = 0$. Consequently,

$$\mathrm{Ch}\, P = 0.$$

The Chern marker is additive in all dimensions. Thus, applying the same reasoning to equation (2.34), it is easy to show that projectors associated with CSOBs are Chern trivial in all dimensions.

2.6 Conclusions

In this paper, we have obtained necessary and sufficient conditions for a band or a set of bands to be spanned by compactly supported Wannier functions, or in the absence of lattice translational invariance, for a subspace of the Hilbert space to possess an orthogonal basis consisting of compactly supported wavefunctions. In 1d tight-binding models, we have established that there exists a compactly supported orthogonal basis spanning the occupied subspace iff. the corresponding projection operator is strictly local. In the process, we presented an algorithm for constructing a compactly supported orthogonal basis for the image of any strictly local projector. This algorithm generates wavefunctions having a maximum spatial extent three times the maximum hopping distance of the projector. Nearest neighbor projectors on a Bethe lattice with arbitrary coordination number also have a compactly supported orthonormal basis.

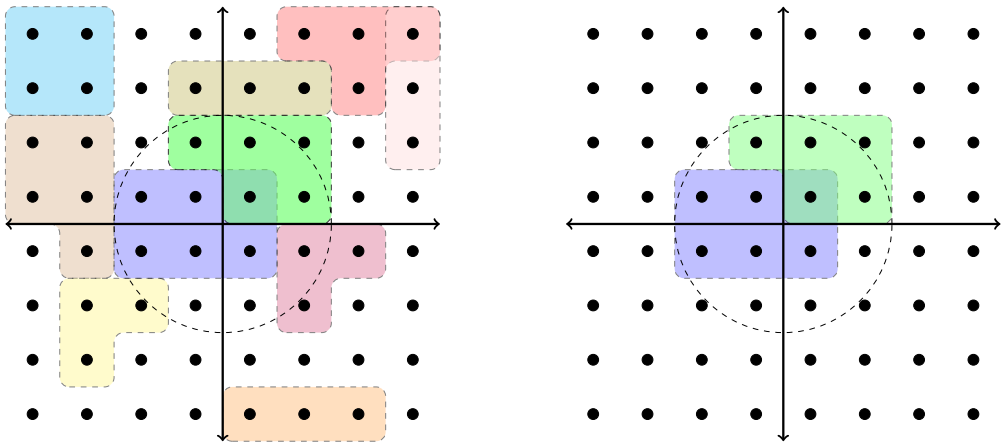

(a) (b)

Figure 2.13: An illustrative example in 2d. (a) Each basis state $|\psi_i\rangle$ of a CSOB of size $R = 2$ is shown by a colored region, and has non-zero support only on the sites within that region. (b) Only those wavefunctions that have their centers $\vec{c}_i$'s inside the dashed circle have non-zero contributions to the Chern marker. Retaining only these wavefunctions defines a new projector $\tilde{P}$, which has the same Chern number as P.

For higher dimensional lattices, we showed that while strict locality of the projector is a necessary condition for the existence of a compactly supported orthogonal basis, a sufficient condition is that the projector be expressible as a nearest neighbor projector using a change of primitive cell vectors or a supercell representation. For such projectors, which we call nearest neighbor reducible, we presented an algorithm for constructing a compactly supported orthogonal basis, or a compactly supported Wannier basis when translationally invariant. Additionally, we showed hybrid Wannier functions that are compactly supported can be constructed for any choice of the localization axis iff. the associated projector is strictly local. Since the localization properties of band projectors and Wannier functions are closely related to band topology, we also showed that all translationally invariant strictly local projectors in systems with dimensions two and higher are topologically trivial. Additionally, using some simple arguments, we have shown that projectors without any symmetry other than possibly lattice translation symmetry, that are associated with compactly supported orthogonal bases are Chern trivial. Moreover, the existence of hybrid Wannier functions

that are compactly supported along the localized axis for any choice of the localized axis implies topological triviality, unlike exponentially localized hybrid Wannier functions, which can exist even for topologically non-trivial bands.

Our results suggest a number of interesting directions for future work. The compactly supported orthogonal bases resulting from our construction may not be maximally localized. It would be interesting to improve the bounds on the spatial support of these basis functions, and also formulate an analytic procedure which results in maximally localized orthogonal basis functions. In the case of translationally invariant projectors, our procedures generate Wannier bases in supercell representations. A natural follow-up would be to find minimal sized supercell representations which have compactly supported Wannier bases. Here, we have shown that a strictly local projector and a compact orthonormal basis are essentially equivalent on 1d lattices. For dimensions two and higher, it would be useful to identify locality conditions on the projector operator that are equivalent to the existence of a compactly supported orthogonal basis. It would also be interesting to prove or disprove the topological triviality of strictly local projectors in arbitrary dimensional systems in the absence of lattice translational invariance.

APPENDIX

2.A Compactly Supported Wannier Functions for an Example Hamiltonian

In this section, we discuss an example of an SL projector in 1d, and compare our results with numerical techniques from the literature. To our knowledge, there are no simple methods in the literature of proving that the span of generic SL projectors possess a compactly supported orthogonal basis (CSOB). Here, we consider the following example of a 1d two-band (translationally invariant) Hamiltonian given in k-space by

$$\begin{aligned} H(k) &= \frac{1}{6}\begin{pmatrix} h_{11} & h_{12} \\ h_{21} & h_{22} \end{pmatrix}, \\ \text{with } h_{11} &= 3\sin k + \cos k\left(2\sqrt{2}\cos k - 2\sqrt{2}\sin k + 8\sqrt{2} + 3\right), \\ h_{12} &= (\cos k - \sin k + 4)\left(i - 2\sqrt{2}\sin k\right), \\ h_{21} &= -(\cos k - \sin k + 4)(i + 2\sqrt{2}\sin k), \\ h_{22} &= (\cos k + 2)(3 - 2\sqrt{2}\cos k) + (2\cos k\sqrt{2} + 3)(\sin k - 2). \end{aligned} \tag{2.37}$$

The two energy bands of this Hamiltonian are $E_1(k) = 2 + \cos k$, and $E_2(k) = -2 + \sin k$. The band projector corresponding to the E_1 band is given by

$$P(k) = \frac{1}{6}\begin{pmatrix} 2\cos(k)\sqrt{2} + 3 & i - 2\sqrt{2}\sin(k) \\ -i - 2\sqrt{2}\sin(k) & 3 - 2\sqrt{2}\cos(k) \end{pmatrix}, \tag{2.38}$$

which is an SL projector. Since the projector is translationally invariant, we seek a Wannier basis. Our theorem implies that there exist CS Wannier functions spanning each of the two bands in a size-two supercell representation.

Usually, Wannier functions are computed by first obtaining the corresponding Bloch wavefunctions. For the example projector, the Bloch wavefunction (upto a phase) is

$$\psi_1(k) = \frac{1}{\sqrt{6}}\begin{pmatrix} \frac{2\sqrt{2}\sin(k) - i}{\sqrt{3 - 2\sqrt{2}\cos(k)}} \\ -\sqrt{3 - 2\sqrt{2}\cos(k)} \end{pmatrix}. \tag{2.39}$$

A corresponding Wannier basis is then obtained through a Fourier transform of the Bloch wavefunction. Specifically, a Wannier function $w_1^R(z)$ localized at cell R can be obtained using

$$w_1^R(z) = \frac{L}{2\pi} \int_{-\pi}^{\pi} dk e^{ik(R-z)} \psi_1(k), \tag{2.40}$$

where L is the system size. Since $\psi_1(k)$ is a smooth function of k, the corresponding Wannier function is exponentially localized (see figure 2.14). However, Wannier functions are not unique, because of a gauge degree of freedom:

$$\psi_1(k) \to e^{i\theta(k)} \psi_1(k).$$

A more localized Wannier basis can be obtained by using a 'better' gauge $\theta(k)$.

While it is not the objective of this paper to obtain maximally localized Wannier functions (MLWFs) for SL projectors, it is useful to compare our approach with the MLWF procedure [20]. The k-space MLWF procedure converges to the optimal gauge using a gradient descent procedure on an initial 'guess' Wannier basis. While our numerical experiments indicate that the MLWF procedure generates compactly supported Wannier functions (which are usually different from the ones obtained using procedure 2), they do not guarantee the existence of compactly supported Wannier functions for arbitrary SL projectors. In contrast, our procedure is analytical, and generates wavefunctions which are exactly compactly supported.

For non-translationally invariant projectors, a notable point of similarity between the MLWF procedure and our approach is the starting point which involves choosing 'trial orbitals' on which the projector is operated. In both procedures, the post-projection wavefunctions are orthonormalized (followed by gradient descent in the case of the MLWF algorithm). While the MLWF procedure uses the Lowdin (i.e. symmetric) orthogonalization procedure [59], we use the Gram-Schmidt procedure. This is intentional: the Lowdin procedure is applicable only if the set to be orthogonalized is linearly independent, while the Gram-Schmidt procedure lacks this restriction. Hence, for generic SL projectors, the real space MLWF procedure requires suitably chosen trial orbitals. While such a choice may exist,

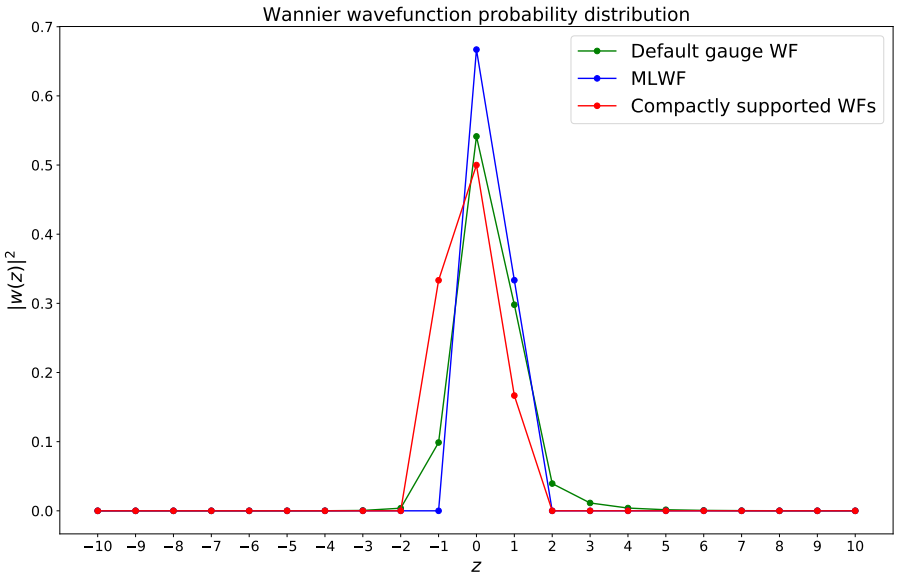

Figure 2.14: Wannier functions (WFs) centered at $R = 0$, corresponding to three different gauge choices and corresponding to the span of (2.38) are shown. The wavefunction probability is plotted a function of position. Green: Numerically obtained Wannier function corresponding to (2.39) is exponentially localized. Blue: Numerically obtained MLWF is compactly supported upto numerical precision. Red: The two compactly supported Wannier functions obtained analytically using algorithm 2 in a size 2 supercell representation have the same probability distribution in the primitive cell representation.

we are not aware of a general method for obtaining one for arbitrary SL projectors. A much simpler approach (which we adopt) is to choose all the orbitals $|\vec{r}, n\rangle$ as trial orbitals. The set $\Pi^P_{\vec{r}}$ (defined in (2.3)) which is generally linearly dependent can then be orthonormalized using the Gram-Schmidt procedure.

CHAPTER 3

Compact Wannier functions in One Dimension

This chapter has been adapted from the preprint (Ref. [73])[1]:

Pratik Sathe, and Rahul Roy. "Compact Wannier Functions in One Dimension." arXiv preprint arXiv:2302.11608 (2023).

3.1 Abstract

Wannier functions have widespread utility in condensed matter physics and beyond. Topological physics, on the other hand, has largely involved the related notion of compactly-supported Wannier-*type* functions, which arise naturally in flat bands. In this work, we establish a connection between these two notions, by finding the necessary and sufficient conditions under which compact Wannier functions exist in one dimension. We present an exhaustive construction of models with compact Wannier functions and show that the Wannier functions are unique, and in general, distinct from the corresponding maximally-localized Wannier functions.

[1]The following acknowledgement appeared in the original manuscript: We thank Adrian Culver, Dominic Reiss, Steven Kivelson and Bartholomew Andrews for discussions, and Fenner Harper for collaboration on a related project. We acknowledge financial support from the University of California Laboratory Fees Research Program funded by the UC Office of the President (UCOP), grant number LFR-20-653926. P.S. acknowledges financial support from Bhaumik Graduate Fellowship (UCLA).

3.2 Introduction

Wannier functions find applications in almost all areas of condensed matter physics. In addition to providing a formal justification for the tight-binding approach [5], they help in understanding a broad range of properties of crystalline materials (see Ref. [74] and the references therein).

Maximally-localized Wannier functions are often used as a starting point in numerical studies [20, 75]. The localization properties of Wannier functions also have a direct bearing on the topological properties of electronic bands [45, 76, 77, 78, 79]. Exponentially-localized Wannier functions can be constructed if and only if the Chern number and Hall conductivity of the corresponding filled band(s) are zero [45, 48, 46]. An even stronger form of localization is compact support, a property of 'compactly-supported Wannier-type functions', which feature in topological no-go theorems [30, 28, 29].

Compactly-supported Wannier-type functions necessarily exist in bands which are completely flat. Flat-band Hamiltonians have attracted a lot of recent attention [31]. They can host a variety of interesting phases, from the extensively studied integer and fractional quantum Hall effects in Landau levels [1] to more recent examples such as unconventional superconductivity in bilayer graphene [80, 81, 32, 33, 82, 83, 84] and fractional Chern insulators [85, 86, 87]. Consequently, a substantial body of work focuses on systematically constructing flat-band models [35, 36, 88], often exploiting compactly-supported Wannier-type functions, which are commonly also known as compact localized states. When such wavefunctions form an orthogonal basis (a situation arising for example when all bands are flat [89, 90, 91], or otherwise [38]), the corresponding projector is Chern trivial regardless of lattice periodicity [10, 92].

Compactly-supported Wannier-type functions, in general, are not orthogonal, and are therefore not truly Wannier functions (which are orthogonal). In this work, we relate these two concepts and identify the necessary and sufficient conditions required for the existence of compactly supported Wannier functions (or compact Wannier functions in short) in one

dimension, i.e. Wannier functions that vanish outside a finite region of the lattice. Building on previous work [10], we show that compact Wannier functions (CWFs) can be constructed if and only if the band projector (or equivalently the appropriate single particle Green's function) is strictly local (SL). Our proof leads us to an exhaustive construction in 1d of all possible models that have CWFs, and thus also of SL projectors. We also show that CWFs are unique when they span a single band while CWFs that span multiple bands together are not unique. Finally, we relate compact Wannier functions to compactly supported Wannier-type functions by showing that the latter must be the same as the former when the former exist.

Contrary to the intuition that compact localization is a stronger form of localization than exponential localization, we show that maximally-localized Wannier functions (MLWFs) are generally *not* compactly supported but are exponentially localized instead, even when CWFs can be constructed. However, for nearest-neighbor-hopping projectors, we show that the MLWFs are compactly supported, and provide a construction to obtain such wavefunctions. For systems without lattice translational invariance (LTI), we extend this construction to obtain generalized Wannier functions [93]. Using this method, we show how to obtain an orthogonal basis of compactly-supported wavefunctions that spans the image of a non-LTI strictly local projector, with the size of each wavefunction being twice the maximum hopping range of the projector.

3.3 Setup and Notation

We consider 1d models expressed in tight-binding representations so that single particle operators are represented by matrices with rows and column labeled by two indices each: an integer-valued position index x, and an orbital index $i = 1, \ldots, n$.

A compact (i.e. compactly supported) wavefunction is one with non-zero support only on a finite region of the lattice. We refer to the length of that region as the size of the wavefunction. We also consider orthogonal projectors (i.e. operators satisfying $P = P^\dagger =$

P^2), and call a projector P strictly local (SL) if $\langle x_1, i| P |x_2, j\rangle = 0$ whenever $|x_1 - x_2| > R$ for some finite integer R. We call the smallest value of R the maximum hopping range of the projector. For finite systems, this terminology is meaningful only if R is less than the system size. Our methods and results apply to finite as well as infinite systems. For simplicity of notation, we will work with the latter.

3.4 Equivalence of compact Wannier functions and strictly local projectors

In Ref. [10], it was shown by construction that strict locality (SL) of 1d projectors is equivalent to the existence of an orthogonal basis of compactly-supported wavefunctions. For projectors with lattice translational invariance (LTI) however, the method of construction did not always result in Wannier functions.

We will now show that in LTI systems, strict locality of a projector is equivalent to the existence of CWFs corresponding to the band(s). First, we note that if a set of CWFs spans a set of $s \geq 1$ bands, then the corresponding projector P is SL. This follows from the fact that $P(k) = \sum_i^s |\psi_i(k)\rangle \langle\psi_i(k)|$, where $|\psi_1(k)\rangle, \ldots, |\psi_s(k)\rangle$ are the Fourier representations of distinct CWF flavors. Clearly, $P(k)$ has matrix elements that are all Laurent polynomials (i.e. Laurent series with finite number of terms) in e^{ik}. The proof of the converse is more subtle as we will now see.

Consider an SL projector with maximum hopping range $R \geq 1$. (The case $R = 0$ is trivial, since P can be diagonalized with an intra-cell rotation thus giving us compact Wannier functions.) In $k-$space, it corresponds to a projection matrix $P(k)$ with elements that are Laurent polynomials in e^{ik} with degrees $\leq R$. Each step of our iterative procedure implements an SL unitary rotation $U_r(k)$ that reduces the maximum hopping range of the projector by 1.

We will now discuss the iterative step. Consider an intermediate step, at the start of which we have a projector $P^{(r)}$ that has a maximum hopping range r with $R \geq r \geq 1$. Note

that $P^{(r)}$ can be expressed as

$$P^{(r)}(k) = P_0 + \sum_{m=1}^{r} \left(P_m e^{ikm} + P_m^\dagger e^{-ikm} \right), \tag{3.1}$$

First, we obtain a singular value decomposition (SVD) of P_r, which we conveniently write as

$$P_r = \sum_{\sigma \neq 0} \sum_{i=1}^{n_\sigma} \sigma \left| \psi_{\sigma,i} \right\rangle \left\langle \phi_{\sigma,i} \right|. \tag{3.2}$$

σ denotes the non-zero singular values, and n_σ denotes the degeneracy of σ. By construction, all the ψ's are mutually orthogonal, and so are the ϕ's.

We note that $P_r^2 = 0$, which follows from $(P^{(r)})^2 = P^{(r)}$, and (3.1). Squaring (3.2) and using $P_r^2 = 0$, we conclude that $\langle \psi_{\sigma,i} | \phi_{\sigma',j} \rangle = 0$. Therefore, the set S of all ϕ's and ψ's together is a set of orthonormal wavefunctions. If $|S| < n$ (the number of orbitals per cell), then one can obtain enough wavefunction $\{|\mu\rangle\}$ such that together with S, they form an orthogonal basis for the orbital space $\mathcal{H}$.

We now implement a unit cell redefinition, so that all the ϕ wavefunctions at cell $x-1$, and all the ψ and μ wavefunctions at cell x together are grouped into a new cell at x. This corresponds to a unitary transformation U_r, given by

$$U_r(k) = \sum_{\phi} e^{-ik} \left| \phi \right\rangle \left\langle \phi \right| + \sum_{\psi} \left| \psi \right\rangle \left\langle \psi \right| + \sum_{\mu} \left| \mu \right\rangle \left\langle \mu \right|, \tag{3.3}$$

with $\sum_\psi$ and $\sum_\phi$ being shorthands for $\sum_{\sigma \neq 0} \sum_{i=1}^{n_\sigma}$. In this new basis, $P^{(r)}$ transforms to $P^{(r-1)} = U_r^\dagger P^{(r)} U_r$ (which is also a projection matrix), and has a maximum hopping range of $r-1$, as we will show below.

Before proceeding, let us introduce some useful notation. We find it convenient to represent the Hilbert space $\mathcal{H}_{\text{total}}$ in two forms, (1) as a tensor product of the position space and the orbital space $\mathcal{H}$, and (2) as a direct sum of spaces at each cell as follows:

$$\begin{aligned} \mathcal{H}_{\text{total}} &= \mathbb{Z} \otimes \mathcal{H}, \\ \mathcal{H}_{\text{total}} &= \bigoplus_{x \in \mathbb{Z}} \mathcal{H}^x, \end{aligned} \tag{3.4}$$

where $\mathcal{H}$ denotes the n dimensional orbital space, while $\mathcal{H}^x$ denotes the Hilbert space at cell x. (The expressions can be suitable modified for finite systems.)

At the start of an intermediate step of the procedure, let the projector have a maximum hopping range $r \geq 1$, and be denoted by $P^{(r)}$. Hence, in $k-$space, we can write $P^{(r)} = P_0 + \sum_{m=1}^{r} P_r e^{ikr} + P_r^\dagger e^{-ikr}$. We first compute an SVD of P_r:

$$P_r = \sum_{\sigma \neq 0} \sum_{i=1}^{n_\sigma} \sigma \left|\psi_{\sigma,i}\right\rangle \left\langle \phi_{\sigma,i}\right| . \tag{3.5}$$

It follows from $P_r^2 = 0$ that all ϕ's and ψ's are mutually orthogonal. If the total number of these wavefunctions is less than n, the number of orbitals per cell, then one can straightforwardly obtain a set of wavefunction $\{|\mu\rangle\}$ which completes the basis for $\mathcal{H}$ (i.e. the orbital space).

Now consider the unitary rotation

$$U_r(k) = \sum_{\sigma \neq 0} \sum_{i=1}^{n_\sigma} e^{-ik} \left|\phi_{\sigma,i}\right\rangle \left\langle \phi_{\sigma,i}\right| + \sum_{\sigma \neq 0} \sum_{i=1}^{n_\sigma} \left|\psi_{\sigma,i}\right\rangle \left\langle \psi_{\sigma,i}\right| + \sum_{\mu} \left|\mu\right\rangle \left\langle \mu\right| . \tag{3.6}$$

This is equivalent to first implementing an intra-cell rotation followed by a unit-cell redefinition.

In the new basis, the projector is represented by the matrix $U_r(k)^\dagger P(k) U_r(k)$. Clearly, all the matrix elements of $U_r(k)^\dagger P(k) U_r(k)$ are Laurent polynomials in e^{ik}. We will now show that the degree of each polynomial in $U_r(k)^\dagger P(k) U_r(k)$ is less than r.

The calculation below is straightforward to carry out in the general case with multiple, possibly degenerate σ's. For notational simplicity, we will go through the calculation only for the case with a single non-zero σ, with no degeneracy. This allows us to safely drop the subscripts σ, i for ψ and ϕ and proceed with a much simpler notation. We then have

$$P_r = \sigma \left|\phi\right\rangle \left\langle \psi\right| , \tag{3.7}$$

$$\text{and } U_r(k) = e^{-ik} \left|\phi\right\rangle \left\langle \phi\right| + \left|\psi\right\rangle \left\langle \psi\right| + \sum_{\mu} \left|\mu\right\rangle \left\langle \mu\right| \tag{3.8}$$

It is straightforward to show that the coefficients of all powers greater than r of e^{ik} in

$U_r^\dagger(k)P(k)U_r(k)$ are 0. We will now show that the coefficient of e^{ikr} is also zero. We have:

$$\begin{aligned}
\text{Coefficient of } e^{ikr} \text{ in } U_r^\dagger(k)P(k)U_r(k) = \text{Coefficient of } e^{ikr} \text{ in } & \\
& \left(e^{ik}\left|\phi\right\rangle\left\langle\phi\right| + \left|\psi\right\rangle\left\langle\psi\right| + \sum_\mu \left|\mu\right\rangle\left\langle\mu\right|\right) \\
& \times \left(P_0 + \sum_{m=1}^{r} P_m e^{ikm} + \sum_{m=1}^{r} P_m^\dagger e^{-ikm}\right) \\
& \times \left(e^{-ik}\left|\phi\right\rangle\left\langle\phi\right| + \left|\psi\right\rangle\left\langle\psi\right| + \sum_\mu \left|\mu\right\rangle\left\langle\mu\right|\right) \\
& = \underbrace{\left|\phi\right\rangle\left\langle\phi\right| P_r \left|\phi\right\rangle\left\langle\phi\right|}_{t_1} \\
& + \underbrace{\left(\left|\psi\right\rangle\left\langle\psi\right| + \sum_\mu \left|\mu\right\rangle\left\langle\mu\right|\right) P_r \left(\left|\psi\right\rangle\left\langle\psi\right| + \sum_\mu \left|\mu\right\rangle\left\langle\mu\right|\right)}_{t_2} \\
& + \underbrace{\left|\phi\right\rangle\left\langle\phi\right| P_{r-1} \left(\left|\psi\right\rangle\left\langle\psi\right| + \sum_\mu \left|\mu\right\rangle\left\langle\mu\right|\right)}_{t_3} \\
& = 0.
\end{aligned} \tag{3.9}$$

This is because, t_1, t_2 and t_3 above are all zero. That t_1 and t_2 vanish follows from (3.7) and the mutual orthogonality of $\left|\psi\right\rangle$, $\left|\phi\right\rangle$ and $\left|\mu\right\rangle$'s. t_3 can be seen to vanish because $\left\langle\phi\right| P_{r-1} \left|\mu\right\rangle = \left\langle\phi\right| P_{r-1} \left|\psi\right\rangle = 0$. To see this, note that for the case $r > 1$, equating the coefficients of $e^{i(2r-1)k}$ on both sides of $P(k) = P(k)^2$ gives us

$$\begin{aligned}
P_r P_{r-1} + P_r P_{r-1} &= 0, \\
\text{and thus } \left|\psi\right\rangle\left\langle\phi\right| P_{r-1} + P_{r-1} \left|\psi\right\rangle\left\langle\phi\right| &= 0.
\end{aligned} \tag{3.10}$$

Let $\left\langle\alpha\right| (\dots) \left|\beta\right\rangle$ denote left-multiplying by $\left\langle\alpha\right|$ and right-multiplying by $\left|\beta\right\rangle$ both sides of equation $(\dots)$. Then, we have

$$\begin{aligned}
\left\langle\phi\right| (3.10) \left|\phi\right\rangle &\implies \left\langle\phi\right| P_{r-1} \left|\psi\right\rangle = 0 \\
\text{and } \left\langle\psi\right| (3.10) \left|\mu\right\rangle &\implies \left\langle\phi\right| P_{r-1} \left|\mu\right\rangle = 0.
\end{aligned} \tag{3.11}$$

On the other hand, for $r = 1$, we have

$$\begin{aligned} P_0 P_1 + P_1 P_0 &= P_1 \\ \therefore P_0 \left|\psi\right\rangle \left\langle\phi\right| + \left|\psi\right\rangle \left\langle\phi\right| P_0 &= \left|\psi\right\rangle \left\langle\phi\right|, \end{aligned} \tag{3.12}$$

so that

$$\begin{aligned} \left\langle\phi\right| (3.12) \left|\phi\right\rangle &\implies \left\langle\phi\right| P_0 \left|\psi\right\rangle = 0 \\ \text{and } \left\langle\psi\right| (3.12) \left|\mu\right\rangle &\implies \left\langle\phi\right| P_0 \left|\mu\right\rangle = 0. \end{aligned} \tag{3.13}$$

Thus, in either case, $t_3 = 0$ and hence the largest positive power of e^{ik} with a non-zero coefficient in $P_1(k)$ is less than r. It follows similarly that all powers of e^{ik} that are $\leq (-r)$ are also zero, since $P(k)$ is a Hermitian matrix.

We have thus shown that the iterative step transforms an SL projector with a maximum hopping range r to a projector with a maximum hopping range of at most $r - 1$.

Thus, after at most R steps, the projector is an on-site hopping projector, so that one final k-independent rotation U_0 finally diagonalizes it. The total unitary transformation is

$$\begin{aligned} P(k) \to U^\dagger(k) P(k) U(k) &= \text{diag}(1, \ldots, 1, 0, \ldots, 0) \\ \text{with } U(k) &= U_R(k) \ldots U_1(k) U_0. \end{aligned} \tag{3.14}$$

All matrix elements of $U(k)$ are Laurent polynomials in e^{ik}. Hence, the inverse Fourier transforms of the columns of $U(k)$ corresponding to the 1 eigenvalues are CWFs spanning the bands corresponding to $P(k)$.

It is straightforward to show that the size of the CWFs can be at most $R + 1$ cells, if the projector has a maximum hopping range R. To that end, we note that each CWF obtained via the procedure described above is actually a bare orbital in the rotated basis determined by $U(k)$. A CWF in the original orbital basis can be obtained by implementing the rotations in reverse on a bare orbital. Since the application of each U_i increases the size of a wavefunction in position space by 1 cell, the CWFs cannot be larger than $R + 1$ cells. Additionally, at least one of the obtained CWF flavors must have a size of $R + 1$ cells.

(Otherwise, the maximum hopping range of the projector can be inferred to be less than R, which contradicts the assumption.)

Therefore, the procedure for obtaining CWFs from an SL projector, implemented in reverse, is a recipe for an exhaustive construction of CWFs as well as of SL projectors with LTI. For example, if one wants to construct an SL projector spanning a single band in a three band model, and which has a maximum hopping range of 2, then one can start with $\mathrm{diag}(1,0,0)$, and repeatedly transform it using intra-cell unitaries and unit-cell re-definitions.

In the absence of LTI, the crystal momentum k is no longer a good quantum number, and as a result, this procedure is not directly applicable. Nonetheless, an orthogonal basis of compact wavefunctions can be constructed for an SL projector without LTI, as shown in Sec 3.7.

3.5 Application of the Procedure to an Example Projector

In order to the procedure described above in action, we walk through its application for an example projector and show how to obtain the corresponding compact Wannier functions. Consider a strictly-local projector with a maximum hopping range of 2, that in k-space is represented by

$$P(k) = \begin{pmatrix} \frac{1}{3} + \frac{e^{-ik}}{6} + \frac{e^{ik}}{6} & -\frac{e^{-ik}}{6\sqrt{2}} + \frac{e^{-2ik}}{6\sqrt{2}} - \frac{1}{3\sqrt{2}} & \frac{e^{-ik}}{2\sqrt{6}} + \frac{e^{-2ik}}{2\sqrt{6}} \\ -\frac{e^{ik}}{6\sqrt{2}} + \frac{e^{2ik}}{6\sqrt{2}} - \frac{1}{3\sqrt{2}} & \frac{5}{12} - \frac{e^{-ik}}{6} - \frac{e^{ik}}{6} & \frac{1}{4\sqrt{3}} - \frac{e^{-ik}}{2\sqrt{3}} \\ \frac{e^{ik}}{2\sqrt{6}} + \frac{e^{2ik}}{2\sqrt{6}} & \frac{1}{4\sqrt{3}} - \frac{e^{ik}}{2\sqrt{3}} & \frac{1}{4} \end{pmatrix} \tag{3.15}$$

The coefficient of e^{2ik}, i.e. P_2 is

$$P_2 = \frac{1}{6\sqrt{2}} \begin{pmatrix} 0 & 0 & 0 \\ 1 & 0 & 0 \\ \sqrt{3} & 0 & 0 \end{pmatrix} \tag{3.16}$$

An SVD of P_2 can be conveniently written as:

$$\begin{aligned} P_2 &= \frac{1}{3\sqrt{2}} |\psi\rangle \langle\phi| \\ \text{with } |\psi\rangle &= \frac{1}{2}\begin{pmatrix} 0 & 1 & \sqrt{3} \end{pmatrix}^T, \\ |\phi\rangle &= \begin{pmatrix} 1 & 0 & 0 \end{pmatrix}^T \end{aligned} \tag{3.17}$$

To complete the basis for $\mathcal{H}$, we obtain $|\mu\rangle = \frac{1}{2}\begin{pmatrix} 0 & -\sqrt{3} & 1 \end{pmatrix}^T$. The first rotation according to the procedure is then $U_2(k) = e^{ik} |\phi\rangle \langle\phi| + |\psi\rangle \langle\psi| + |\mu\rangle \langle\mu|$ which in this case turns out to be $U_2(k) = \text{diag}(e^{-ik}, 1, 1)$. The projector after the rotation is represented by

$$\begin{aligned} P^{(1)} &= U_2^\dagger P U_2 \\ &= \frac{1}{6}\begin{pmatrix} e^{-ik} + e^{ik} + 2 & -\sqrt{2}e^{ik} + \frac{e^{-ik}}{\sqrt{2}} - \frac{1}{\sqrt{2}} & \sqrt{\frac{3}{2}} + \sqrt{\frac{3}{2}}e^{-ik} \\ -\sqrt{2}e^{-ik} + \frac{e^{ik}}{\sqrt{2}} - \frac{1}{\sqrt{2}} & -e^{-ik} - e^{ik} + \frac{5}{2} & \frac{\sqrt{3}}{2} - \sqrt{3}e^{-ik} \\ \sqrt{\frac{3}{2}} + \sqrt{\frac{3}{2}}e^{ik} & \frac{\sqrt{3}}{2} - \sqrt{3}e^{ik} & \frac{3}{2} \end{pmatrix}. \end{aligned} \tag{3.18}$$

As expected, all entries are Laurent polynomials with degrees less than or equal to 1. In the next step, we obtain an SVD of the P_1 corresponding to $P^{(1)}$:

$$\begin{aligned} P_1 &= \frac{1}{6}\begin{pmatrix} 1 & -\sqrt{2} & 0 \\ \frac{1}{\sqrt{2}} & -1 & 0 \\ \sqrt{\frac{3}{2}} & -\sqrt{3} & 0 \end{pmatrix}, \\ \text{which has an SVD given by } P_1 &= \frac{1}{2} |\psi\rangle \langle\phi| \\ \text{with } |\psi\rangle &= \frac{-1}{\sqrt{6}}\begin{pmatrix} \sqrt{2} & 1 & \sqrt{3} \end{pmatrix}^T, \\ |\phi\rangle &= \frac{1}{\sqrt{3}}\begin{pmatrix} -1 & \sqrt{2} & 0 \end{pmatrix}^T. \end{aligned} \tag{3.19}$$

The basis for $\mathcal{H}$ can be completed by adding the vector $|\mu\rangle = \begin{pmatrix} -\sqrt{2} & -1 & \sqrt{3} \end{pmatrix}^T$ to the set $\{|\phi\rangle, |\psi\rangle\}$. The second rotation, $U_1 = e^{-ik} |\phi\rangle \langle\phi| + |\psi\rangle \langle\psi| + |\mu\rangle \langle\mu|$ is then found to be

$$U_1 = \frac{1}{3}\begin{pmatrix} 2 + e^{-ik} & \sqrt{2}\left(1 - e^{-ik}\right) & 0 \\ \sqrt{2}\left(1 - e^{-ik}\right) & 1 + 2e^{-ik} & 0 \\ 0 & 0 & 3 \end{pmatrix}. \tag{3.20}$$

Implementing this rotation, we get

$$\begin{aligned} P^{(1)} \to P^{(0)} &= U_1^\dagger P^{(1)} U_1 \\ &= \frac{1}{12}\begin{pmatrix} 8 & -2\sqrt{2} & 2\sqrt{6} \\ -2\sqrt{2} & 1 & -\sqrt{3} \\ 2\sqrt{6} & -\sqrt{3} & 3 \end{pmatrix} \end{aligned} \tag{3.21}$$

The final step is diagonalizing $P^{(0)}$ with a unitary U_0:

$$\begin{aligned} P^{(0)} \to U_0^\dagger P^{(0)} U_0 &= \mathrm{diag}(1,0,0) \\ \text{with } U_0 &= \begin{pmatrix} \sqrt{\frac{2}{3}} & -\sqrt{\frac{3}{11}} & \frac{1}{3} \\ -\frac{1}{2\sqrt{3}} & 0 & \frac{2\sqrt{2}}{3} \\ \frac{1}{2} & 2\sqrt{\frac{2}{11}} & 0 \end{pmatrix} \end{aligned} \tag{3.22}$$

Thus, we have implemented a net unitary transformation $P \to U^\dagger P U = \mathrm{diag}(1,0,0)$, with $U = U_2 U_1 U_0$, given by

$$U = \begin{pmatrix} \frac{e^{-2ik}\left(1+e^{ik}\right)}{\sqrt{6}} & -\frac{e^{-2ik}\left(1+2e^{ik}\right)}{\sqrt{33}} & \frac{1}{3}e^{-2ik}\left(-1+2e^{ik}\right) \\ \frac{e^{-ik}\left(-2+e^{ik}\right)}{2\sqrt{3}} & -\sqrt{\frac{2}{33}}e^{-ik}\left(-1+e^{ik}\right) & \frac{1}{3}\sqrt{2}e^{-ik}\left(1+e^{ik}\right) \\ \frac{1}{2} & 2\sqrt{\frac{2}{11}} & 0 \end{pmatrix} \tag{3.23}$$

The family of Wannier function $\{|w\rangle_x | x \in \mathbb{Z}\}$ corresponding to P is obtained by simply taking the inverse Fourier transform of the first column of U. Clearly, $|w\rangle_x$ (up to lattice translation and phase re-definitions) is

$$|w\rangle_x = |x\rangle \otimes \begin{pmatrix} \frac{1}{\sqrt{6}} \\ 0 \\ 0 \end{pmatrix} + |x+1\rangle \otimes \begin{pmatrix} \frac{1}{\sqrt{6}} \\ \frac{-1}{\sqrt{3}} \\ 0 \end{pmatrix} + |x+2\rangle \otimes \begin{pmatrix} 0 \\ \frac{1}{2\sqrt{3}} \\ \frac{1}{2} \end{pmatrix} \tag{3.24}$$

As a corollary, we also obtain Wannier functions for $(1-P)$, which in this case are the inverse Fourier transforms of the second and third columns of (3.23).

3.6 Maximally-localized Wannier functions for strictly-local projectors

Maximally localized Wannier functions (MLWFs) are defined as Wannier functions that have the least quadratic spread in space [20, 74]. In 1d, MLWFs are eigenstates of the projected position operator, i.e. of $P\hat{x}P$ [20].

In 1d, it has been shown that MLWFs have tails that die off exponentially (or faster) [20]. Since CWFs are compactly supported thus having zero support outside of a finite region of the lattice, it might seem reasonable to assume that they are also maximally localized. We will now show that this is not the case. Specifically, even when a set of bands is spanned by CWFs (or equivalently, the projector is SL), the corresponding MLWFs need not be compactly supported.

To that end, we provide a simple representative example. Consider a two band model with one band that is spanned by a flavor of CWFs, with the CWF at location x being

$$\begin{aligned} |\psi_x\rangle = \frac{1}{\sqrt{6}}(\sqrt{2}\,|x,1\rangle - |x+1,1\rangle + \\ + |x+1,2\rangle + \sqrt{2}\,|x+2,2\rangle). \end{aligned} \tag{3.25}$$

Is it straightforward to express the $P\hat{x}P$ operator in terms of these wavefunctions. We find that

$$\begin{aligned} P\hat{x}P = \sum_x \Big((x+1)\,|\psi_x\rangle\langle\psi_x| \\ + \frac{1}{3\sqrt{2}}(|\psi_{x+1}\rangle\langle\psi_x| + |\psi_x\rangle\langle\psi_{x+1}|)\Big). \end{aligned} \tag{3.26}$$

The MLWFs are then a set, consisting of a wavefunction $|w_x\rangle$ which is a simultaneous eigenstate of $P\hat{x}P$ and P, and all its lattice translates. It is easy to see that no eigenstate of $P\hat{x}P$ (corresponding to a non-zero eigenvalue) can be compactly supported. (If that were the case, then $|w_x\rangle = \sum_{i=l}^{l+m} c_i\,|\psi_i\rangle$ for some c_i and finite l and $m > 0$. We then find that $P\hat{x}P\,|w_x\rangle$ has a larger spatial spread that $|w_x\rangle$, leading to a contradiction.)

Thus for this example, MLWFs are not compactly supported, even though a CWF basis spans the band. However, the MLWFs are exponentially localized, which also follows from

Ref. [20]. We expect that the behavior seen in this example applies more generally; in other words, that the numerical construction of MLWFs will result not in CWFs, but in exponentially decaying Wannier functions.

Even though CWFs are not always MLWFs, when a projector is nearest-neighbor hopping, the MLWFs are actually compactly supported. Furthermore, if such a projector does not have LTI, it is still possible to obtain 'generalized Wannier functions' [93], which are analogs of MLWFs. We will prove both these statements in the next section.

3.7 Maximally Localized Wannier Functions for Nearest Neighbor Projectors

We showed in section 3.4 that strict locality of projectors is equivalent to the existence of compactly-supported Wannier functions (CWFs) for systems with LTI. However, maximally-localized Wannier functions (MLWFs) corresponding to a strictly-local (SL) projector can be exponentially localized and not compact in some cases.

In this section, we will provide some key results for projectors that are nearest-neighbor (NN) hopping in one dimension, with or without LTI. Specifically, we will show that MLWFs for NN projectors are always compactly supported. We will provide a procedure for such a construction. In addition, we will show that even in the absence of LTI, one can construct analogs of MLWFs called generalized Wannier functions [93] for any NN projector. We highlight that the MLWFs and generalized Wannier functions have a size of 1 or 2 cell only. In either case, the obtained wavefunctions are eigenstates of $P\hat{x}P$.

The procedure for constructing $P\hat{x}P$ eigenstates for NN projectors without LTI is also applicable to NN projectors with LTI. However, for the latter, we desire to obtain a set of Wannier functions, which have the property that the set they form is invariant under any lattice translation operation. Hence, the procedure developed for non-LTI systems requires modifications in order to obtain MLWFs for LTI NN projectors. Hence we first present the procedure for NN projectors without LTI, followed by a presentation of the procedure for

NN projectors with LTI. Finally, we discuss how to extend these results to SL projectors with larger hopping ranges.

3.7.1 Nearest Neighbor Projectors without Lattice Translational Invariance

First we describe some notation and conventions. We will say that P 'connects' two orbitals if P has a non-zero matrix element between them. We find it convenient to define 'hopping matrices' as follows. For any cell x, hopping matrices P_i^x are defined as:

$$P_i^x \coloneqq \langle x+i| \, P \, |x\rangle \,, \tag{3.27}$$

thus being matrices of size $n \times n$, where n is the number of orbitals per cell. Since P is NN hopping, for each x only P_0^x and $P_{\pm 1}^x$ can be non-zero. Furthermore, $P_{-1}^{x+1} = (P_1^x)^\dagger$, since P is Hermitian.

The primary tool in our procedure is again the singular value decomposition (SVD). Given an NN projector P, our objective is to obtain eigenvectors of P that are also eigenstates of the $P\hat{x}P$ operator. To that end, we leverage the properties of various blocks in the matrix representation of P.

Our procedure is iterative, with each step resulting in an intra-cell unitary rotation. Each unitary rotation corresponds to a change of basis, and is accompanied by a reduction in the connectivity of the projector in the new basis. At the end of the procedure, we obtain states that are simultaneous eigenstates of P as well as $P\hat{x}P$. We will now present this procedure.

The first step is to diagonalize P_0^x for each x. Thus, at each cell x, we obtain an orthogonal basis $\{|x, \lambda_i\rangle\}$ comprising eigenvectors of P_0^x, that spans the local Hilbert space $\mathcal{H}^x$. Here, the index i distinguishes degenerate states (if λ is degenerate). For the steps that follow, we refer to orbitals as being the eigenvectors of the P_0^x matrices. When clear from the context, we will drop the position index and the degeneracy index if inessential.

We note that all eigenvalues of P_0^x matrices lie in $[0, 1]$. To see this, consider an eigenvector $|\lambda\rangle$ of P_0^x with eigenvalue λ. Then,

$$P_0^x = (P_0^x)^2 + (P_1^x)^\dagger P_1^x + P_1^{x-1}(P_1^{x-1})^\dagger$$

$$\begin{aligned} &\implies \lambda - \lambda^2 = ||P_1^x |\lambda\rangle||^2 + ||P_1^{x-1} |\lambda\rangle||^2 \\ &\implies \lambda - \lambda^2 \geq 0 \\ &\qquad \therefore 0 \leq \lambda \leq 1. \end{aligned} \tag{3.28}$$

Next, we note that P connects orbitals at adjacent cells only if their eigenvalues add to 1. In other words, $\langle x+1, \lambda'| P |x, \lambda\rangle = 0$, unless $\lambda + \lambda' = 1$. This follows from

$$\begin{aligned} &P_1^x = P_1^x P_0^x + P_0^{x+1} P_1^x \\ &\implies \langle\lambda'| P_1^x |\lambda\rangle = \langle\lambda'| P_1^x P_0^x |\lambda\rangle + \langle\lambda'| P_0^{x+1} P_1^x |\lambda\rangle \\ &\qquad \therefore 0 = (\lambda + \lambda' - 1) \langle\lambda'| P_1^x |\lambda\rangle . \end{aligned} \tag{3.29}$$

A corollary is that if they exist, $\lambda = 0$ states are annihilated by P, while $\lambda = 1$ states are eigenvectors of P with eigenvalue 1. Additionally, it follows that if P_0^x has an eigenvalue λ, then at least one of $P_0^{x\pm1}$ must have an eigenvalue of $1 - \lambda$. (Otherwise, we reach the contradiction that P has eigenvalues other than 0 and 1.)

With these properties at our disposal, we proceed to the next step, which is to obtain an SVD of all the P_1^x matrices simultaneously. Specifically, we will show that judicious unitary rotations at each cell can bring all the P_1^x matrices into diagonal forms simultaneously. We will show that such rotations can be obtained by implementing SVDs (with particular properties) of the P_1^x matrices sequentially. [At face value, it is not obvious that this can be done, because (for example) an SVD of P_1^x can interfere with an SVD of P_1^{x-1}, since the domain space and the target space respectively of the two are the same (i.e. $\mathcal{H}^x$).] To explain how this can be done, we first discuss properties of the SVD of a single P_1^x matrix.

First, we note that orbitals corresponding to $\lambda = 0$ and $\lambda = 1$ at x (when they exist) can be ignored, since P_1^x annihilates them. For eigenvalues $\lambda \neq 0$ or 1 of P_0^x, as noted before, P connects $|x, \lambda_i\rangle$ only to the $1 - \lambda$ orbitals at cells $x \pm 1$. Thus, P_1^x has a particular block structure, with non-zero blocks $P^x_{\lambda \to 1-\lambda}$ that connect the λ subspace at x to the $(1-\lambda)$ subspace at $x+1$. If $\mathcal{H}^y_\beta$ denotes the eigenvalue β subspace at cell y, then the block structure

of P_1^x can be inferred to be:

$$P_1^x = \begin{array}{c|ccccc} \mathcal{H}_\lambda^x & \dots & \mathcal{H}_\mu^x & \mathcal{H}_0^x & \mathcal{H}_1^x & \\ \hline \left(\begin{array}{c|ccccc} P^x_{\lambda\to 1-\lambda} & 0 & 0 & 0 & 0 \\ \hline 0 & \ddots & 0 & 0 & 0 \\ \hline 0 & 0 & P^x_{\mu\to 1-\mu} & 0 & 0 \\ \hline 0 & 0 & 0 & 0 & 0 \\ \hline 0 & 0 & 0 & 0 & 0 \end{array}\right) & \begin{array}{c} \mathcal{H}^{x+1}_{1-\lambda} \\ \vdots \\ \mathcal{H}^{x+1}_{1-\mu} \\ \mathcal{H}^{x+1}_1 \\ \mathcal{H}^{x+1}_0 \end{array} \end{array}, \tag{3.30}$$

where $\lambda, \dots, \mu$ denote the non-zero eigenvalues of P_0^x. [Note that it is possible for some eigenvalues to not be 'paired' in the matrix representation above. For example P_0^x may have an eigenvalue $\gamma \in (0,1)$, but it is possible for P_0^{x+1} to not have an eigenvalue of $1-\gamma$. Similarly, it is possible that there may not be a 0 or 1 eigenspace at x or $x+1$. In all such cases, the corresponding rows/columns should be understood as being absent in the block structure above.]

We exploit this block structure, and obtain an SVD of P_1^x by combining the SVDs of each of the blocks obtained independently. Thus, we can obtain unitary rotations within each λ subspace at x and each $1-\lambda$ subspace at $x+1$, so that (in the new basis) P_1^x connects every λ orbital at x with either zero, or exactly one 'partner' orbital corresponding to eigenvalue $1-\lambda$ at cell $x+1$. Henceforth, orbitals at x and $x+1$ will refer to these post-rotation orbitals.

Having implemented these rotations, let us now discuss how an SVD of P_1^{x-1} can be obtained without disturbing the partner structure between cells x and $x+1$. To that end, we first note that whenever orbital $|x,\lambda\rangle$ has a partner orbital $|x+1, 1-\lambda\rangle$, P does not connect $|x,\lambda\rangle$ with any orbital at cell $x-1$. (This follows from the fact that $P^2 = P$ is NN-hopping, so that $P_1^x P_1^{x-1} = 0$.) On the other hand, it also follows that if an orbital $|x,\lambda\rangle$ with $\lambda \neq 0, 1$ does not have a partner orbital at cell $x+1$, then $|x,\lambda\rangle$ must be connected to at least one orbital (which must have eigenvalue $1-\lambda$) at cell $x-1$, and thus P_1^{x-1} must have a block $P^{x-1}_{1-\lambda,\lambda}$ that connects these subspaces.

Thus, P_1^{x-1} maps the $1-\lambda$ orbitals at cell $x-1$ only onto those λ orbitals at x that do not have partner orbitals at $x+1$. Thus, an SVD of $P^{x-1}_{1-\lambda\to\lambda}$ can be obtained that leaves untouched the λ orbitals at cell x that have partners at $x+1$. Such an SVD also ensures that all the λ ($\neq 0,1$) orbitals at x now get exactly one partner state, either at $x+1$ or at $x-1$. [This along with (3.28) implies that the non-zero singluar values of $P^x_{\lambda,1-\lambda}$ are all equal to $\sqrt{\lambda(1-\lambda)}$.] Implementing such SVDs of all its blocks, we thus obtain an SVD for P_1^{x-1} which respects the SVD of P_1^x. In a similar fashion, one can obtain an SVD for P_1^{x+1} without disturbing the partner structure between cells $x-1$ and x.

The procedure ends when SVDs of all the P_1s are obtained sequentially following the prescription above. At the end of the procedure, the connectivity of the projector is greatly reduced in the rotated orbitals, and has the property that every $\lambda \neq 0,1$ orbital at a cell x is connected via P only to itself and exactly one partner orbital (with eigenvalue $1-\lambda$) either at cell $x-1$ or at $x+1$. On the other hand any orbital that corresponds to $\lambda = 0$ is annihilated by P, while $\lambda = 1$ orbitals are eigenvectors of P with eigenvalue 1. In this orbital basis, we straightforwardly obtain a generalized Wannier basis, i.e. an orthogonal basis of the image of P, with the property that each basis vector is also an eigenvector of $P\hat{x}P$.

Specifically, the basis consists of 'monomers', i.e. all the $\lambda = 1$ orbitals that exist, along with 'dimers', each of which is a linear combination of a λ orbital (for $\lambda \neq 0,1$), and its $(1-\lambda)$ partner orbital at a neighboring cell. For example, if orbital $|x,\lambda\rangle$ corresponding to eigenvalue $\lambda \neq 0,1$ of P_0^x has a partner orbital $|x+1,1-\lambda\rangle$ at cell $x+1$, then $P_1^x|x,\lambda\rangle = \sqrt{\lambda(1-\lambda)}\,|x+1,1-\lambda\rangle$. Thus, we can define a state $|w\rangle$ which is a simultaneous eigenstate of P and $P\hat{x}P$. Specifically,

$$\begin{aligned} |w\rangle &\coloneqq \sqrt{\lambda}\,|x,\lambda\rangle + \sqrt{1-\lambda}\,|x+1,1-\lambda\rangle\,, \\ \text{is s.t. } & P|w\rangle = |w\rangle\,, \\ \text{and } & P\hat{x}P|w\rangle = (x+1-\lambda)\,|w\rangle\,. \end{aligned} \tag{3.31}$$

The set of all such monomer and dimer states forms the set of generalized Wannier functions for P, since it spans the image of P, and consists of simultaneous eigenstates of P and $P\hat{x}P$.

3.7.2 Nearest Neighbor Projectors with Lattice Translational Invariance

We now return to the case of NN projectors with LTI. While the procedure for obtaining generalized Wannier functions also generates simultaneous eigenstates of P and $P\hat{x}P$ operators for LTI NN projectors, the obtained basis may not be Wannier functions, since they may lack the property of forming a set that is invariant under any lattice translation operation. We will now provide a modification that generates compact Wannier functions (which are also the maximally-localized Wannier functions).

First, we note that because of LTI, we have only two hopping matrices P_1 and P_0 [see (3.27)] that determine the projector, since $P(k) = P_0 + P_1 e^{ik} + P_1^\dagger e^{-ik}$. Additionally, many of the statements from the non-LTI case carry over. Since $P_0^\dagger = P_0$ and $P_0 = P_0^2 + P_1 P_1^\dagger + P_1^\dagger P_1$, eigenvalues of P_0 are real and lie in $[0, 1]$. As before, we diagonalize P_0 and obtain an orthonormal eigen-basis $\{|\lambda_i\rangle \mid \lambda \text{ is an eigenvalue of } P_0\}$ for the orbital space $\mathcal{H}$, with λs denoting P_0 eigenvalues and i distinguishing degenerate states. Until specified otherwise, from this point onwards, by orbitals, we will mean vectors from this basis.

Since $P_1 = P_1 P_0 + P_0 P_1$, we note that $\langle\mu| P_1 |\lambda\rangle \neq 0$ for $\lambda \neq 0, 1$ only if $\mu + \lambda = 1$. Thus, P connects orbitals λ and μ at neighboring cells only if the sum of the P_0 eigenvalues they correspond to add to 1. We also note that if P_0 has an eigenvalue $\lambda \neq 0, 1$, then it also must have an eigenvalue $1 - \lambda$. So, if n_λ denotes the multiplicity of eigenvalue λ, then for $\lambda \in (0, 1)$, $n_\lambda \neq 0 \iff n_{1-\lambda} \neq 0$. Therefore, P_1 has a block structure similar to (3.30).

Dropping all the position indices from (3.30), we can write it as

$$P_1 = \begin{array}{c|ccccccc} & \mathcal{H}_\lambda & \mathcal{H}_{1-\lambda} & \dots & \mathcal{H}_\mu & \mathcal{H}_{1-\mu} & \mathcal{H}_0 & \mathcal{H}_1 \\ \hline \mathcal{H}_\lambda & 0 & P_{(1-\lambda)\to\lambda} & 0 & 0 & 0 & 0 & 0 \\ \mathcal{H}_{1-\lambda} & P_{\lambda\to(1-\lambda)} & 0 & 0 & 0 & 0 & 0 & 0 \\ \vdots & 0 & 0 & \ddots & 0 & 0 & 0 & 0 \\ \mathcal{H}_\mu & 0 & 0 & 0 & 0 & P_{(1-\mu)\to\mu} & 0 & 0 \\ \mathcal{H}_{(1-\mu)} & 0 & 0 & 0 & P_{\mu\to(1-\mu)} & 0 & 0 & 0 \\ \mathcal{H}_0 & 0 & 0 & 0 & 0 & 0 & 0 & 0 \\ \mathcal{H}_1 & 0 & 0 & 0 & 0 & 0 & 0 & 0 \end{array} , \tag{3.32}$$

with $\lambda, \dots, \mu$ denoting eigenvalues of P_0 that lie in $(0, 0.5]$, and $\mathcal{H}_\lambda$ denoting the λ eigenspace. $\lambda = 1 - \lambda$ when $\lambda = 0.5$, so the two corresponding rows/columns collapse to one in this case. Rows (and columns) corresponding to eigenvalues that do not exist for a particular example should be understood as being absent in the representation above. Similarly to the procedure for the non-LTI projectors, we will obtain an SVD of the P_1 matrix by obtaining the SVDs of its various blocks.

Let us first consider the blocks corresponding to λ and $1-\lambda$ for $\lambda \in (0, 0.5)$. We start with an SVD of $P_{\lambda\to(1-\lambda)}$. If $|\lambda\rangle$ and $|1-\lambda\rangle$ are two vectors corresponding to a non-zero singular value σ so that $P_1 |\lambda\rangle = \sigma |1-\lambda\rangle$ and $P_1^\dagger |1-\lambda\rangle = \sigma |\lambda\rangle$, then $P_1 |1-\lambda\rangle = 0$ and $P_1^\dagger |\lambda\rangle = 0$. [This follows from $P^2 = P$ being an NN operator, so that $P_1^2 = (P_1^\dagger)^2 = 0$.] In position space, this means that P maps the span of $\{|x, \lambda\rangle, |x+1, 1-\lambda\rangle\}$ onto itself. Thus, such vectors are 'paired' with each other. As a consequence, $P_{(1-\lambda)\to\lambda}$ has possibly non-zero matrix elements only between vectors corresponding to zero singular values of $P_{\lambda\to(1-\lambda)}$. An SVD of $P_{(1-\lambda)\to\lambda}$ can thus be implemented via rotations affecting only these subspaces, leaving the subspaces of the paired vectors untouched. At the end of all these rotations, every λ orbital at a cell is connected to one and only one $1-\lambda$ ('partner') orbital at a neighboring cell, and similarly for $1-\lambda$. We note again that all the non-zero singular values of both $P_{(1-\lambda)\to\lambda}$ and $P_{\lambda\to(1-\lambda)}$ are equal to $\sqrt{\lambda(1-\lambda)}$. This follows from the equation $P_0 = P_0^2 + P_1^\dagger P_1 + P_1 P_1^\dagger$.

Let us now consider the case of $P_{0.5\to0.5}$. Suppose an SVD of this matrix is given by

$P_{0.5\to 0.5} = \sum_{\sigma\neq 0} \sigma \left|\psi_\sigma\right\rangle \left\langle\phi_\sigma\right|$. Since $P_1^2 = 0$, all the ψ and ϕ vectors are orthogonal to each other. Thus, the set of all $|\psi\rangle$s and $|\phi\rangle$s form an orthonormal basis of $\mathcal{H}_{0.5}$. (This is because if there were to exist any $|\mu\rangle \in \mathcal{H}_{0.5}$ orthogonal to both $|\phi\rangle$s and $|\psi\rangle$s, then we would find that $P_1 |\mu\rangle = P_1^\dagger |\mu\rangle = 0$, implying that $P |x, \mu\rangle = 0.5 |x, \mu\rangle$, which is impossible.) In addition, $P_0 = P_0^2 + P_1^\dagger P_1 + P_1 P_1^\dagger$ implies that every singular value $\sigma = \sqrt{0.5(1-0.5)} = 0.5$. Thus, in this basis for $\mathcal{H}_{0.5}$, each orbital has a partner orbital, so that for every partner pair ψ and ϕ, P maps the span of $\{|x, \phi\rangle, |x+1, \psi\rangle\}$ onto itself.

It is now straightforward to construct Wannier functions using these orbitals. For each eigenvalue $\lambda \in (0, 0.5]$ of P_0, every orbital $|\lambda\rangle$ is paired with exactly one orbital $|1-\lambda\rangle$. For every such pair, $\{\sqrt{\lambda} |x, \lambda\rangle + \sqrt{1-\lambda} |x+1, 1-\lambda\rangle |x\}$ forms one flavor of Wannier functions. Similarly, if an eigenvalue of 1 exists, every corresponding eigenvector and all its lattice translates form a flavor of Wannier functions. It is straightforward to see that all these wavefunctions are eigenstates of $P\hat{x}P$ as well, and are thus the maximally-localized Wannier functions (MLWFs) for the span of the projector.

3.7.3 Larger Hopping Range Projectors without Lattice Translational Invariance

For lattice translationally invariant (LTI) strictly-local (SL) projectors with maximum hopping range $R > 1$, as shown in Section 3.4, we can always construct CWFs spanning its image, with each wavefunction having a maximum size of no more than $R+1$. However, the technique is not applicable to projectors that are not LTI. In order to obtain an orthogonal basis of compact wavefunction for such projectors with a maximum hopping range R, we first consider a supercell representation, so that R cells in the original lattice are clubbed together to form one supercell. In the supercell representation, the SL projector is now an NN projector. We can now apply the procedures from the previous subsections, and obtain a basis that spans the image of P. Reverting back to the original (i.e. primitive cell) lattice representation, this basis is then an orthogonal basis of compactly-supported wavefunctions that spans the image of P. These wave-functions then have a maximum spatial extent of no

more than $2R$ cells.

3.8 Uniqueness of compact Wannier functions

We will now show that if a single band is spanned by CWFs $\{|\psi_x\rangle\,|x \in \mathbb{Z}\}$, then these CWFs form a unique set of Wannier functions (up to a phase) that are compactly supported for that band.

We prove this by contradiction. Suppose there exists another flavor of CWFs, $\{|\phi_x\rangle\,|x \in \mathbb{Z}\}$ that spans the band. Then every $|\phi_x\rangle$ can be expressed as a superposition of a finite number of $|\psi_y\rangle$'s, so that

$$|\phi_x\rangle = \sum_{k\leq i\leq l} c_i\,|\psi_{x+i}\rangle\,, \tag{3.33}$$

with integers k and l such that both c_k and $c_l \neq 0$. Since the ϕ's are Wannier functions, they are orthogonal to their translates. With T denoting translation by one unit cell, we thus have

$$\begin{aligned} 0 &= \langle\phi_x|\,T^{l-k}\,|\phi_x\rangle \\ &= \sum_{k\leq i,m\leq l} c_i^* c_m \delta_{i+k,m+l} \\ &= c_l^* c_k, \end{aligned} \tag{3.34}$$

which is impossible since both c_l and c_k are non-zero. Thus, every other WF of the band is a superposition of an infinite number of translates of $|\psi\rangle$'s, implying that CWFs for a single band are unique up to inconsequential phases.

In contrast, the CWFs for multiple bands are not unique, so that when a set of multiple bands are together spanned by a set of CWFs, one can generate many such sets. For example, if two band are together spanned by CWFs $\{|\psi_x\rangle\,|x \in \mathbb{Z}\} \cup \{|\phi_x\rangle\,|x \in \mathbb{Z}\}$, then $\{(|\psi_x\rangle + |\phi_x\rangle)/\sqrt{2} \mid x \in \mathbb{Z}\} \cup \{(|\psi_x\rangle - |\phi_x\rangle)/\sqrt{2} \mid x \in \mathbb{Z}\}$ forms a distinct set of CWFs spanning the same set of bands.

3.9 Uniqueness of compactly-supported Wannier-type functions for a strictly-local projector

Wannier-type functions are a generalization of Wannier functions, in that they form a possibly non-orthogonal or even an over-complete basis for a set of bands. The existence of compactly-supported Wannier-type functions (CWTs) implies topological triviality in dimensions $d > 1$ [29]. A flat band (in a lattice of any dimensionality) is spanned by such wavefunctions, which are called compact localized states or CLSs in that context [35], and are eigenstates of the Hamiltonian.

SL projectors can be associated with flat, i.e. dispersionless bands (for example, see Ref. [89, 91, 91]) as well as dispersive bands. However, not all flat-band projectors are strictly local, and in general one cannot construct CWFs for flat bands. (For a detailed discussion, see section 2 of Ref. [10]). Consequently, CLSs or CWTs are not, in general, expected to form an orthogonal basis.

We will now show that if a single flavor of CWTs spans a band described by an SL projector P, then the CWTs are actually the unique CWFs spanning the band. To that end, we will show that if a single flavor of CWTs spans a band, the CWTs form an orthogonal set of wavefunctions. In Fourier space, the CWTs, say $\{|\psi_x\rangle\,|x \in \mathbb{Z}\}$ each of size p, correspond to a possibly unnormalized, but non-vanishing Bloch-like wavefunction $|\psi(k)\rangle = \sum_{j=0}^{p-1} |\phi_j\rangle\, e^{ikj}$ (with $|\phi_0\rangle \neq 0$ and $|\phi_{p-1}\rangle \neq 0$). Thus, the band projector $P(k)$ can be expressed as $P(k) = \frac{\mathcal{P}(k)}{\mathcal{Q}(k)}$, with $\mathcal{P}(k) = |\psi(k)\rangle\langle\psi(k)|$ and $\mathcal{Q} = \langle\psi(k)|\psi(k)\rangle$. Each element of $\mathcal{P}$, and $\mathcal{Q}$ are then Laurent polynomials in e^{ik} with degrees at most $p-1$. Since each matrix element $\mathcal{P}_{ij} = \mathcal{Q}P_{ij}$, the degree of $\mathcal{Q}$ is $< p-1$ (or else, it equals $p-1$ and $P(k)$ has degree 0, in which case the problem is trivial and hence we will not discuss it further). Thus $\langle\phi_{p-1}|\phi_0\rangle = 0$, with both vectors being non-zero. One can thus iteratively implement unit-cell redefinitions similar to (3.3) with the identification $\phi_0 \to \phi$ and $\phi_{p-1} \to \psi$, and conclude that $U(k)\,|\psi(k)\rangle = \begin{pmatrix}1 & 0\ldots & 0\end{pmatrix}^T$, and therefore $|\psi(k)\rangle$ is normalized for all k after all. In other words, the CWTs are actually CWFs, and it then follows from the uniqueness of

CWFs that the CWTs are the unique CWFs. We note that a similar procedure was used in Ref. [91] for constructing compact localized states for Hamiltonians that only have flat bands.

3.10 Conclusions

Flat, or dispersion-less electronic bands in tight-binding models are spanned by compactly-supported Wannier-type functions, which in general can form a non-orthogonal set. In line with the localization-topology correspondence, their existence is known to be incompatible with topological non-triviality of the band(s) they span. Wannier-type functions are nevertheless not true Wannier functions. In one-dimensional models, we answered the question of when one can form compact Wannier functions from compact Wannier-type functions. We showed that the existence of compact Wannier functions is equivalent to the strict locality of the band projector (or the single-particle Green's function). We provided a method for constructing compact Wannier functions corresponding to a strictly-local projector. We also showed that they are unique if they span a single band, and furthermore, compactly-supported Wannier-type functions are equivalent to compact Wannier functions when the latter exist.

For bands spanned by compact Wannier functions, we showed that maximally-localized Wannier functions are in general exponentially localized and not compactly supported, except when the band projector is nearest-neighbor hopping. In the latter case, we presented a procedure for obtaining maximally-localized Wannier functions (generalized Wannier functions) for projectors with (without) lattice translational invariance. We also presented a method for constructing all possible 1d models that have compact Wannier functions, which we expect will find applications in the construction of flat-band models with a rich variety of applications in single-particle and many-particle physics.

A simple corollary of our work is that in higher dimensions, hybrid Wannier functions that are compactly supported along one direction can exist if and only if the band projector

is strictly local along that direction. While our methods do not directly apply to higher dimensions, they could conceivably be modified to identify conditions equivalent to the existence of compact Wannier functions in higher dimensions. A lot of our results and discussion can also be rephrased in terms of the single-particle Green's function which suggest generalizations to interacting systems.

CHAPTER 4

Flat Hamiltonians are Topologically Trivial

This chapter has been adapted from the following preprint (Ref. [94]) [1]:

Pratik Sathe, and Rahul Roy. "Topological Triviality of Strictly-Local Flat Hamiltonians." arXiv:2309.06487 (2023).

4.1 Abstract

Landau levels play a key role in theoretical models of the quantum Hall effect. Each Landau level is degenerate, flat and topologically non-trivial. Motivated by Landau levels, we study tight-binding Hamiltonians whose energy levels are all flat. We demonstrate that in two dimensions, for such Hamiltonians, the flat bands must be topologically trivial. To that end, we show that the projector onto each flat band is necessarily strictly local. Our conclusions do not need the assumption of lattice translational invariance.

4.2 Introduction

Topological phases of matter are a cornerstone of modern condensed matter physics. Beginning with the discovery of the quantum Hall effects (QHE) [95, 96], topology has played an important role in understanding and predicting novel phases of matter ranging from topo-

[1]The following acknowledgement appeared in the original manuscript: We thank Adrian Culver for providing helpful comments on the manuscript. P.S. and R.R. acknowledge financial support from the University of California Laboratory Fees Research Program funded by the UC Office of the President (UCOP), grant number LFR-20-653926. P.S. acknowledges financial support from the Center for Quantum Science and Engineering Fellowship (UCLA) and the Bhaumik Graduate Fellowship (UCLA).

logical insulators and superconductors to topologically ordered phases of matter [97, 98].

The Hall conductivity of a filled Landau level or a Bloch band is proportional to a topological invariant called the Chern number [99, 100, 101]. Much like Landau levels, a Bloch band that is flat or dispersionless and which has a non-zero Chern number can host fractional quantum Hall phases when subject to interactions. Such systems are known as fractional Chern insulators (FCIs) and hold significant experimental appeal since they have the potential to exhibit fractional QHE at small (or even zero) magnetic fields and high temperatures [102]. Consequently, a substantial amount of research has focused on the study of topological flat-band models (see Refs. [51, 86, 103] for reviews).

Hamiltonians with flat bands are also interesting because of numerous other phenomena they exhibit [31]. The effects of interactions are pronounced in flat-band Hamiltonians, and hence they serve as a platform to explore novel correlated phases of matter. In addition to FCIs, some prominent examples include unconventional superconductivity in bilayer graphene [32, 84, 81, 33], flat-band superfluidity [104, 105] and flat-band ferromagnetism [106].

Various no-go theorems restrict the possibility of topological flat bands. Strict localization of a band projector, a condition more restrictive than band flatness, was shown to imply a vanishing Hall conductance [76]. Further, if a strictly local (SL) Hamiltonian has a flat band, then it must have a Chern number of zero [30, 29]. These results apply to Hamiltonians with lattice translational invariance (LTI). It has also been shown that local commuting projector Hamiltonians cannot exhibit the QHE [92]. The non-interacting limit of such a model has a flat band which is spanned by an orthogonal basis of compactly supported wavefunctions [10, 73].

Non-interacting Hamiltonians that exclusively have flat bands, which we call flat Hamiltonians, have also attracted significant attention. Flat Hamiltonians can exhibit unconventional behavior when interactions are introduced. Some examples include many-body localization in translationally-invariant Hamiltonians [107, 108], non-linear caging [91, 109] and transport via two-particle bound states [110, 111]. Furthermore, the spectrum of a flat

Hamiltonian is similar to Landau levels since all the energies are flat and degenerate. Due to this resemblance, topological flat Hamiltonians that have SL hoppings seem to be particularly promising as platforms for fractional QHE. Indeed, many of the initial proposals for FCIs were Hamiltonians with all bands being approximately flat [112, 113, 114, 115].

In this Letter, we prove some unique properties of SL flat Hamiltonians with exactly flat bands and establish a no-go theorem. First, we show that the projection operators associated with all the flat bands in a SL flat Hamiltonian are also SL, regardless of lattice dimension or the system having LTI. Next, we show that the spectrum of such a Hamiltonian is unchanged even with twisted boundary conditions. By utilizing properties unique to SL projectors, we show that each flat band in a flat Hamiltonian has a Chern number of zero. (We compute the many-body Chern number defined in terms of the twist angles [100].) More generally, our statement applies to any Hamiltonian that has a highly degenerate spectrum, regardless of whether it has LTI. The no-go theorem is summarized below.

Theorem. *Consider a SL tight-binding Hamiltonian defined on a 2d system of size $L_x \times L_y$ cells with periodic boundary conditions. Let n denote the number of distinct energies and R denote the maximum hopping range of the Hamiltonian. If $L_{x,y} \geq 3nR$, then the Chern number associated with each energy is* 0.

We note that within the context of flat Hamiltonians with LTI, the inequality above is broadly satisfied. However, exotic models (such as those in Ref. [116] which have an extensive number of flat bands) that do not have this property can evidently be topological.

4.3 Notation and Setup

We consider 2d tight-binding Hamiltonians with orbitals $|\mathbf{r}, \alpha\rangle$ where $\mathbf{r} = (x, y)$ denotes cell position and $\alpha = 1, \ldots, N$ denotes different orbitals in a unit cell. We will restrict our discussion to systems that lie on a torus (i.e. those that satisfy periodic boundary conditions). Without loss of generality, we consider square lattices of size $L_x \times L_y$ with lattice constant 1.

The concepts of strict localization of operators and wavefunctions will play an important role in our arguments. A wavefunction is compactly supported if it has non-zero support only on a finite region of the lattice. On the other hand, an operator $\mathcal{O}$ in an infinite sized system is said to be strictly local (SL) if $\langle \mathbf{r}, \alpha | \mathcal{O} | \mathbf{r}', \beta \rangle = 0$ (for any α, β) whenever $|\mathbf{r} - \mathbf{r}'| > R$ for some finite number R. We call the smallest value of R for which this is true the maximum hopping range of the operator. For finite sized systems, this condition is satisfied by every operator. Therefore, we instead propose the following definition for finite-sized systems on a torus: an operator is called SL if it does not connect any two cells that are maximally separated from each other. This is equivalent to the conditions $2R + 2 \leq L_{x/y}$.

The central focus of this manuscript is on flat Hamiltonians, which we now define. We recall that in an infinite sized system, the spectrum of a Hamiltonian with LTI consists of a finite number of continuous bands following Bloch's theorem. The energy eigenvalues of a Hamiltonian on a finite system are necessarily discrete but are still arranged in the form of bands if the Hamiltonian is LTI. In particular, each band is spanned by Bloch wavefunctions at a set of discrete values of the crystal momentum that are equal in number to the system size. If a Hamiltonian with LTI only has flat bands, then we call it a flat Hamiltonian. Thus, each energy level has a degeneracy equal to the system size. In the case of Hamiltonians without LTI, we consider Hamiltonians that have a similar property of possessing highly degenerate energy levels. In a slight abuse of notation, we will refer to the distinct energy levels of such Hamiltonians as flat bands even in the absence of LTI. Regardless of LTI, all our results are derived for Hamiltonians and system sizes which satisfy $3nR \leq L_{x,y}$, where n denotes the number of distinct energies or flat bands, and R denotes the maximum hopping range of H. Strictly speaking, in addition to the condition $L_{x,y} \geq 3nR$, we also require that the Hamiltonian satisfy $L_{x,y} \geq 2nR + 2$ to ensure that all the projectors are SL. Except for the special (and uninteresting) case of $nR \in \{0, 1\}$, it is always true that $3nR \geq 2nR + 2$, so that we simply require $L_{x,y} \geq 3nR$.

Each energy eigenspace of a Hamiltonian may be associated with an orthogonal projector, i.e., a Hermitian operator P which satisfies $P^2 = P$. The locality properties of projectors

associated with energy eigenspaces will form an important part of our subsequent discussion.

We will also find it useful to use a simple kind of dimensional reduction. Specifically, any 2d SL operator can always be regarded as a 1d SL operator by grouping together all the lattice sites in every row (or column) into a single 1d lattice site. In particular, a 2d next-nearest-neighbor (NNN)-hopping projector P (i.e. one with $R = \sqrt{2}$) is also a nearest-neighbor (NN)-hopping projector (with $R = 1$) on a 1d lattice with one truncated dimension.

We will find it useful to define 'hopping matrices' for 1d SL projectors. Specifically, we define P_i^x for a SL projector P as follows:

$$P_i^x \coloneqq \langle x + i| \, P \, |x\rangle \, . \tag{4.1}$$

The number of rows or columns in this matrix is equal to the number of orbitals in each cell. We note that such hopping matrices can also be defined for 2d SL projectors by regarding them as 1d projectors using the dimensional reduction described above.

4.4 All Projectors of a Flat Hamiltonian are Strictly Local

Proposition: If a Hamiltonian is strictly local (SL), and has a finite number of distinct energies, then each of the projectors onto individual energies is also SL. Furthermore, if the maximum hopping distance of the Hamiltonian is r, and the number of distinct energies is n, then the maximum hopping distance of each of the band projectors cannot be more than rn.

Proof: Let H be the Hamiltonian, with a finite number of distinct energies $E_1, \ldots, E_n$, arranged in increasing order. Let the corresponding projectors be denoted by $P_1, \ldots, P_n$. Without loss of generality, all the energies can be chosen to be non-zero. (In case an energy is zero, one can always add a constant energy shift that makes all the energies non-zero. This has no effect on the projectors and hence our conclusions.)

We then find that

$$\begin{aligned} H &= \sum_{i=1}^{n} E_i P_i \\ H^2 &= \sum_{i=1}^{n} E_i^2 P_i \\ &\vdots \\ H^n &= \sum_{i=1}^{n} E_i^n P_i, \end{aligned} \tag{4.2}$$

where we have used the property $P_i^2 = P_i$ for every i.

Note that H^n has a maximum hopping distance no more than Rn. Hence, each of the operators $H, \ldots, H^n$ has vanishing matrix elements between any locations separated by a distance greater than Rn. Let $i \equiv (\vec{r}_1, \alpha)$ and $j \equiv (\vec{r}_2, \beta)$ label orbitals α and β at locations $\vec{r}_1$ and $\vec{r}_2$ satisfying $|\vec{r}_1 - \vec{r}_2| > Rn$. Equating the (i, j) matrix elements of both sides of equations (4.2) gives us

$$\begin{pmatrix} E_1 & E_2 & \ldots & E_n \\ E_1^2 & E_2^2 & \ldots & E_n^2 \\ \vdots & & & \vdots \\ E_1^n & E_2^n & \ldots & E_n^n \end{pmatrix} \begin{pmatrix} (P_1)_{i,j} \\ (P_2)_{i,j} \\ \vdots \\ (P_n)_{i,j} \end{pmatrix} = \begin{pmatrix} 0 \\ 0 \\ \vdots \\ 0 \end{pmatrix} \tag{4.3}$$

We note that the determinant of the matrix on the left hand side is non-zero. This is because

$$\begin{aligned} \det \begin{pmatrix} E_1 & E_2 & \ldots & E_n \\ E_1^2 & E_2^2 & \ldots & E_n^2 \\ \vdots & & & \vdots \\ E_1^n & E_2^n & \ldots & E_n^n \end{pmatrix} &= \left(\prod_{i=1}^{n} E_i \right) \det \begin{pmatrix} 1 & 1 & \ldots & 1 \\ E_1 & E_2 & \ldots & E_n \\ \vdots & & & \vdots \\ E_1^{n-1} & E_2^{n-1} & \ldots & E_n^{n-1} \end{pmatrix} \\ &= \prod_{i=1}^{n} E_i \prod_{1 \le i < j \le n} (E_i - E_j) \\ &\neq 0 \end{aligned} \tag{4.4}$$

The last line follows from E_i being distinct, non-zero energies, while the intermediate determinant is the well-known Vandermonde determinant.

Recalling that a homogeneous system of linear equations has non-trivial solutions if and only if the coefficient matrix is non-singular, we conclude that the only solution for (4.3) is the trivial one (i.e. the zero vector).

In other words, each of the projectors $P_1, \ldots, P_n$ are strictly-local with maximum hopping ranges less than or equal to nR, since the conclusion about the uniqueness of the solution is applicable to all $\mathbf{r}_1, \mathbf{r}_2$ that satisfy $|\mathbf{r}_1 - \mathbf{r}_2| > nR$. This statement is independent of the dimensionality of the lattice as well as whether the Hamiltonian is invariant under lattice translations. (In Ref. [91], it was stated without proof that strictly-local flat Hamiltonians must have strictly-local projectors, in the context of 1d Hamiltonians with lattice translational invariance. [See the discussion below equation (A22) in that paper.] By proving this conjecture, we fill a gap in their proof for the statement that each band in a 1d flat Hamiltonian can be spanned by compact Wannier function.)

For systems of infinite size and finite n, all the projectors are thus SL. However, for finite-sized systems, the projectors may not be SL if nR is comparable to the system size. Since $p_i \geq R$ for at least one i, $q \coloneqq \max\{R, p_1, \ldots, p_n\}$ is such that $q \leq nR$. Thus, all the projectors are SL if $2q + 2 \leq L_{x/y}$. This is guaranteed if $2nR + 2 \leq L_{x/y}$.

In the subsequent sections, the following observation will be useful. If we group the unit cells so that $q \times q$ primitive cells form a supercell, then all the projectors and the Hamiltonian are NNN-hopping operators. If L_x is not divisible by q, then we choose the first $\lfloor L_x/q \rfloor - 1$ number of supercells along $\hat{x}$ to consist of q cells each (where $\lfloor . \rfloor$ denotes the floor function), while the last supercell will comprise $L_x - q(\lfloor L_x/q \rfloor - 1)$ number of primitive cells. We implement a similar grouping along $\hat{y}$ if L_y is not divisible by q.

4.5 Niu-Thouless-Wu (NTW) Invariant

In the presence of disorder and/or interactions, there is no band structure, and hence one cannot express the transverse conductivity in terms of the Chern number of a Bloch band [see (1.25)]. However, Niu, Thouless and Wu [100] showed that even in the presence of interactions

and disorder, Hall conductance is still quantized and is equal to the Chern number computed with a base manifold corresponding not to the Brillouin zone, but to certain magnetic fluxes (or equivalently, 'twist angles' for twisted boundary conditions). Specifically, the parameter space consists of the two fluxes inserted through the two holes of a torus, on which the lattice of the system is considered lie on; see Fig. 4.1. Substrate potential that may or may not be periodic, as well as electron-electron Coulomb interactions are allowed. It is assumed that at any values of fluxes, the (many-body) ground state is always gapped.

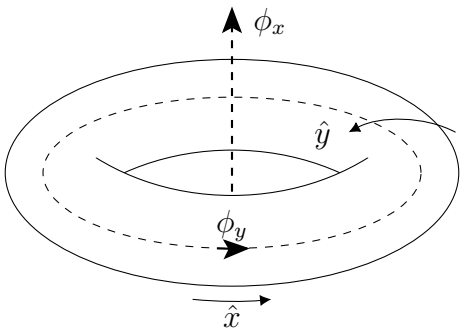

Figure 4.1: Periodic boundary conditions are imposed on the system, so that it lies on a torus. Two magnetic fluxes ϕ_x and ϕ_y are inserted through the two holes of the torus. The $\hat{x}$ and $\hat{y}$ directions are shown for reference.

Then, using the Kubo formula, they show that the transverse conductivity is essentially proportional to the Berry curvature at the particular parameter values. At this point, they argue that in the infinite system size limit, the boundary conditions should not matter, and hence the actual transverse conductivity must be this quantity, averaged over all the twist angles. This is, of course the Chern number of the many-body ground state wavefunction, in the flux parameter space, and is hence quantized. For finite system sizes, the Chern number can be defined using the same formula.

Let us go through the derivation of the formula. With magnetic vector potential given by $\mathbf{A} = \frac{\phi_x}{L_x}\hat{x} + \frac{\phi_y}{L_y}\hat{y}$, the Hamiltonian is then

$$H = \sum_i \frac{(\mathbf{p}_i + e\mathbf{A})^2}{2m} + \sum_i U_i(\mathbf{r}_i) + \sum_{i<j} V(|\mathbf{r}_i - \mathbf{r}_j|) \tag{4.5}$$

Let $\mathbf{E}$ denote an external electric field. This results into a perturbation to the Hamiltonian, given by $e\mathbf{E}.\mathbf{r}$. Denoting by $\partial_\mu \equiv \frac{\partial}{\partial E_\mu}$, we note that

$$er_\mu = \partial_\mu H. \tag{4.6}$$

The current density is given by $\mathbf{j} = e\mathbf{v}/A$, where $A = L_x L_y$ is the surface area. Let $|\Psi\rangle \equiv |\Psi(\phi_x, \phi_y)\rangle$ denote the many-body ground state as a function of the fluxes. Using linear response theory [see (1.19) and (1.18)], we thus get

$$\begin{aligned}\sigma_{\mu\nu} = \partial_\mu \langle j_\nu \rangle &= \frac{2e}{A} \operatorname{Re} \langle \Psi | \, OTQ \, | \partial_\mu \Psi \rangle \\ &= \frac{2e^2}{A} \operatorname{Re} \langle \Psi | \, v_\nu T r_\mu \, | \Psi \rangle \\ &= \frac{\hbar e^2}{A} 2 \operatorname{Im} \langle \Psi | \, v_\nu T^2 v_\mu \, | \Psi \rangle \, .\end{aligned} \tag{4.7}$$

The velocity operator components are given by $v_\mu = \frac{-i}{\hbar}[r_\mu, H] = \frac{L_\mu}{e}\frac{\partial H}{\partial \phi_\mu}$. Plugging into (1.18), we have

$$T v_\mu \, |\Psi\rangle = \frac{L_\mu}{e} Q \, \big| \partial_{\phi_\mu} \Psi \big\rangle \tag{4.8}$$

Plugging into (4.7), we get

$$\sigma_{xy} = -i\hbar [\big\langle \partial_{\phi_x} \Psi \big| \partial_{\phi_y} \Psi \big\rangle - \text{h.c.}] \tag{4.9}$$

This quantity is not quantized. However, for large system sizes, the physical properties would not depend on the boundary condition, and hence the magnetic flux values. Hence, Niu, Thouless and Wu argued that one could replace σ_{xy} by the average over all flux values $\phi_x, \phi_y \in [0, \Phi_0)$, where $\Phi_0 = h/e$. Taking an average, we find that

$$\begin{aligned}\bar{\sigma}_{xy} &= \frac{e^2}{h} C \\ \text{where } C &= \left(\frac{1}{2\pi i} \int_0^{\Phi_0} \int_0^{\Phi_0} \mathrm{d}\phi_x \, \mathrm{d}\phi_y \; \big\langle \partial_{\phi_x} \Psi \big| \partial_{\phi_y} \Psi \big\rangle - \big\langle \partial_{\phi_y} \Psi \big| \partial_{\phi_x} \Psi \big\rangle \right).\end{aligned} \tag{4.10}$$

where C is the Chern number and only has integer values.

While the actual conductivity is equal to the flux-averaged conductivity only in the thermodynamic limit, the Chern number, as defined above, is well-defined for any system size.

Even for finite systems, the transverse conductivity has been shown to be proportional to this Chern number up to exponentially small errors in the system size [117, 118]. Consequently, the transverse conductivity for finite system sizes is also equal to e^2C/h up to exponentially small errors. We can straightforwardly generalize (4.10) in order to define a Chern number for an isolated flat band or energy in a flat Hamiltonian. Specifically, we use expression Eq. (4.10) but with $|\Psi\rangle$ taken to be the 'flat band wavefunction', i.e. the many-body wavefunction corresponding to only the flat band states being fully occupied, with the rest of the energies being unoccupied. We will henceforth use this definition.

4.6 Spectrum and Projectors after Flux Insertion

The spectrum of a non-flat Hamiltonian generally changes when magnetic fluxes are threaded through the two holes of a torus as shown in Fig. 4.1. However, for flat Hamiltonians which have SL projectors (and which further satisfy $L_{x,y} \geq 3q$ and $L_{x,y} \geq 2q+2$), the spectrum is unchanged even after threading any amount of flux, as we will show below.

Let us first consider the case when only ϕ_x is inserted, so that H changes to $H(\phi_x)$ following Peierls substitution [7]. We choose a gauge for the substitution that corresponds to twisted boundary conditions (TBCs) [100], so that only those hopping elements that cross the boundary at $x = L_x$ are modified. In other words, every hopping elements that connects a cell with an x-coordinate in $\{L_x - R + 1, \ldots, L_x\}$ to a cell with an x-coordinate in $\{1, 2, \ldots, R\}$ is multiplied by a phase of $e^{-2\pi i \phi_x/\Phi_0}$, while hoppings in the reverse direction get multiplied by $e^{2\pi i \phi_x/\Phi_0}$. ($\Phi_0 = h/e$ is the magnetic flux quantum.) The rest of the hopping elements are unchanged in the substitution.

Similarly, we can implement TBCs for all the P_i as well, if they are SL. Denoting the post-transformation operators by $P_i(\phi_x)$s, we note that

$$H(\phi_x) = \sum_{i=1}^{N} E_i P_i(\phi_x). \tag{4.11}$$

While it is not immediately obvious, this equation is actually a spectral decomposition of $H(\phi_x)$ when $L_x \geq 3q$, as shown in Appendix 4.A.

This fact can also be used to obtain a spectral decomposition for the Hamiltonian $H(\phi_x, \phi_y)$, the Hamiltonian with both the fluxes are inserted, if $L_y \geq 3q$ and $L_y \geq 2q + 2$. The key idea is to treat $H(\phi_x)$ as the 'initial Hamiltonian' and repeat the steps above. Specifically, we obtain $H(\phi_x, \phi_y)$ by applying TBCs to $H(\phi_x)$ along $\hat{y}$. Transforming the projectors similarly, so that $P_i(\phi_x) \to P_i(\phi_x, \phi_y)$, we get

$$H(\phi_x, \phi_y) = \sum_{i=1}^{N} E_i P_i(\phi_x, \phi_y). \tag{4.12}$$

Applying the proof from Appendix 4.A again, we conclude that (4.12) is also a spectral decomposition. Thus, flat Hamiltonians have the interesting property of having an unchanging spectrum if $L_{x,y} \geq 2q + 2$ and $L_{x,y} \geq 3q$. Both these conditions are satisfied if $L_{x,y} \geq 3nR$ and $L_{x,y} \geq 2nR + 2$.

4.7 Many-Body Wavefunctions after Magnetic Flux Insertion

Let us proceed with the task of computing the Chern number corresponding to a flat band in a flat Hamiltonian. Let the energy of the flat band be E and the corresponding projector, P. We assume that $L_{x,y} \geq 3nR$ so that the spectrum of a flat Hamiltonian is unaffected by the fluxes as shown above. Thus, for any ϕ_x, ϕ_y, while the state of the system corresponding to that energy level being fully filled is unique, the corresponding wavefunction $|\Psi(\phi_x, \phi_y)\rangle$ has a phase ambiguity. We will now provide a prescription that fixes the phase to obtain a global expression for $|\Psi(\phi_x, \phi_y)\rangle$ that can then be used to compute the Chern number.

We will start with a brief outline of our approach. First, we obtain a particular type of orthogonal basis of single-particle wavefunctions spanning the energy E subspace when no fluxes are inserted. The Slater determinant then yields $|\Psi\rangle$ at zero flux. Next, we consider the case when only ϕ_x is inserted, so that P transforms to $P(\phi_x)$. We show that wavefunctions obtained for $\phi_x = 0$, when modified appropriately, are eigenstates of $P(\phi_x)$ and thus span E at flux ϕ_x. The corresponding Slater determinant yields $|\Psi(\phi_x)\rangle$, which by construction is shown to be a smooth function of ϕ_x. In the last step, we insert flux ϕ_y in addition to ϕ_x. Specifically, for each value of ϕ_x, we follow a similar procedure to obtain a smooth family of

wavefunctions as a function of ϕ_y. This finally results in a global expression for $|\Psi(\phi_x, \phi_y)\rangle$.

For the remainder of the manuscript we will work within the size $q \times q$ supercell representation described previously. Thus, H and all P_is are then NNN operators in this representation, and we have a supercell grid of a size of at least 3×3 since we assumed $L_{x,y} \geq 3nR$. The wavefunctions obtained in this representation can always be expressed in the original primitive cell representation at the end.

The first step involves obtaining the flat band many-body wavefunction before inserting ϕ_x. First, we demote the y index to an orbital index so that P can be regarded as a NN projector on a 1d lattice with position coordinate x. Next, we will use the property that the image of a 1d SL projector can always be spanned by an orthogonal basis of compactly-supported wavefunctions [10, 73]. Specifically, we use the construction of generalized Wannier functions presented in Ref. [73] for 1d NN projectors. The wavefunction so obtained are of two types: 'monomers' and 'dimers'. A monomer has support on only one cell, while a dimer has support only on two consecutive cells. (In the original 2d picture, each such wavefunction is strictly localized along $\hat{x}$ but is possible delocalized along $\hat{y}$.)

Monomer-dimer bases have an important property which we call the 'support property'. Specifically, whenever two wavefunctions from such a basis have non-zero support at a common cell, say x_0, then their supports at x_0 are also mutually orthogonal.

We note further that a monomer-dimer basis so obtained is not unique. For instance, multiplying any monomer or dimer in a given basis by a phase itself results in a different basis. Less trivial possibilities arise whenver any P_1^x hopping matrix [defined in (4.1)] has degenerate singular values; see Ref. [73]. However, for our purpose, it suffices to choose any valid monomer-dimer basis for P. For convenience, let us denote the chosen basis by a set $\mathcal{B}$. We obtain the flat band many-body wavefunction $|\Psi\rangle$ at zero flux by computing the Slater determinant of $\mathcal{B}$.

Next, we insert flux ϕ_x so that P now transforms to $P(\phi_x)$. The hopping matrices of P that connect $x = 0$ and $x = 1$ get transformed, with the rest being unaffected. The

substitution can be summarized as:

$$\begin{aligned} P_1^0 &\xrightarrow{\phi_x} e^{-2\pi i\phi_x/\Phi_0} P_1^0 \\ \text{and } P_{-1}^1 &\xrightarrow{\phi_x} e^{2\pi i\phi_x/\Phi_0} P_{-1}^1. \end{aligned} \tag{4.13}$$

While $\mathcal{B}$ is not an orthonormal basis for the image of $P(\phi_x)$, a simple modification of it does span the image. Consider two subsets of $\mathcal{B}$, namely $\mathcal{C}$ which consists only of those dimers that have support at both $x = 0$ and $x = 1$, and $\mathcal{U}$ that consists of all other wavefunctions from $\mathcal{B}$, so that $\mathcal{B} = \mathcal{U} \cup \mathcal{C}$. It is easy to see that every element of $\mathcal{U}$ is also an eigenvector of $P(\phi_x)$ (with an eigenvalue of 1), since $P(\phi_x)$ is the same as P except for hopping elements between $x = 0$ and $x = 1$. However, the elements of $\mathcal{C}$ are not eigenvectors of $P(\phi_x)$. They can however be modified as follows. Consider a wavefunction $|w\rangle \in \mathcal{C}$. Let

$$|w\rangle = \alpha\,|x = 0, \psi_0\rangle + \beta\,|x = 1, \psi_1\rangle\,, \tag{4.14}$$

for some support vectors $|\psi_{0,1}\rangle$. We now define $|w_{\phi_x}\rangle$ as follows:

$$|w_{\phi_x}\rangle \coloneqq \alpha\,|x = 0, \psi_0\rangle + e^{-i2\pi\phi_x/\Phi_0}\beta\,|x = 1, \psi_1\rangle\,. \tag{4.15}$$

Using (4.13) and the fact that $P\,|w\rangle = |w\rangle$, we conclude that $P(\phi_x)\,|w_{\phi_x}\rangle = |w_{\phi_x}\rangle$. Let us denote by $\mathcal{C}_{\phi_x}$ the set obtained after modifying every element of $\mathcal{C}$ in this way, and define $\mathcal{B}_{\phi_x} \coloneqq \mathcal{U} \cup \mathcal{C}_{\phi_x}$. Then, using the support property of monomer-dimer bases, we furthermore conclude that $\mathcal{B}_{\phi_x}$ is an orthogonal basis (and actually a monomer-dimer basis) for the image of $P(\phi_x)$. For any value of ϕ_x, the Slater determinant of $\mathcal{B}_{\phi_x}$ thus yields $|\Psi(\phi_x)\rangle$. Clearly, $|\Psi(\phi_x)\rangle$ is a smooth function of ϕ_x. Furthermore, since $\mathcal{B}_{\phi_x=\Phi_0}$ is the same as $\mathcal{B}_{\phi_x=0}$, we also find that $|\Psi(\phi_x = 0)\rangle = |\Psi(\phi_x = \Phi_0)\rangle$.

Having obtained $|\Psi(\phi_x)\rangle$, we will now discuss the last step, i.e. obtaining the many-body wavefunction when ϕ_y is also inserted. To that end, for any value of ϕ_x, we first set $H(\phi_x)$ to be the 'initial' flat Hamiltonian and then apply the entire procedure discussed above, but for the flux ϕ_y. [We thus obtain monomer-dimer states for each band projector $P_i(\phi_x, \phi_y)$, with the states being strictly localized along $\hat{y}$.] The Slater determinant of these wavefunctions, denoted $|\tilde{\Psi}_{\phi_x}(\phi_y)\rangle$, corresponds to the flat band at those flux values. Since the many-body

state corresponding to the flat band is unique for any flux values, $|\Psi(\phi_x)\rangle$ and $|\tilde{\Psi}_{\phi_x}(\phi_y = 0)\rangle$ must be the same up to a phase, so that $|\Psi(\phi_x)\rangle = e^{i\theta_{\phi_x}}|\tilde{\Psi}_{\phi_x}(\phi_y = 0)\rangle$ for some $\theta_{\phi_x} \in \mathbb{R}$. Finally we define $|\Psi(\phi_x, \phi_y)\rangle \coloneqq e^{i\theta_{\phi_x}}|\tilde{\Psi}_{\phi_x}(\phi_y)\rangle$.

We find that by construction, for all values of ϕ_x and ϕ_y,

$$\begin{aligned} |\Psi(\phi_x, 0)\rangle &= |\Psi(\phi_x, \Phi_0)\rangle\,, \\ \text{and } |\Psi(0, \phi_y)\rangle &= |\Psi(\Phi_0, \phi_y)\rangle\,. \end{aligned} \tag{4.16}$$

Using Stokes' theorem, we can write (4.10) as

$$C = \frac{1}{2\pi} \oint_\Gamma i \langle \Psi | \nabla_\phi \Psi \rangle \,.\mathrm{d}\phi, \tag{4.17}$$

where Γ is the boundary $(0,0) \to (\Phi_0, 0) \to (\Phi_0, \Phi_0) \to (0, \Phi_0) \to (0,0)$.

From (4.16), we conclude that the line integral contributions from $(0,0) \to (\Phi_0, 0)$ and $(\Phi_0, \Phi_0) \to (0, \Phi_0)$ cancel each other, and so do those from $(\Phi_0, 0) \to (\Phi_0, \Phi_0)$ and $(0, \Phi_0) \to (0,0)$. Consequently, $C = 0$. Let us note that while our proof of Chern triviality was stated for flat bands in flat Hamiltonians, all the steps can also be used to prove that the Chern number associated with an isolated degenerate energy (or a flat band) that has SL projector is zero, regardless of whether the rest of the bands are flat.

While our arguments apply only to tight-binding models, we find it interpret them in the context of Landau levels. The fact that Landau levels are infinite in number seems to provide an escape route, since it does not imply that the projection operators are strictly local, which forms a crucial part of the remaining proof.

4.8 Conclusions

We showed that all bands of a two dimensional strictly local (SL) flat Hamiltonians have a Chern number of zero. To that end, we showed that each band in such a system is described by a SL projector. We also showed that the spectrum of such Hamiltonians is unchanged even after flux threading in a toroidal geometry. We demonstrated all our results without the requirement of lattice-translational invariance (LTI) thereby going beyond existing no-go

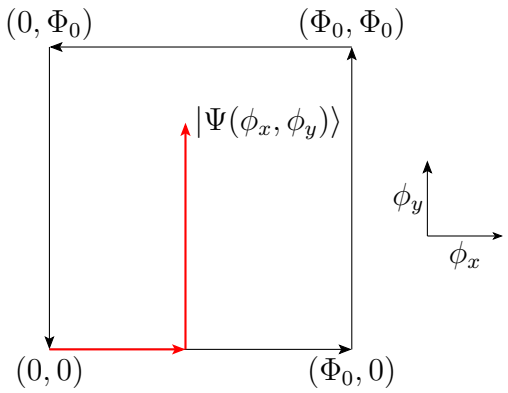

Figure 4.2: The (ϕ_x, ϕ_y) parameter space with $\phi_x, \phi_y \in [0, \Phi_0]$. For any pair of values (ϕ_x, ϕ_y), wavefunction $|\Psi(\phi_x, \phi_y)\rangle$ is obtained in two steps – by applying the single-flux procedure for the flux insertions corresponding to each of the two red arrows in sequence. The line integral in (4.17) is computed along the boundary of the region (black arrows).

theorems concerning flat bands. Furthermore, we clarified the role of a subtle condition that allows for a topological flat Hamiltonian in finite systems.

An important step of our proof involved showing that each band projector is strictly local. Since projection operators are equal-time Green's functions in non-interacting systems, generalizations to interacting cases might be possible. Our no-go theorem was proven for system sizes that are greater than a lower bound expressible in terms of the number of energies and maximum hopping range of the Hamiltonian. It would be interesting to obtain an improved lower bound.

APPENDIX

4.A Proof of Spectrum not changing after Flux Insertion

In the main text, it was asserted that when a flux ϕ_x is inserted, the spectrum of a flat Hamiltonian does not change (if $L_x \geq 3q$ and $L_x \geq 2q+2$). Here, we provide a proof for this statement.

Let us denote the spectral decomposition of the flat Hamiltonian H by

$$H = \sum_{i=1}^{n} E_i P_i, \tag{4.18}$$

where $P_i P_j = P_j P_i = P_i \delta_{ij}$. R and p_i denote the maximum hopping ranges of H and P_i respectively, and $q \coloneqq \max\{R, p_1, \ldots, p_n\}$. As described in the main text, the Hamiltonian gets transformed according to Peierls substitution upon inserting ϕ_x. We chose a gauge for the substitution which corresponds to twisted boundary conditions (TBCs) with a boundary at $x = L_x$ (or equivalently, $x = 0$). In order to implement Peierls substitution on the projectors as well, we require that they be SL along $\hat{x}$. This requires that $L_x \geq 2q+2$. Denoting by $P_i(\phi_x)$ the post-substitution version of P_i, we obtain

$$H(\phi_x) = \sum_{i=1}^{n} E_i P_i(\phi_x). \tag{4.19}$$

We will now show that similar to the original P_is, each $P_i(\phi_x)$ is an orthogonal projector and that any two distinct projectors from this transformed set are mutually orthogonal.

We will find it convenient to work in the size $q \times q$ supercell representation described in the main text, so that H and all the P_is are NNN-hopping. Since the y-coordinate does not play a role here, the problem is effectively 1d. Hence, we suppress the y-coordinate for the following steps. Each P_i can then effectively be treated as a 1d NN projector.

We will start by showing that each $P_i(\phi_x)$ is an orthogonal projector. To that end, let us consider any projector $P \in \{P_1, \ldots, P_n\}$. If $L_x \geq 3q$, then there are at least 3 supercells in the lattice. Peierls substitution for P (implemented in the primitive cell representation) is

then equivalent to modifying only those hopping matrices [as defined in Eq. (4.1) in the main text] that connect $x = 0$ and $x = 1$ in the supercell representation. Thus, in the supercell representation, the changes are captured by the following transformations of the hopping matrices:

$$\begin{aligned} P_1^0 &\xrightarrow{\phi_x} e^{-2\pi i\phi_x/\Phi_0} P_1^0 \\ \text{and } P_{-1}^1 &\xrightarrow{\phi_x} e^{2\pi i\phi_x/\Phi_0} P_{-1}^1. \end{aligned} \tag{4.20}$$

Note that if $L_x < 3q$, then we only have two supercells, and Peierls substitution implemented in the primitive cell representation is not equivalent to (4.20) in the supercell representation. Since we make use of (4.20) below, we require that $L_x \geq 3q$ at this point.

Before inserting a flux, P is an orthogonal projector and hence satisfies $P^2 = P = P^\dagger$. This is equivalent to the conditions

$$\begin{aligned} (P_j^x)^\dagger &= P_{-j}^{x+j}, \\ P_0^x &= (P_0^x)^2 + (P_1^x)^\dagger(P_1^x) + (P_1^{x-1})(P_1^{x-1})^\dagger, \\ \text{and } P_1^x &= P_0^{x+1}P_1^x + P_1^x P_0^x, \end{aligned} \tag{4.21}$$

for all cell positions x. It is straightforward to show P continues to satisfy (4.21) even after undergoing Peierls substitution (4.20). Thus, every $P_i(\phi_x)$ is also an orthogonal projector.

Now let us consider any two distinct projectors $P, Q \in \{P_1, \ldots, P_n\}$. They necessarily satisfy $PQ = QP = 0$. Expressed in terms of the hopping matrices, these equalities can be written as

$$\begin{aligned} P_0^x Q_0^x = Q_0^x P_0^x &= 0 \\ P_1^x Q_0^x + P_0^{x+1} Q_1^x = Q_1^x P_0^x + Q_0^{x+1} P_1^x &= 0 \\ P_1^{x+1} Q_1^x = Q_1^{x+1} P_1^x &= 0. \end{aligned} \tag{4.22}$$

It is easy to show that P and Q continue to satisfy (4.22) even after undergoing the substitution (4.20) (and its analog for Q). Thus, all the $P_i(\phi_x)$s together are a set of mutually orthogonal projectors. Eq. (4.19) is therefore a spectral decomposition.

CHAPTER 5

Delocalization Transition in Chiral Floquet Topological Insulators

5.1 Introduction

The localization of eigenstates of a non-interacting Hamiltonian in the presence of disorder, a phenomenon known as Anderson localization, has broad implications in condensed matter physics, and statistical mechanics in general [119]. While any amount of disorder localizes all eigenstates in a one-dimensional system, in dimensions three and higher, a metal-insulator transition exists as a function of disorder strength [120]. (In the special case of two-dimensional systems, the eigenstates are localized, but with possibly large localization lengths.)

Quite broadly, topological non-triviality (of a kind that depends on the context) can provide an obstruction to the localization of eigenstates. We have already encountered some examples in the previous chapters, wherein non-trivial topology restricts the possibility of Wannier functions that are well-localized. Another related connection between localization and topology arises in the plateau transition [121]. Specifically, in the integer quantum Hall effect, disorder localizes all states except for those at the center of every Landau level, where at least one delocalized state exists because of the topological non-triviality of Landau levels. The localization length of eigenstates as a function of energy difference from the center of the band diverges with an exponent believed to be universal.

In this chapter, we present some analogous results in the context of Floquet topological insulators, i.e. systems with non-interacting, time-periodic Hamiltonians. We find a

localization-delocalization transition which is universal for a certain class of models. Furthermore, these results are interesting in their own right in the context of Floquet phases. A rich variety of topological phases can be observed in the context of driven systems, with characteristics unique to Floquet systems which are absent in static systems [122]. Similar to the periodic table of (static) topological insulators [123] which provides a classification of the phases corresponding to different symmetry classes and dimensions in the Altland-Zirnbauer classification of symmetries [124], an analogous periodic table classifying Floquet topological insulators has been established [125].

We consider the simplest type of a Floquet topological insulator, a one-dimensional class AIII Floquet insulator (which has chiral or sublattice symmetry but does not have time-reversal or particle-hole symmetries). The focus of the current chapter is to analyze the localization properties of topologically non-trivial Hamiltonians in this class of models in the presence of disorder. Instead of considering localization lengths as a function of energy, we study them as a function of time. In particular, we find that in loop drives (see below), the localization length L_{loc} of all the eigenstates of the time evolution operator as a function of time diverge to infinity as

$$L_{\text{loc}} \sim (t - T_{\text{drive}}/2)^{-2}, \tag{5.1}$$

when $t \to T_{\text{drive}}/2$, where T_{drive} is the time period of the drive [i.e. of $H(t)$].

A forthcoming manuscript aims to present various aspects of our results in a comprehensive manner and to provide an analytical explanation for the universality of the exponent of 2, and by expanding on the scope of our results. We also note that some preliminary results have also been reported in Ref. [126]. In this chapter, we focus on presenting the main result and a derivation of the exponent in a particular ensemble of disordered drives. Let us start with a discussion of some the setup and relevant definitions.

5.2 Overview of Chiral Floquet Topological Insulators

The Hamiltonian $H(t)$ have a time period of T_{drive}. The study of Floquet topological insulators often revolves around the time-evolution operator $U(t)$, for values $0 \leq t \leq T_{\text{drive}}$. $U(t)$ can be computed using

$$U(t) = \mathcal{T} \exp\left[-i \int_0^t \mathrm{d}t' H(t')\right],$$

where $\mathcal{T}$ is the time-ordering symbol.

Unlike Hamiltonians, which have real eigenvalues, unitary operators have eigenvalues which lie on the complex unit circle. Thus, for any t, we have eigen-equations of the type

$$U(t) \left|\Psi\right\rangle = e^{-i\epsilon t} \left|\Psi\right\rangle, \tag{5.2}$$

wherein ϵt is defined modulo 2π. ϵ is called a quasi-energy. Similar to Bloch's theorem for Hamiltonians, if $H(t)$ has lattice translational invariance, the quasienergies are arranged in a quasi-energy band structure.

We recall that topological insulators have a gap in their spectrum when the system is closed (i.e. has periodic boundary conditions), and when the insulator is in a topologically non-trivial phase, the corresponding open system has one or more edge modes in a gap. Similarly, in the case of Floquet topological insulators, we consider drives that have a gap in the quasienergy spectrum for $U(T_{\text{drive}})$. It is then possible to define the 'Floquet Hamiltonian' H_F, defined via the expression

$$U(T_{\text{drive}}) = \exp(-iH_F T_{\text{drive}}).$$

Equivalence classes have been defined in Ref. [125] using a notion of homotopy. Specifically, two gapped drives U_1 and U_2 in a symmetry class $\mathcal{S}$ are said to be homotopically equivalent if there exists a function $h(s)$ for $s \in [0, 1]$ such that $h(0) = U_1$ and $h(1) = U_2$, with $h(s)$ being a gapped unitary in the symmetry class $\mathcal{S}$ for all value of s.

Let us now discuss loop drives, which are the center of focus of this chapter. First, let us note that in general, $U(T_{\text{drive}}) \neq \mathbb{1}$. However, in Ref. [125] it was argued that an

arbitrary Floquet unitary can be decomposed into a combination of a static evolution, and a 'loop' evolution. The loop component is a unitary operator $\mathcal{U}(t)$ for $0 \leq t < 1$ such that (upto an appropriate scaling of time) $\mathcal{U}(0) = \mathcal{U}(1) = \mathbb{1}$. The properties of the drive that are uniquely Floquet were then shown to be captured by the loop component. While any Floquet drive can be decomposed into a loop and a constant part, here, we will only consider Floquet drives that have the loop property without requiring a decomposition, so that $U(t = 0) = U(T_{\text{drive}}) = \mathbb{1}$.

Returning to the class AIII Floquet drives, i.e. the objects of interest in this chapter, we note that are defined by the following properties of the corresponding Hamiltonian $H(t)$:

$$CH(t)C^{-1} = -H(-t), \tag{5.3}$$
$$\text{and by implication } CU(T_{\text{drive}})C^{-1} = U^{\dagger}(T_{\text{drive}}).$$

Here, the chiral operator C is a unitary operator such that $C^2 = CC^{\dagger} = 1$. For the case with two orbitals per site, we choose a basis in which $C = \mathbb{1} \otimes \begin{pmatrix} 1 & 0 \\ 0 & 1 \end{pmatrix}$. A class AIII Floquet loop drive is then a drive which furthermore satisfies $U(T_{\text{drive}}) = U(0) = \mathbb{1}$.

It may be verified that at the midpoint of drive, we have [127]

$$CU(T_{\text{drive}}/2)C^{-1} = U(T/2),$$

so that $U(T_{\text{drive}}/2)$ has a block diagonal form

$$U(T_{\text{drive}}/2) = \begin{pmatrix} U_+ & 0 \\ 0 & U_- \end{pmatrix}.$$

The topological invariant characterizing one dimensional class AIII loop drives is then the flow invariant of U_+ as defined in Ref. [127]:

$$\nu[U] = F[U_+] = \sum_{j \geq 0} \sum_{k < 0} (|U_+^{jk}|^2 - |U_+^{kj}|^2),$$

where U_+^{jk} is the j,k-component of the unitary matrix U_+, j is summed over all orbitals with positions ≤ 0, while k is summed over all orbitals with positions > 0. The flow invariant $F[V]$ for any 1d unitary V has been shown to be integer valued by Kitaev [128]. Consequently, the topological invariant as defined above for the class AIII loop drives is also integer-valued.

5.2.1 The Model Drive

Much of the analysis in this chapter will revolve around a simple drive, henceforth referred to as the 'model drive', which was introduced in Ref. [127].

The model drive is defined on a chain with orbitals $|n, A\rangle$ and $|n, B\rangle$ for $n \in \mathbb{Z}$, and has the following Hamiltonian:

$$H(t) = \begin{cases} H_1 & \text{if } 0 < t < \frac{T_{\text{drive}}}{4} \\ H_2 & \text{if } \frac{T_{\text{drive}}}{4} < t < \frac{T_{\text{drive}}}{2} \\ H_2 & \text{if } \frac{T_{\text{drive}}}{2} < t < \frac{3T_{\text{drive}}}{4} \\ H_1 & \text{if } \frac{3T_{\text{drive}}}{4} < t < T_{\text{drive}} \end{cases}, \tag{5.4}$$

with

$$\begin{aligned} H_1 &= \frac{2\pi}{T_{\text{drive}}} \sum_n (|n, A\rangle \langle n, B| + |n, B\rangle \langle n, A|); \\ H_2 &= -\frac{2\pi}{T_{\text{drive}}} \sum_n (|n+1, A\rangle \langle n, B| + |n, B\rangle \langle n+1, A|). \end{aligned} \tag{5.5}$$

Without loss of generality, we choose $T_{\text{drive}} = 2\pi$. The minus sign in the expression for H_2 ensures that at the midpoint of the drive, the Floquet unitary moves A orbitals to the right, and B orbitals to the left without adding a phase. Much of our analysis will revolve around analyzing the model drive with some added disorder.

Before proceeding, let us study the eigenstates of the time evolution operator $U(t)$ around the midpoint, i.e. for $\pi/2 < t < 3\pi/2$. With $\Delta t \coloneqq t - T_{\text{drive}}/2$, we are therefore concerned with the range of values $-\pi/2 < \Delta t < \pi/2$. An eigenstate of $|\Psi\rangle$ satisfies $U(t)|\Psi\rangle = e^{-i\epsilon t}|\Psi\rangle$. We may express $|\Psi\rangle$ in position space as

$$|\Psi\rangle = \sum_n \left(\Psi^A(n)|n, A\rangle + \Psi^B(n)|n, B\rangle\right).$$

It is straightforward to see that the eigenequation can also be written in terms of these components as

$$\cos(\Delta t)\Psi^A(n-1) + i\sin(\Delta t)\Psi^B(n) = e^{-\epsilon t}\Psi^A(n)$$

$$i\sin(\Delta t)\Psi^A(n) + \cos(\Delta t)\Psi^B(n+1) = e^{-i\epsilon t}\Psi^B(n),$$

for all n. This formula can be more conveniently written as

$$\begin{pmatrix} \Psi^A(n+1) \\ \Psi^B(n+1) \end{pmatrix} = \underbrace{\begin{pmatrix} e^{i\epsilon t}\sec\Delta t & i\tan\Delta t \\ -i\tan\Delta t & e^{-i\epsilon t}\sec\Delta t \end{pmatrix}}_{M_n} \begin{pmatrix} \Psi^A(n) \\ \Psi^B(n) \end{pmatrix}. \tag{5.6}$$

We call M_n the position-space transfer matrix, since it tell us how the amplitudes of an eigenstate at a cell $n+1$ are related to the amplitudes of the same eigenstate at cell n.

5.2.2 Disordering the Model Drive

In order to obtain a family of drives that are in some sense a 'disordering' of the model drive, the simplest approach might be to replace H_1 or H_2 in (5.5) by some disordered variants. However, the loop property is unlikely to hold for an arbitrary drive picked from such an ensemble.

We instead propose an ensemble of Floquet Hamiltonians with the following form:

$$H(t) = \begin{cases} H_d & \text{if } 0 < t < \Delta \\ H_1 & \text{if } \Delta < t < \Delta + \frac{T_{\text{drive}}}{4} \\ H_2 & \text{if } \Delta + \frac{T_{\text{drive}}}{4} < t < \Delta + \frac{T_{\text{drive}}}{2} \\ H_2 & \text{if } \Delta + \frac{T_{\text{drive}}}{2} < t < \Delta + \frac{3T_{\text{drive}}}{4} \\ H_1 & \text{if } \Delta + \frac{3T_{\text{drive}}}{4} < t < T_{\text{drive}} + \Delta \\ -H_d & \text{of } T_{\text{drive}} + \Delta < t < T_{\text{drive}} + 2\Delta \end{cases} \tag{5.7}$$

Here, H_1 and H_2 are those defined in (5.5). In order to ensure that the drive has the loop property, the random Hermitian matrix H_d must satisfy the condition:

$$CH_dC = H_d, \tag{5.8}$$

so that H_d can be written as

$$H_d = H_d^A \oplus H_d^B, \tag{5.9}$$

wherein the pieces $H_d^{A/B}$ act on the A and B sublattices individually.

We find it convenient to take $\Delta \to 0^+$ by scaling H_d appropriately, so that $H(t)$ is has a period of T_{drive} instead of $T_{\text{drive}} + 2\Delta$. Clearly, the time evolution operator is then given by

$$U(t) = U_{\text{clean}}(t)U_d \quad 0 < t < T_{\text{drive}}$$

wherein $U_d = \exp(-iH_d)$ and $U_{\text{clean}}(t)$ corresponds to the time evolution operator of the model drive without disorder. It is to be understood that at $t = T_{\text{drive}}$, we also multiply by $U_d^\dagger$, i.e. $U(T_{\text{drive}}) = U_d^\dagger U_{\text{clean}}(t)U_d = \mathbb{1}$.

Any ensemble of H_ds which satisfies this property generates AIII Floquet loop drives. For the remainder of the thesis, we work with a particular ensemble. Specifically, we choose H_d that acts on each A and B orbital separately, so that U_d defined above can be written as

$$U_d = \sum_{n=1}^{N} \left(e^{i\phi_{n,A}} \left|n, A\right\rangle \left\langle n, A\right| + e^{i\phi_{n,B}} \left|n, B\right\rangle \left\langle n, B\right| \right) \tag{5.10}$$

Expressing an eigenvector of $U(t)$ for $\pi/2 < t < 3\pi/2$ in position space and plugging into the eigenequation $U(t)\left|\Psi\right\rangle = e^{-i\epsilon t}\left|\Psi\right\rangle$, we obtain a position-space transfer matrix similar to (5.6):

$$\begin{pmatrix} \Psi^A(n+1) \\ \Psi^B(n+1) \end{pmatrix} = \underbrace{\begin{pmatrix} e^{i\epsilon t + \phi_{n,A}} \sec \Delta t & i \tan \Delta t \\ -i \tan \Delta t e^{i(\phi_{n,A} - \phi_{n+1,B})} & e^{-i\epsilon t - i\phi_{n+1,B}} \sec \Delta t \end{pmatrix}}_{M_n} \begin{pmatrix} \Psi^A(n) \\ \Psi^B(n) \end{pmatrix}. \tag{5.11}$$

Such a transfer matrix can be used to numerically compute the localization lengths of eigenvectors as a function of the quasienergy ϵ and Δt (time away from the midpoint of the drive). Specifically, for any combination of ϵ and Δt, one may obtain many transfer matrices by randomly generating $\phi_{n,A}$ and $\phi_{n,B}$ for a given ensemble, and obtain the rate at which the logarithm of the larger eigenvalue of the product $M_N \ldots M_1$ increases as a function of N. The inverse of this rate yields the localization length. For more details of this procedure as well as the corresponding numerical results, we refer the reader to Ref. [126].

5.3 Fyodorov-Sommers Method

We now switch gears and derive the position-space transfer matrix using an alternate procedure, based on the Fyodorov-Sommers (FS) formalism [129]. We start with a basic overview of the FS formalism. Then, we focus on the model drive with full on-site disorder, beginning with a discussion for two arrangements of the leads, which we refer to as the 'A-B' and '1-2' arrangements. For this problem, we show that the FS formalism applied to a particular setup is equivalent to the real space transfer matrix approach discussed above that resulted in Eq. (5.11). Specifically, the scattering matrix obtained using FS is the same as the scattering matrix corresponding to the tranfer matrix corresponding to (5.11). We also derive the log additivity of the transmission probability, which gives us the exact localization length for all Δt's.

5.3.1 Scattering Formalism in Discrete Time Systems

We will now discuss the general development of the Fyodorov-Sommers approach [129]. Let U be a unitary operator which acts on a 1d lattice, and dictates the evolution of a wavefunction $\Psi[T]$, where $T \in \mathbb{Z}$ denotes the time. Thus,

$$\Psi[T+1] = U\Psi[T]. \tag{5.12}$$

Here, we interpret $\Psi[T]$ as a column vector, and U as a unitary matrix. Consider a system with three subspaces, E_{in}, E_{out} and E_0, which can be interpreted as the incoming, outgoing and 'sample' spaces. These subspaces need not be mutually orthogonal, nor is it necessary for $E_{in} \oplus E_{out} \oplus E_0$ to equal the total Hilbert space.

In the context of scattering, the change in one time step of the probability of the particle being in the sample region, is equal to the difference between the incoming probability $\phi_{in}[T]^\dagger \phi_{in}[T]$ and the outgoing probability $\phi_{out}[T]^\dagger \phi_{out}[T]$, i.e. the particle conservation condition:

$$\psi[T+1]^\dagger \psi[T+1] - \psi[T]^\dagger \psi[T] = \phi_{in}[T]^\dagger \phi_{in}[T] - \phi_{out}[T]^\dagger \phi_{out}[T]. \tag{5.13}$$

The vectors Ψ and $\phi_{in/out}$ are projections onto the corresponding subspaces, i.e.

$$\begin{aligned}\psi[T] &= P_0\Psi[T],\\ \phi_{in}[T] &= P_{in}\Psi[T],\\ \phi_{out}[T] &= P_{out}\Psi[T].\end{aligned}$$

These projectors are rectangular matrices with the number of rows equaling the dimension of the space to be projected onto, and the number of columns equaling the dimension of the Hilbert space (the projectors satisfy $PP^T = 1$, but not $P^TP = 1$).

The sample vector at time $T+1$ depends only on the sample vector and incoming vector at time T, while the outgoing vector only depends on the sample and incoming vectors. To summarize, the action of the unitary restricted to these subspaces is given by

$$\begin{aligned}\begin{pmatrix}\psi[T+1]\\ \phi_{out}[T]\end{pmatrix} &= V\begin{pmatrix}\psi[T]\\ \phi_{in}[T]\end{pmatrix};\\ V &= \begin{pmatrix}A & W_{out}\\ W_{in} & S_0\end{pmatrix}.\end{aligned} \tag{5.14}$$

Note: Intuitively, one would want to write $\phi_{out}[T+1]$ instead of $\phi_{out}[T]$ as the second component of the vector on the left hand side. However, this only results in an overall change of phase for the scattering matrix, i.e. $S[\omega] \to e^{-i\omega}S[\omega]$. Hence, to keep the notation consistent with [129], we use their convention.

It is easy to show that if equations (5.12) and (5.14) are both true, then V is a unitary matrix.

Now, let us decompose the wavefunction $\Psi[t]$ in the Fourier space, so that

$$\begin{aligned}\Psi[T] &= \sum_{\omega} e^{-i\omega T}\Psi[\omega];\\ \Psi[\omega] &= \sum_{T} e^{i\omega T}\Psi[t].\end{aligned} \tag{5.15}$$

With similar decompositions for ψ and $\phi_{in/out}$ vectors. In the Fourier space, equation (5.14)

becomes

$$\sum_{\omega} e^{-i\omega T} \left[\begin{pmatrix} \psi[\omega] e^{-i\omega} \\ \phi_{out}[\omega] \end{pmatrix} - V \begin{pmatrix} \psi[\omega] \\ \phi_{in}[\omega] \end{pmatrix} \right] = 0. \tag{5.16}$$

Setting T to 1, we conclude that the matrix equation inside the square brackets must be zero. We eliminate $\psi[\omega]$ from this system of two equations. It is easy to show that we finally obtain:

$$\begin{aligned} \phi_{out}[\omega] &= S[\omega]\phi_{in}[\omega]; \\ \text{with } S[\omega] &= S_0 + W_{out} \frac{1}{e^{-i\omega} - A} W_{in}. \end{aligned} \tag{5.17}$$

It is straightforward to prove that $S[\omega]$ is unitary for any ω. The unitarity of S can be inferred from the unitarity of V. One way to prove the unitarity of S is to multiply $V^\dagger$ to both sides of equation (5.16). This gives us $\phi_{in}[\omega] = S[\omega]^\dagger \phi_{out}$, with the same S as in (5.17). Since this equation as well as equation (5.17) is valid for all values of $\phi_{in}[\omega]$, $S[\omega]$ has to be unitary.

5.3.2 Rotated Basis Formula

Here, we derive in detail an alternate and more compact expression, equation (5) in [129], for the V matrix in (5.14).

Let the dimensions of the $E_{in/out}$ and E_0 spaces be m and p respectively. The unitarity of V gives us the following conditions:

$$AW_2^\dagger + W_1 S_0^\dagger = 0 \tag{5.18}$$

$$AA^\dagger + W_1 W_1^\dagger = 1 \tag{5.19}$$

$$W_2 W_2^\dagger + S_0 S_0^\dagger = 1 \tag{5.20}$$

$$A^\dagger W_1 + W_2^\dagger S_0 = 0 \tag{5.21}$$

$$A^\dagger A + W_2^\dagger W_2 = 1 \tag{5.22}$$

$$W_1^\dagger W_1 + S_0^\dagger S_0 = 1. \tag{5.23}$$

Here, W_1 and W_2 are the W_{in} and W_{out} matrices. Now, W_2 is an $m \times p$ matrix. We now obtain an SVD of W_2, Clearly, there exist unitary matrices $U^{(1)}$ and $V^{(1)}$, and a $p \times m$ sized diagonal rectangular matrix τ such that

$$W_2 = U^{(1)} \tau^\dagger V^{(1)}.$$

Equation (5.20) implies that

$$\begin{aligned} S_0 S_0^\dagger &= U^{(1)}(1 - \tau^\dagger \tau) U^{(1)\dagger} \\ \implies \exists\ V^{(2)} \text{ s.t. } S_0 &= U^{(1)} \sqrt{1 - \tau^\dagger \tau} V^{(2)} \end{aligned}$$

Equation (5.22) implies that

$$A^\dagger A = V^{(1)\dagger}(1 - \tau\tau^\dagger) V^{(1)}.$$

Clearly, this implies the existence of a unitary X of size $p \times p$ s.t.

$$A = X \sqrt{1 - \tau\tau^\dagger} V^{(1)}.$$

We can always define a new unitary $U = V^{(1)\dagger} X$. In terms of U, we thus get

$$A = V^{(1)\dagger} \left[U \sqrt{1 - \tau\tau^\dagger} \right] V^{(1)}$$

Similarly, (5.19) implies that

$$W_1 W_1^\dagger = V^{(1)\dagger} U (\tau\tau^\dagger) U^\dagger V^{(1)}.$$

This implies the existence of a unitary matrix Y such that

$$W_1 = V^{(1)\dagger} U \Delta t Y.$$

Plugging these all into (5.18), we get

$$\begin{aligned} V^{(1)\dagger} U \left[\sqrt{1 - \tau\tau^\dagger}\tau + \tau Y V^{(2)\dagger} \sqrt{1 - \tau^\dagger\tau} \right] U^{(1)^\dagger} &= 0 \\ \implies \sqrt{1 - \tau\tau^\dagger}\tau + \tau Y V^{(2)\dagger} \sqrt{1 - \tau^\dagger\tau} &= 0. \end{aligned}$$

Since τ is a diagonal matrix, this implies that $Y = -V^{(2)}$, and consequently,

$$W_1 = -V^{(1)^\dagger} U \tau V^{(2)}.$$

Putting this all together, we get

$$V = \begin{pmatrix} V^{(1)\dagger} & 0 \\ 0 & U^{(1)} \end{pmatrix} \begin{pmatrix} U\sqrt{1-\tau\tau^\dagger} & -U\tau \\ \tau^\dagger & \sqrt{1-\tau^\dagger\tau} \end{pmatrix} \begin{pmatrix} V^{(1)} & 0 \\ 0 & V^{(2)} \end{pmatrix}. \tag{5.24}$$

Thus, this special form can always be attained by separately rotating the left and right incoming and outgoing subspaces. In this rotated basis, (5.17) becomes

$$S[\omega] = \sqrt{1-\tau^\dagger\tau} - \tau^\dagger \frac{1}{e^{-i\omega} - U\sqrt{1-\tau\tau^\dagger}} U\tau. \tag{5.25}$$

5.3.3 Scattering Matrix for Model Drive with Onsite Disorder

In this section, we start by discussing the various scattering setups for the model drive with on-site disorder. Specifically, we are interested in analyzing the properties of the model drive at times $T_{\text{drive}}/2 + \Delta t$ for small Δt. The time evolution operator for model drive with onsite disorder discussed in Section 5.2.2 at $T_{\text{drive}}/2 + \Delta t$ is given by

$$\begin{aligned} U(T_{\text{drive}}/2 + \Delta t)\,|n, A\rangle &= e^{i\phi_{nA}}(\cos\Delta t\,|n+1, A\rangle + i\sin\Delta t\,|n, B\rangle) \\ U(T_{\text{drive}}/2 + \Delta t)\,|n, B\rangle &= e^{i\phi_{nB}}(\cos\Delta t\,|n-1, B\rangle + i\sin\Delta t\,|n, A\rangle). \end{aligned} \tag{5.26}$$

While it might be possible to explicitly calculate the scattering matrix for multiple scatterers using formulas for finding the inverse of band diagonal matrices, here we only calculate the scattering matrices explicitly for a single scatterer. For all the setups we consider in this section, we find that it is possible to obtain a scattering transfer matrix associated with a single scatterer. This can be used to analytically study the scattering properties of a larger scattering sample. Interestingly, the scattering transfer matrix we obtain for this model is identical to the position space transfer matrix. However, we find that for other Floquet drives, including the model drive with other types of disorder, it may or may not be possible to obtain a simple 'chainable' scattering matrix.

First, we discuss the 'A-B' and '1-2' leads, for which we make a distinction between the disordered sample region, and the disorder-free leads. Then, we discuss the case where there is no qualitative distinction between the sample and the leads. This is equivalent to considering 1-2 leads with disorder. In this case, we find that the scattering matrix is in fact equal to the scattering matrix corresponding to the position-space transfer matrix in Eq. (5.11). As we will see, this is not surprising. In the case of the model drive with onsite disorder, this third setup corresponds exactly to the problem of relating the amplitudes (of the eigenvector of $U(T_{\text{drive}}/2 + \Delta t)$) at two different sites relative to each other.)

Before proceeding, we introduce a notation that will be used in this section. Specifically, we assume that a vector Ψ satisfies (5.12), and is expressed in the orbital basis as

$$|\Psi[T]\rangle = \sum_{n\in\mathbb{Z}} \sum_{\alpha=A}^{B} \Psi[n,\alpha,T]\,|n,\alpha\rangle\,. \tag{5.27}$$

5.3.3.1 A-B Leads

In this setup, we assume that the dynamics in the sample are the same as that of $U(T_{\text{drive}}/2+\Delta t)$ given in (5.26). On the other hand, the dynamics in the leads, which we call A-B dynamics, is set to be identical to the dynamics of $U(T_{\text{drive}}/2)$. That is, the action of U moves the A orbital to the right and the B orbitals to the left. At the boundary region of the sample, the dynamics is intermediate between the two.

Specifically, we denote the unitary of the scattering setup by $\mathcal{U}$, with its action given by

$$\mathcal{U}\,|n,A\rangle = \begin{cases} e^{i\phi_{n,A}}(\cos\Delta t\,|n+1,A\rangle + i\sin\Delta t\,|n,B\rangle), & \text{if } 1\le n<L; \\ e^{i\phi_{n,A}}\,|n+1,A\rangle\,, & \text{otherwise.} \end{cases} \tag{5.28}$$

$$\mathcal{U}\,|n,B\rangle = \begin{cases} e^{i\phi_{n,B}}(\cos\Delta t\,|n-1,B\rangle + i\sin\Delta t\,|n,B\rangle), & \text{if } 1<n\le L; \\ e^{i\phi_{n,B}}\,|n+1,A\rangle\,, & \text{otherwise.} \end{cases} \tag{5.29}$$

The connectivity of the unitary $\mathcal{U}$ is shown schematically in figure 5.1. We restrict the disorder to sites 1 to L, i.e. we set $\phi_{n,A/B} = 0$ for $n < 1$ and $n > L$. We also note that the 'scatterers' at sites 1 and L are qualitatively different from the scatterers at sites 2 to L-1.

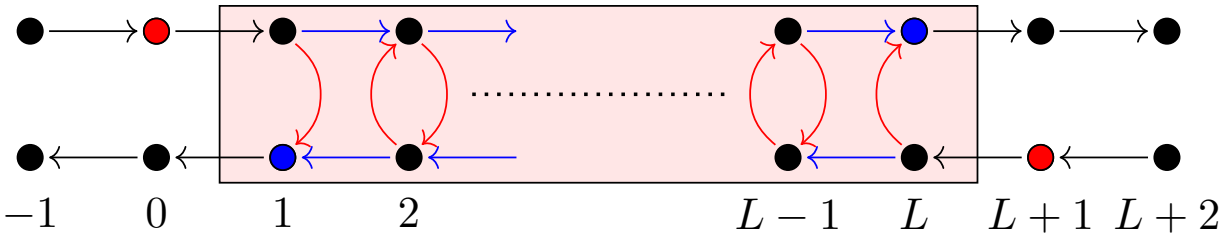

Figure 5.1: The scattering setup with A-B leads: The upper and lower rows of circles correspond to the A and B orbitals respectively. We designate the colored region to be the 'sample' subspace. The red (blue) circles correspond to the in (out) subspaces. The arrows denote the connectivity of the scattering unitary U. The black arrows correspond to a hopping amplitude of 1, while the red and blue arrows correspond to hopping amplitudes of $i \sin \Delta t$ and $\cos \Delta t$ respectively (upto on-site phases).

Specifically, the unitary lacks a hopping from $|1, B\rangle$ to $|1, A\rangle$ and from $|L, A\rangle$ to $|L, B\rangle$. (We interpret this as the sites 1 and L being 'lead connectors', which we will not modify when we consider increasing the size of the sample. Instead, we will add a scatterer to the region 2 to L-1.)

To apply the FS formalism, we first need to identify the sample, incoming and outgoing spaces. It is natural to choose the sample vector to be

$$\psi[T] = \begin{pmatrix} \Psi[1A,T] & \Psi[1B,T] & \dots & \Psi[L,A,T] & \Psi[L,B,T] \end{pmatrix}^T \tag{5.30}$$

In order to identify the in/out subspaces, we first obtain the corresponding particle conservation equation. A few lines of algebra give us

$$\begin{aligned} \psi[T+1]^\dagger \psi[T+1] - \psi[T]^\dagger \psi[T] = (|\Psi[0,A,T]|^2 + |\Psi[L+1,B,T]|^2) \\ - (|\Psi[1,B,T]|^2 + |\Psi[L,A,T]|^2) \end{aligned} . \tag{5.31}$$

Hence, we define the the in/out vectors to be

$$\begin{aligned} \phi_{in}[T] &= \begin{pmatrix} \Psi[0,A,T] & \Psi[L+1,B,T] \end{pmatrix}^T \\ \phi_{out}[T] &= \begin{pmatrix} \Psi[1,B,T] & \Psi[L,A,T] \end{pmatrix}^T . \end{aligned} \tag{5.32}$$

Thus, the $S[\omega]$ matrix connects the wavefunction amplitudes as follows:

$$\begin{pmatrix} \Psi[1, B, \omega] \\ \Psi[L, A, \omega] \end{pmatrix} = S[\omega] \begin{pmatrix} \Psi[0, A, \omega] \\ \Psi[L+1, B, \omega] \end{pmatrix}. \tag{5.33}$$

One may straightforwardly obtain the matrices A, W_{in}, W_{out} and S_0 at this point. Specifically, let P_{in}, P_{out} and P_0 denote rectangular projection matrices onto the in, out and sample spaces. (Recall that these matrices satisfy $PP^T = 1$ but not $P^T P = 1$.) For example, let P_{in} is a $2 \times \dim \mathcal{H}$ matrix, with all elements being zero, except for those corresponding to $(0, A)$ and $(L+1, B)$. Then, it is easy to see that $A = P_0 U P_0^T$, $W_{in} = P_0 U P_{in}^T$, $W_{out} = P_{out} P_0^T$ and $S_0 = P_{out} P_{in}^T$. Clearly, $S_0 = 0$ as expected.

Here, we don't explicitly express these is matrix form. We note that the rather awkward choice for the incoming subspace, which is $(0, A)$ and $(L+1, B)$ instead of $(1, A)$ and (L, B) as one would want, is due to the fact that we used (5.14), with $\phi_{in}[T]$ instead of $\phi_{in}[T+1]$ on the right hand side. If we use the latter, then ϕ_{out} will correspond to $(1, A)$ and (L, B) as we want. This will result in an overall phase change in the corresponding $S[\omega]$.

Let us briefly discuss how to interpret this setup as one corresponding to 'scattering of waves'. Let us decompose Ψ in Fourier space for time as well as position space. In particular, let Ψ be an eigenvector of $\mathcal{U}$, so that $\mathcal{U}\Psi = e^{-i\omega}\Psi$, and let $\Psi[T] = \mathcal{U}^T \Psi = e^{-i\omega t}$ be a vector which evolves according to $\mathcal{U}$ and has the value of Ψ at $T = 0$. Thus, we have

$$\begin{aligned} \Psi[n, \alpha, T] &= \sum_{k, \omega'} e^{i(kn - \omega' T)} \Psi[k, \alpha, \omega'], \\ &= e^{-i\omega} \sum_k e^{ikn} \Psi[k, \alpha, \omega]. \end{aligned}$$

For $n < 1$ and $n \geq L$, we note that

$$\begin{aligned} & \Psi[n+1, A, T+1] = \Psi[n, A, T] \\ \implies & e^{-i\omega T} \sum_k e^{ikn} (e^{i(k-\omega)} - 1) \Psi[k, A, \omega] = 0 \\ \implies & \Psi_{n<1, n \geq L}[k, A, \omega] = 0 \quad \text{if } k \neq \omega, \\ \implies & \Psi_{n<1(n \geq L)} \Psi[n, A, \omega] = e^{i\omega n} \Psi_{n<1(n \geq L)}[\omega, A, \omega]. \end{aligned}$$

Similarly, for the B channel, get get

$$\Psi_{n\leq 1,n>L}[k,B]=0,\quad \text{if } k\neq -\omega.$$
$$\implies \Psi_{n\leq 1(n>L)}\Psi[n,B,\omega]=e^{-i\omega n}\Psi_{n\leq 1(n>L)}[-\omega,B,\omega].$$

Here, the subscripts denoting the position denote the fact that the $k-$space decomposition has been done only in the corresponding region. Thus, the only waves moving on the left and right of the sample are right moving $k=\omega$ waves in the A channel, and left moving $k=\omega$ waves in the B channel. Let us denote the incoming an outgoing wave amplitudes as follows:

$$\Psi_{n\leq 1}[\omega,A,\omega]=L^{+}$$
$$\Psi_{n\geq L}[\omega,A,\omega]=e^{i\omega L}R^{+}$$
$$\Psi_{n\leq 1}[-\omega,B,\omega]=e^{-i\omega}L^{-}$$
$$\Psi_{n\geq L}[-\omega,B,\omega]=e^{-i\omega(L+1)}R^{-},$$

where the phases have been adjusted, so as to get a nice form upon substitution in (5.33):

$$\begin{pmatrix}L_{-}\\R_{+}\end{pmatrix}=S[\omega]\begin{pmatrix}L+\\R-\end{pmatrix}.$$

Thus, the scattering matrix relates the incoming wave amplitudes to the outgoing wave amplitudes.

5.3.3.2 1-2 Leads

In this setup, the dynamics everywhere is the same as that of $U(T_{\text{drive}}/2+\Delta t)$. The disorder is turned on in the sample, and turned off everywhere else. Specifically, the evolution is determined by a unitary given by

$$\begin{aligned}\mathcal{U}\,|n,A\rangle &= e^{i\phi_{n,A}}(\cos\Delta t\,|n+1,A\rangle + i\sin\Delta t\,|n,B\rangle),\\ \mathcal{U}\,|n,B\rangle &= e^{i\phi_{n,B}}(\cos\Delta t\,|n-1,B\rangle + i\sin\Delta t\,|n,A\rangle),\end{aligned}\tag{5.34}$$

with $\phi_{n,A/B}=0$ for $n<1$ and $n>L$, along with $\phi_{1,A}=0$ and $\phi_{L+1,B}=0$. The setup is shown schematically in figure 5.2. The reason for choosing this 'tilted' box, rather than a

rectangular box will become clear soon. (Choosing a rectangular box makes the probability conservation equation complicated, with the in and out spaces being mixtures of two orbitals each. Additionally, the combination on the left is not the same as the combination on the right, making it harder to obtain the desirable chainable form similar to the transfer matrix approach. This choice necessitates obtaining appropriate rotations as in (5.24).)

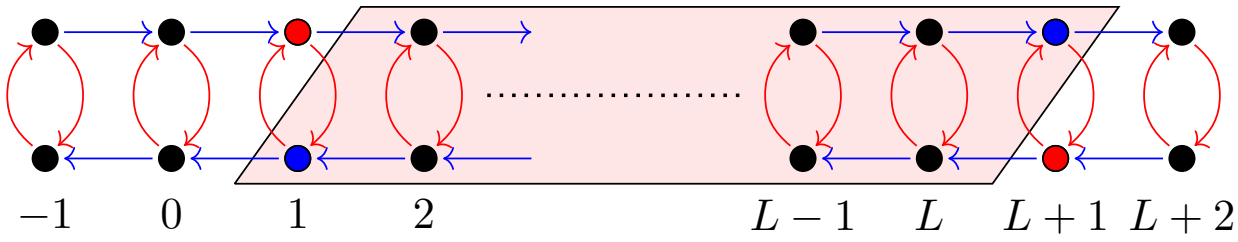

Figure 5.2: The scattering setup for 1-2 leads. The red (blue) circles correspond to the in (out) subspaces. The arrows denote the connectivity of the scattering unitary $\mathcal{U}$. The red and blue arrows correspond to hopping amplitudes of $i \sin \Delta t$ and $\cos \Delta t$ respectively (upto an on-site phase). We designate the colored region to be the 'sample' subspace.

As before, in order to obtain the S matrix, we first obtain the particle conservation relation. We note that for a wavefunction $|\Psi\rangle$ evolving according to U, the change in the probability in one time step at any A or B orbital is given by

$$\begin{aligned} |\Psi[n, A, T+1]|^2 - |\Psi[n, A, T]|^2 &= \cos^2 \Delta t |\Psi[n-1, A, T]|^2 + \sin^2 \Delta t |\Psi[n, B, T]|^2 \\ &+ \sin(2\Delta t)\, \mathrm{Re}[i e^{i(\phi_{n,B} - \phi_{n-1,A})} \Psi^*[n-1, A, T] \Psi[n, B, T]] \\ &- |\Psi[n, A, T]|^2; \end{aligned} \tag{5.35}$$

$$\begin{aligned} |\Psi[n-1, B, T+1]|^2 - |\Psi[n-1, B, T]|^2 &= \sin^2 \Delta t |\Psi[n-1, A, T]|^2 + \cos^2 \Delta t |\Psi[n, B, T]|^2 \\ &- \sin(2\Delta t)\, \mathrm{Re}[i e^{i(\phi_{n,B} - \phi_{n-1,A})} \Psi^*[n-1, A, T] \Psi[n, B, T]] \\ &- |\Psi[n-1, B, T]|^2. \end{aligned} \tag{5.36}$$

We note that adding the two equations leads to the cancellation of the cross terms on the right hand side. Thus, we get the particle conservation equation (5.13) with the following

choice:

$$\begin{aligned}
\psi[T] &= \begin{pmatrix} \Psi[1B,T] & \Psi[2A,T] & \dots & \Psi[L,A,T] & \Psi[L,B,T] & \Psi[L+1,A,T] \end{pmatrix}^T \\
\phi_{in}[T] &= \begin{pmatrix} \Psi[1,A,T] & \Psi[L+1,B,T] \end{pmatrix}^T \\
\phi_{out}[t] &= \begin{pmatrix} \Psi[1,B,T] & \Psi[L+1,A,T] \end{pmatrix}^T .
\end{aligned} \tag{5.37}$$

As before, the matrices A, $W_{in/out}$ and S_0 can be obtained straightforwarly, although it is less trivial to obtain the $S[\omega]$ matrix from these because of the matrix inversion.

5.3.4 Connection to Real-Space Transfer Matrix Approach

In the previous subsections, we implemented the FS approach from the point of view of a scattering matrix corresponding to a scattering experiment with incoming and outgoing waves. However, one may also interpret the FS approach in the following manner: for an eigenvector corresponding to an assumed quasienergy of the unitary, $S[\omega]$ relates the amplitude of the eigenvector at on site, to that at another site. This is precisely the real space transfer matrix approach, as done in [126].

This can be shown to be true straightforwardly. Let Ψ be an eigenvector of a unitary U corresponding to an eigenvalue of $e^{-i\omega}$. Let $\Psi[T]$ be a time-dependent vector which evolves according to U, and which equals Ψ at time $T = 0$. Thus, this vector satisfies

$$\Psi[T] = U^T \Psi[0] = e^{-i\omega T}\Psi. \tag{5.38}$$

Thus, in the Fourier space, $\Psi[T]$ has only one component, with $\Psi[\omega'] = 0$ whenever $\omega' \neq \omega$. Since the sample and in/out vectors are simply projections of Ψ, they too obey this statement. Therefore, the scattering matrix provides the a relationship between the amplitudes of an assumed eigenvector at the ends of the sample region. Note that in the section on 1-2 leads, whether the disorder outside the sample region was zero or not did not affect our conclusions, and hence we borrow that setup, except that the disorder outside is not set to zero.

We will now calculate the scattering matrix corresponding to one scatterer. Consider the

sample region to consist of (n, B) and $(n+1, A)$. Thus, we choose

$$\begin{aligned}
\psi[T] &= \begin{pmatrix} \Psi[n, B, T] & \Psi[n+1, A, T] \end{pmatrix}^T, \\
\phi_{in}[T] &= \begin{pmatrix} \Psi[n, A, T] & \Psi[n+1, B, T] \end{pmatrix}^T, \\
\phi_{out}[T] &= \begin{pmatrix} \Psi[n, B, T] & \Psi[n+1, A, T] \end{pmatrix}^T = \psi[T].
\end{aligned}$$

The submatrices of V are then given by

$$W_{out} = \begin{pmatrix} 1 & 0 \\ 0 & 1 \end{pmatrix}, \qquad S_0 = \begin{pmatrix} 0 & 0 \\ 0 & 0 \end{pmatrix}$$

$$W_{in} = \begin{pmatrix} i \sin \Delta t e^{i\phi_{nA}} & \cos \Delta t e^{i\phi_{n+1,B}} \\ \cos \Delta t e^{i\phi_{n,A}} & i \sin \Delta t e^{i\phi_{n+1,B}} \end{pmatrix}, \qquad A = \begin{pmatrix} 0 & 0 \\ 0 & 0 \end{pmatrix}.$$

Thus, the scattering matrix is

$$\begin{aligned}
S[\omega] &= 0 + 1 \frac{1}{e^{-i\omega} - 0} W_{in} \\
&= e^{i\omega} \begin{pmatrix} i \sin \Delta t e^{i\phi_{nA}} & \cos \Delta t e^{i\phi_{n+1,B}} \\ \cos \Delta t e^{i\phi_{n,A}} & i \sin \Delta t e^{i\phi_{n+1,B}} \end{pmatrix}.
\end{aligned} \tag{5.39}$$

Thus, we have:

$$\begin{pmatrix} \Psi[n, B, \omega] \\ \Psi[n+1, A, \omega] \end{pmatrix} = S[\omega] \begin{pmatrix} \Psi[n, A, \omega] \\ \Psi[n+1, B, \omega] \end{pmatrix}$$

Since $\Psi[n, \alpha, \omega] = \Psi[n, \alpha]$, we can drop the omega dependence from the left hand side for an eigenvector of quasienergy ω. We would like to obtain a relationship instead between the amplitude of Ψ at sites $n+1$ and n. In other words, we would like to obtain a transfer matrix. To that end, recall that a scattering matrix S and a transfer matrix M are related as follows:

$$S = \begin{pmatrix} r & t' \\ t & r' \end{pmatrix} \iff \quad M = \begin{pmatrix} \frac{1}{t^*} & -\frac{r^*}{t^*} \\ -\frac{r}{t'} & \frac{1}{t} \end{pmatrix},$$

Thus, we obtain

$$\begin{pmatrix} \Psi[n+1, A] \\ \Psi[n+1, B] \end{pmatrix} = \underbrace{\begin{pmatrix} \sec \Delta t e^{i(\omega + \phi_{n,A})} & i \tan \Delta t \\ -i \tan \Delta t e^{i(\phi_{n,A} - \phi_{n+1,B})} & \sec \Delta t e^{-i(\omega + \phi_{n,A})} \end{pmatrix}}_{M} \begin{pmatrix} \Psi[n, A] \\ \Psi[n, B] \end{pmatrix}.$$

This is precisely the position-space transfer matrix derived above, i.e. the matrix in (5.11). Note that ω here is identical to the quasienergy $t\epsilon$.

5.4 Model Drive with Full Onsite Disorder

In this section, we will show that for the model drive with full on-site disorder, i.e. with $\phi_{n,A}$ and $\phi_{n,B}$ in (5.10) being uniformly distributed over $[-\pi, \pi]$, the exponent is indeed 2, i.e. we will show that $L_{\text{loc}} \propto \Delta t^{-2}$.

Furthermore, we will show that the logarithm of the transmission coefficient in this case follows the Fokker-Planck equation.

Much of the calculations here follow the treatment in Ref. [130].

5.4.1 Derivation of the Exponent

To that end, we obtain a relationship between transmission coefficients corresponding to different sample sizes. We will use the Neumann series, so that

$$\begin{aligned} S[\omega] &= S_0 + W_{out}\frac{1}{e^{-i\omega} - A}W_{in}. \\ &= S_0 + W_{out}(1 + e^{i\omega}A + e^{2i\omega}A^2 + \dots)e^{i\omega}W_{in}. \end{aligned}$$

Now, consider the scattering matrix corresponding to a sample of size L, as shown in figure 5.2. Let us denote the transmission and reflection amplitudes by t_{1-L}, t'_{1-L} and r_{1-L}, r'_{l-L} respectively. Now if we increase the sample region by one unit to the right, then the transmission amplitude $t_{1-(L+1)}$ will be related (using the series form above) to those of S_L through the following relationship:

$$\begin{aligned} t_{1-(L+1)} &= t_{1-L}f_1 + t_{1-L}f_2 r'_{l-L}f_1 + t_{1-L}f_L f_2 r'_{l-L}f_2 r'_{l-L}f_1 + \dots \\ &= t_{1-L}f_1(1 + (f_2 r'_{l-L}) + (f_2 r'_{l-L})^2 + \dots) \\ &= \frac{t_{1-L}f_1}{1 - f_2 r'_{l-L}}, \end{aligned} \tag{5.40}$$

with $f_1 = \cos\tau e^{i(\omega+\phi_{L+2,A})}$ and $f_2 = i\sin\tau e^{i(\omega+\phi_{L+1,A})}$. We note that $t_{L-(L+1)} = f_1$, and $r'_{L-(L+1)} = f_2$ so that we may write

$$t_{1-(L+1)} = \frac{t_{1-L}t_{L-(L+1)}}{1 - r'_{l-L}r'_{L-(L+1)}}. \tag{5.41}$$

In fact using the Neumann series, we can see that this is true for any two sample spaces which share a boundary. The same conclusion can be reached at following the arguments in [130].

In the equation above, if we choose $L = 1$ and use the notation $t_{12} = t_{1-3}$, $t_1 = t_{1-2}$, $t_2 = t_{2-3}$, $r'_1 = r'_{1-2}$ and $r_2 = r_{2-3}$, then we have

$$t_{1-2} = \frac{t_1 t_2}{1 - r'_1 r_2},$$

This is precisely equation (12) from [130]. We now proceed analogously. Taking the square of the absolute values of both the sides, we get

$$T_{12} = \frac{T_1 T_2}{|1 - \sqrt{R_1 R_2}e^{i\theta}|^2}, \tag{5.42}$$

wherein we have absorbed the arguments of r'_1 and r_2 into θ. In general, the distribution of θ is disorder dependent. In our case, we can show that θ is uniformly distributed in $[-2w, 2w]$, or $[-\pi, \pi]$ with the choice $w = \pi$. This is straightforward:

$$\theta = \arg r'_1 r_2. \tag{5.43}$$

Reading of the r' and r from equation (5.39), we have

$$r'_1 = i\sin(\Delta t)\exp(i(\omega + \phi_{2,B})) \tag{5.44}$$

$$r_2 = i\sin(\Delta t)\exp(i(\phi_{2,A} + \omega)) \tag{5.45}$$

Thus,

$$\theta = \phi_{2,A} + \phi_{2,B} - \pi + 2\omega. \tag{5.46}$$

Note that $\phi_{2,A}$ and $\phi_{2,B}$ are both distributed uniformly over $[-\pi, \pi]$. The sum of uniform I.I.D. distributions is given by the Irwin-Hall distribution. Thus $\phi_{2,A} + \phi_{2,B}$ has a triangular

probability density function:

$$f_{\phi_{2,A}+\phi_{2,B}}(x) = \begin{cases} \frac{1}{2\pi}x + 1 & \text{for } -2\pi < x < 0 \\ -\frac{1}{2\pi}x + 1 & \text{for } 0 \leq x < 2\pi \end{cases} \tag{5.47}$$

However, note that the value of $\phi_{2,A} + \phi_{2,B}$ is only meaningful modulo 2π. Thus, θ is uniformly distributed over $[-\pi, \pi]$.

We consider now the logarithm of the transmission probability upon combining two scatterers. Taking the average of (5.42), we see that

$$\begin{aligned} \langle \ln T_{12} \rangle_d &= \left\langle \ln T_1 + \ln T_2 - \ln |1 - \sqrt{R_1 R_2} e^{i\theta}|^2 \right\rangle_\theta \\ &= \ln T_1 + \ln T_2 - \int_0^{2\pi} \mathrm{d}\theta \ln |1 - \sqrt{R_1 R_2} e^{i\theta}|^2 \\ &= \ln T_1 + \ln T_2 + 2i \oint_C \mathrm{d}x \frac{|1 - \sqrt{R_1 R_2} x|}{x} \qquad (5.48) \\ &= \ln T_1 + \ln T_2. \end{aligned}$$

Note that in step (5.48), C denotes the unit circle in the complex plane, with a counterclockwise orientation. Using Cauchy's residue theorem, the integral vanishes. Thus, the log of the transmission value is additive. Thus, the transmission from sites 1 to L satisfies

$$\langle \ln T_{1 \cdots L} \rangle = \sum_i^L \ln T_i \tag{5.49}$$

From (5.39), note that each $T_i = \cos^2(\Delta t)$, and thus

$$\langle \ln T_{1 \cdots L} \rangle = 2L \ln \cos(\Delta t). \tag{5.50}$$

Recall that the localization length ξ is defined through the equation:

$$\langle \ln T_{1 \cdots L} \rangle = -\frac{L}{\xi}. \tag{5.51}$$

Thus, the localization length has the value

$$\begin{aligned} \xi &= -\frac{1}{2 \ln \cos(\Delta t)} \qquad (5.52) \\ &= \frac{1}{\Delta t^2 + \mathcal{O}(\Delta t^4)} \end{aligned}$$

$$\text{so that } \xi \propto \Delta t^{-2} \qquad \text{for } \tau \to 0 \tag{5.53}$$

5.4.2 Fokker-Planck Equation for Log Transmission

Now, let us use equation (5.40) in order to derive the Fokker-Planck equation for the log of the transmission probability. This enables us to derive an expression for the probability distribution of the log of the transmission probability for large lengths. We note that we are only able to derive this equation for the case when $\tau \to 0$.

To aid readability, let us replace subscripts $1-L$ and $1-(L+1)$ by simply L and $L+1$. (This notation is different than the one we used while deriving the log additivity of the transmission probability.) Thus, we have

$$t_{L+1} = \frac{t_L \cos\tau e^{i(\omega+\phi_{L+2,A})}}{1 - i\sin\tau e^{i(\omega+\phi_{L+1,A})} r'_L}. \tag{5.54}$$

Taking the absolute value square on both sides, we get

$$T_{L+1} = \frac{T_L \cos^2\tau}{1 + (1-T_L) + 2\sin\tau\sqrt{1-T_L}\sin\Gamma_L},$$

with $\Gamma_L = \omega + \phi_{L+1,A} + \arg r'_L$. Taking the logarithm on both sides, and using the notation $\eta_L = -\log T_L$, we get

$$\eta_{L+1} = \eta_L - 2\log\cos\tau + \log[2 - T_L + 2\sin\tau\sqrt{1-T_L}\sin\Gamma_L].$$

For large lengths, we expect $T_L \to 0$. We Taylor expand to second order in τ, which gives us

$$\eta_{L+1} = \eta_L + \tau^2[2 - e^{-\eta_L} - 2\sin^2\Gamma_L(1-e^{-\eta_L})] + 2\tau\sin\Gamma_L\sqrt{1-e^{-\eta_L}}. \tag{5.55}$$

We can use this to relate the probability distribution of η's for lengths L and $L+1$. Specifically,

$$P_{L+1}(\eta) = \int \frac{\mathrm{d}\Gamma}{2\pi} \int \mathrm{d}P_L(\eta')\delta(\eta' + \tau^2[2 - e^{-\eta'} - 2\sin^2\Gamma(1-e^{-\eta'})] + 2\tau\sin\Gamma\sqrt{1-e^{-\eta'}} - \eta)$$

Inverting the relation (5.55) and opening the δ function, we get

$$P_{L+1}(\eta) = \int \frac{\mathrm{d}\Gamma}{2\pi} P_L(\eta - \tau^2[2 - e^{-\eta} - 2\sin^2\Gamma(1-e^{-\eta})] - 2\tau\sin\Gamma\sqrt{1-e^{-\eta}})$$

Taylor expanding to second order in τ, we get

$$P_{L+1}(\eta) = P_L(\eta) - \tau^2\frac{\partial P_L}{\partial\eta} +' \tau^2(1-e^{-\eta})\frac{\partial^2 P_L}{\partial\eta^2}.$$

Taking the continuum limit, we write $P_{L+1} - P_L \to \frac{\partial P}{\partial L}$. For $L \to \infty$, we expect $\eta \to \infty$, so that $e^{-\eta} \to 0$. This finally gives us

$$\tau^{-2}\frac{\partial P}{\partial L} = -\frac{\partial P}{\partial \eta} + \frac{\partial^2 P}{\partial \eta^2}. \tag{5.56}$$

The solution of this equation is

$$P_L(\eta) = \sqrt{\frac{L_{loc}}{2\pi\eta}} \exp\left[-\frac{(\eta - 2n/L_{loc})^2}{2n/L_{loc}}\right], \tag{5.57}$$

$$\text{with } L_{loc} = 2\tau^{-2} \tag{5.58}$$

5.5 Conclusion

In this chapter, we studied a specific class of disordered chiral Floquet topological insulators in one dimension that are described by loop drives. We further showed that the eigenvectors of the time evolution operator at times t close to the midpoint of the drive have localization lengths that diverge as $L_{\text{loc}} \propto |t - T_{\text{drive}}/2|^{-2}$.

After reviewing the definition of Chiral Floquet topological insulators, we presented an example drive that was proposed in the literature. After discussing various ways to disorder this example drive, we calculated the position-space transfer matrix the model drive with on-site phase disorder. Using the scattering theory approach for discrete time quantum systems, we derived the same formula with an appropriate setup. Finally, we derived the exponent of two using for the model drive with full phase disorder, and showed that the logarithm of the transmission coefficient follows the Fokker-Plank equation.

While the arguments presented here are restricted to the case of the model drive with full on-site phase disorder, it is possible to show that the exponent is universal and appears in all 1d chiral loop drives. These arguments rely on the results presented in Refs. [131, 132], which outline a perturbative scattering theory approach for independently and identically disordered scatterers which are individually almost fully transmitting (i.e. have transmission coefficients close to one). The full argument along with supporting numerical evidence for the universality of the exponent will be presenting in a forthcoming manuscript.

REFERENCES

[1] Daijiro Yoshioka. *The Quantum Hall Effect*, volume 133. Springer Science & Business Media, 2002.

[2] David Tong. The Quantum Hall Effect (TIFR Infosys Lectures).

[3] Alexander Altland and Ben D Simons. *Condensed Matter Field Theory*. Cambridge university press, 2010.

[4] Steven M Girvin and Kun Yang. *Modern Condensed Matter Physics*. Cambridge University Press, 2019.

[5] Neil W. Ashcroft and N. David Mermin. *Solid State Physics*. New York: Holt, Rinehart and Winston,, 1976.

[6] J. M. Luttinger. The Effect of a Magnetic Field on Electrons in a Periodic Potential. *Physical Review*, 84(4):814–817, November 1951.

[7] R. Peierls. Zur Theorie des Diamagnetismus von Leitungselektronen. *Zeitschrift für Physik*, 80(11):763–791, November 1933.

[8] David Vanderbilt. *Berry Phases in Electronic Structure Theory: Electric Polarization, Orbital Magnetization and Topological Insulators*. Cambridge University Press, 2018.

[9] N. Byers and C. N. Yang. Theoretical Considerations Concerning Quantized Magnetic Flux in Superconducting Cylinders. *Physical Review Letters*, 7(2):46–49, July 1961.

[10] Pratik Sathe, Fenner Harper, and Rahul Roy. Compactly supported Wannier functions and strictly local projectors. *Journal of Physics A: Mathematical and Theoretical*, 54(33):335302, July 2021.

[11] Gregory H. Wannier. The Structure of Electronic Excitation Levels in Insulating Crystals. *Phys. Rev.*, 52(3):191–197, August 1937.

[12] Raffaele Resta. Electrical polarization and orbital magnetization: The modern theories. *Journal of Physics: Condensed Matter*, 22(12):123201, 2010.

[13] T. Thonhauser, Davide Ceresoli, David Vanderbilt, and R. Resta. Orbital magnetization in periodic insulators. *Physical Review Letters*, 95(13):137205, September 2005.

[14] Arrigo Calzolari, Nicola Marzari, Ivo Souza, and Marco Buongiorno Nardelli. Ab initio transport properties of nanostructures from maximally localized Wannier functions. *Physical Review B*, 69(3):035108, January 2004.

[15] Jonathan R. Yates, Xinjie Wang, David Vanderbilt, and Ivo Souza. Spectral and Fermi surface properties from Wannier interpolation. *Physical Review B*, 75(19):195121, May 2007.

[16] W. Kohn. Analytic properties of bloch waves and wannier functions. *Physical Review*, 115(4):809–821, August 1959.

[17] Jacques Des Cloizeaux. Energy Bands and Projection Operators in a Crystal: Analytic and Asymptotic Properties. *Physical Review*, 135(3A):A685–A697, August 1964.

[18] Jacques Des Cloizeaux. Analytical properties of n-Dimensional energy bands and wannier functions. *Physical Review*, 135(3A):A698–A707, August 1964.

[19] G Nenciu. Existence of the exponentially localised Wannier functions. *Communications in mathematical physics*, 91(1):81–85, 1983.

[20] Nicola Marzari and David Vanderbilt. Maximally localized generalized Wannier functions for composite energy bands. *Physical review B*, 56(20):12847, 1997.

[21] Gianluca Panati and Adriano Pisante. Bloch Bundles, Marzari-Vanderbilt Functional and Maximally Localized Wannier Functions. *Communications in Mathematical Physics*, 322(3):835–875, September 2013.

[22] S. F. Boys. Construction of Some Molecular Orbitals to Be Approximately Invariant for Changes from One Molecule to Another. *Reviews of Modern Physics*, 32(2):296–299, April 1960.

[23] GF Koster. Localized functions in molecules and crystals. *Physical Review*, 89(1):67, 1953.

[24] Vidvuds Ozoliņš, Rongjie Lai, Russel Caflisch, and Stanley Osher. Compressed modes for variational problems in mathematics and physics. *Proceedings of the National Academy of Sciences*, 110(46):18368–18373, 2013.

[25] JC Budich, J Eisert, EJ Bergholtz, S Diehl, and P Zoller. Search for localized Wannier functions of topological band structures via compressed sensing. *Physical Review B*, 90(11):115110, 2014.

[26] Farzin Barekat, Ke Yin, Russel E Caflisch, Stanley J Osher, Rongjie Lai, and Vidvuds Ozolins. Compressed Wannier modes found from an L_1 regularized energy functional. *arXiv preprint arXiv:1403.6883*, 2014.

[27] Liu Zheng, Liu Feng, and Wu Yong-Shi. Exotic electronic states in the world of flat bands: From theory to material. *Chinese Physics B*, 23(7):077308, 2014.

[28] Jerome Dubail and Nicholas Read. Tensor network trial states for chiral topological phases in two dimensions and a no-go theorem in any dimension. *Physical Review B*, 92(20):205307, 2015.

[29] N. Read. Compactly supported Wannier functions and algebraic K-Theory. *Physical Review B*, 95(11):115309, March 2017.

[30] Li Chen, Tahereh Mazaheri, Alexander Seidel, and Xiang Tang. The impossibility of exactly flat non-trivial Chern bands in strictly local periodic tight binding models. *Journal of Physics A: Mathematical and Theoretical*, 47(15):152001, April 2014.

[31] Daniel Leykam, Alexei Andreanov, and Sergej Flach. Artificial flat band systems: From lattice models to experiments. *Advances in Physics: X*, 3(1):1473052, January 2018.

[32] Yuan Cao, Valla Fatemi, Shiang Fang, Kenji Watanabe, Takashi Taniguchi, Efthimios Kaxiras, and Pablo Jarillo-Herrero. Unconventional superconductivity in magic-angle graphene superlattices. *Nature*, 556(7699):43–50, April 2018.

[33] Matthew Yankowitz, Shaowen Chen, Hryhoriy Polshyn, Yuxuan Zhang, K. Watanabe, T. Taniguchi, David Graf, Andrea F. Young, and Cory R. Dean. Tuning superconductivity in twisted bilayer graphene. *Science (New York, N.Y.)*, 363(6431):1059–1064, March 2019.

[34] RG Dias and JD Gouveia. Origami rules for the construction of localized eigenstates of the Hubbard model in decorated lattices. *Scientific reports*, 5:16852, 2015.

[35] Wulayimu Maimaiti, Alexei Andreanov, Hee Chul Park, Oleg Gendelman, and Sergej Flach. Compact localized states and flat-band generators in one dimension. *Physical Review B*, 95(11):115135, 2017.

[36] Wulayimu Maimaiti, Sergej Flach, and Alexei Andreanov. Universal d = 1 flat band generator from compact localized states. *Physical Review B*, 99(12):125129, March 2019.

[37] Sebastian D. Huber and Ehud Altman. Bose condensation in flat bands. *Physical Review B*, 82(18):184502, November 2010.

[38] Yoshihito Kuno, Tomonari Mizoguchi, and Yasuhiro Hatsugai. Flat band quantum scar. *Physical Review B*, 102(24):241115, December 2020.

[39] Claudia Sgiarovello, Maria Peressi, and Raffaele Resta. Electron localization in the insulating state: Application to crystalline semiconductors. *Physical Review B*, 64(11):115202, August 2001.

[40] Kasra Hejazi, Xiao Chen, and Leon Balents. Hybrid Wannier Chern bands in magic angle twisted bilayer graphene and the quantized anomalous Hall effect. *arXiv:2007.00134 [cond-mat]*, February 2021.

[41] Alexey A. Soluyanov and David Vanderbilt. Computing topological invariants without inversion symmetry. *Physical Review B*, 83(23):235401, June 2011.

[42] Maryam Taherinejad, Kevin F. Garrity, and David Vanderbilt. Wannier center sheets in topological insulators. *Physical Review B*, 89(11):115102, March 2014.

[43] Dominik Gresch, Gabriel Autès, Oleg V. Yazyev, Matthias Troyer, David Vanderbilt, B. Andrei Bernevig, and Alexey A. Soluyanov. Z2Pack: Numerical implementation of hybrid Wannier centers for identifying topological materials. *Physical Review B*, 95(7):075146, February 2017.

[44] Masaya Nakagawa, Robert-Jan Slager, Sho Higashikawa, and Takashi Oka. Wannier representation of Floquet topological states. *Physical Review B*, 101(7):075108, February 2020.

[45] D. J. Thouless. Wannier functions for magnetic sub-bands. *Journal of Physics C: Solid State Physics*, 17(12):L325–L327, April 1984.

[46] Domenico Monaco, Gianluca Panati, Adriano Pisante, and Stefan Teufel. Optimal decay of Wannier functions in Chern and quantum Hall insulators. *Communications in Mathematical Physics*, 359(1):61–100, 2018.

[47] Gianluca Panati. Triviality of bloch and Bloch–Dirac bundles. In *Annales Henri Poincaré*, volume 8, pages 995–1011. Springer, 2007.

[48] Christian Brouder, Gianluca Panati, Matteo Calandra, Christophe Mourougane, and Nicola Marzari. Exponential Localization of Wannier Functions in Insulators. *Physical Review Letters*, 98(4):046402, January 2007.

[49] Xiao-Liang Qi. Generic Wave-Function Description of Fractional Quantum Anomalous Hall States and Fractional Topological Insulators. *Physical Review Letters*, 107(12):126803, September 2011.

[50] Doron L. Bergman, Congjun Wu, and Leon Balents. Band touching from real-space topology in frustrated hopping models. *Physical Review B*, 78(12):125104, September 2008.

[51] Siddharth A. Parameswaran, Rahul Roy, and Shivaji L. Sondhi. Fractional quantum Hall physics in topological flat bands. *Comptes Rendus Physique*, 14(9-10):816–839, November 2013.

[52] Michael Creutz. Aspects of chiral symmetry and the lattice. *Reviews of Modern Physics*, 73(1):119–150, January 2001.

[53] Daniel Leykam, Sergej Flach, Omri Bahat-Treidel, and Anton S. Desyatnikov. Flat band states: Disorder and nonlinearity. *Physical Review B*, 88(22):224203, December 2013.

[54] Yoshihito Kuno. Extended flat band, entanglement, and topological properties in a Creutz ladder. *Physical Review B*, 101(18):184112, May 2020.

[55] J. Jünemann, A. Piga, S.-J. Ran, M. Lewenstein, M. Rizzi, and A. Bermudez. Exploring Interacting Topological Insulators with Ultracold Atoms: The Synthetic Creutz-Hubbard Model. *Physical Review X*, 7(3):031057, September 2017.

[56] Michael Creutz. End States, Ladder Compounds, and Domain-Wall Fermions. *Physical Review Letters*, 83(13):2636–2639, September 1999.

[57] Sebabrata Mukherjee, Marco Di Liberto, Patrik Öhberg, Robert R. Thomson, and Nathan Goldman. Experimental Observation of Aharonov-Bohm Cages in Photonic Lattices. *Physical Review Letters*, 121(7):075502, August 2018.

[58] Jin Hyoun Kang, Jeong Ho Han, and Y Shin. Creutz ladder in a resonantly shaken 1D optical lattice. *New Journal of Physics*, 22(1):013023, January 2020.

[59] Per-Olov Löwdin. On the non-orthogonality problem connected with the use of atomic wave functions in the theory of molecules and crystals. *The Journal of Chemical Physics*, 18(3):365–375, 1950.

[60] Rahul Siddharthan and Antoine Georges. Square kagome quantum antiferromagnet and the eight-vertex model. *Physical Review B*, 65(1):014417, December 2001.

[61] Johannes Richter, Oleg Derzhko, and Taras Krokhmalskii. Finite-temperature order-disorder phase transition in a frustrated bilayer quantum Heisenberg antiferromagnet in strong magnetic fields. *Physical Review B*, 74(14):144430, October 2006.

[62] Oleg Derzhko, Johannes Richter, and Mykola Maksymenko. Strongly correlated flat-band systems: The route from Heisenberg spins to Hubbard electrons. *International Journal of Modern Physics B*, 29(12):1530007, 2015.

[63] Hal Tasaki. Ferromagnetism in the Hubbard models with degenerate single-electron ground states. *Physical review letters*, 69(10):1608, 1992.

[64] Bill Sutherland. Localization of electronic wave functions due to local topology. *Physical Review B*, 34(8):5208–5211, October 1986.

[65] Domenico Monaco and Gianluca Panati. Symmetry and Localization in Periodic Crystals: Triviality of Bloch Bundles with a Fermionic Time-Reversal Symmetry. *Acta Applicandae Mathematicae*, 137(1):185–203, June 2015.

[66] Giovanna Marcelli, Massimo Moscolari, and Gianluca Panati. Localization implies Chern triviality in non-periodic insulators. *arXiv preprint arXiv:2012.14407*, 2020.

[67] Alexander Altland and Martin R. Zirnbauer. Nonstandard symmetry classes in mesoscopic normal-superconducting hybrid structures. *Physical Review B*, 55(2):1142–1161, January 1997.

[68] Alexei Kitaev. Periodic table for topological insulators and superconductors. *AIP Conference Proceedings*, 1134(1):22–30, May 2009.

[69] Shinsei Ryu, Andreas P Schnyder, Akira Furusaki, and Andreas W W Ludwig. Topological insulators and superconductors: Tenfold way and dimensional hierarchy. *New Journal of Physics*, 12(6):065010, June 2010.

[70] Hosho Katsura and Tohru Koma. The noncommutative index theorem and the periodic table for disordered topological insulators and superconductors. *Journal of Mathematical Physics*, 59(3):031903, 2018.

[71] Alexei Kitaev. Anyons in an exactly solved model and beyond. *Annals of Physics*, 321(1):2–111, 2006.

[72] Giovanna Marcelli, Domenico Monaco, Massimo Moscolari, and Gianluca Panati. The Haldane model and its localization dichotomy. *arXiv preprint arXiv:1909.03298*, 2019.

[73] Pratik Sathe and Rahul Roy. Compact Wannier Functions in One Dimension, February 2023.

[74] Nicola Marzari, Arash A. Mostofi, Jonathan R. Yates, Ivo Souza, and David Vanderbilt. Maximally localized Wannier functions: Theory and applications. *Reviews of Modern Physics*, 84(4):1419–1475, October 2012.

[75] Arash A. Mostofi, Jonathan R. Yates, Young-Su Lee, Ivo Souza, David Vanderbilt, and Nicola Marzari. Wannier90: A tool for obtaining maximally-localised Wannier functions. *Computer Physics Communications*, 178(9):685–699, May 2008.

[76] Roman Bezrukavnikov and Anton Kapustin. Localization Properties of Chern Insulators. *Arnold Mathematical Journal*, 5(1):15–21, March 2019.

[77] Giovanna Marcelli, Massimo Moscolari, and Gianluca Panati. Localization of Generalized Wannier Bases Implies Chern Triviality in Non-periodic Insulators. *Annales Henri Poincaré*, September 2022.

[78] Jianfeng Lu and Kevin D. Stubbs. Algebraic localization implies exponential localization in non-periodic insulators. *arXiv:2101.02626*, January 2021.

[79] Alexey A. Soluyanov and David Vanderbilt. Wannier representation of Z 2 topological insulators. *Physical Review B*, 83(3):035108, January 2011.

[80] N. B. Kopnin, T. T. Heikkilä, and G. E. Volovik. High-temperature surface superconductivity in topological flat-band systems. *Physical Review B*, 83(22):220503(R), June 2011.

[81] Xiaobo Lu, Petr Stepanov, Wei Yang, Ming Xie, Mohammed Ali Aamir, Ipsita Das, Carles Urgell, Kenji Watanabe, Takashi Taniguchi, Guangyu Zhang, Adrian Bachtold, Allan H. MacDonald, and Dmitri K. Efetov. Superconductors, orbital magnets and correlated states in magic-angle bilayer graphene. *Nature*, 574(7780):653–657, October 2019.

[82] D. Marchenko, D. V. Evtushinsky, E. Golias, A. Varykhalov, Th. Seyller, and O. Rader. Extremely flat band in bilayer graphene. *Science Advances*, 4(11):eaau0059, November 2018.

[83] Hideo Aoki. Theoretical Possibilities for Flat Band Superconductivity. *Journal of Superconductivity and Novel Magnetism*, 33(8):2341–2346, August 2020.

[84] G. E. Volovik. Graphite, Graphene, and the Flat Band Superconductivity. *JETP Letters*, 107(8):516–517, April 2018.

[85] Rahul Roy and Shivaji L. Sondhi. Fractional quantum Hall effect without Landau levels. *Physics*, 4:46, June 2011.

[86] Emil J Bergholtz and Zhao Liu. Topological flat band models and fractional Chern insulators. *International Journal of Modern Physics B*, 27(24):1330017, 2013.

[87] Eric M. Spanton, Alexander A. Zibrov, Haoxin Zhou, Takashi Taniguchi, Kenji Watanabe, Michael P. Zaletel, and Andrea F. Young. Observation of fractional Chern insulators in a van der Waals heterostructure. *Science (New York, N.Y.)*, 360(6384):62–66, April 2018.

[88] Luis Morales-Inostroza and Rodrigo A. Vicencio. Simple method to construct flat-band lattices. *Physical Review A: Atomic, Molecular, and Optical Physics*, 94(4):043831, October 2016.

[89] Aamna Ahmed, Ajith Ramachandran, Ivan M. Khaymovich, and Auditya Sharma. Flat band based multifractality in the all-band-flat diamond chain. *Physical Review B*, 106(20):205119, November 2022.

[90] Carlo Danieli, Alexei Andreanov, Thudiyangal Mithun, and Sergej Flach. Quantum caging in interacting many-body all-bands-flat lattices. *Physical Review B*, 104(8):085132, August 2021.

[91] Carlo Danieli, Alexei Andreanov, Thudiyangal Mithun, and Sergej Flach. Nonlinear caging in all-bands-flat lattices. *Physical Review B*, 104(8):085131, August 2021.

[92] Anton Kapustin and Lukasz Fidkowski. Local Commuting Projector Hamiltonians and the Quantum Hall Effect. *Communications in Mathematical Physics*, 373(2):763–769, January 2020.

[93] S. Kivelson. Wannier functions in one-dimensional disordered systems: Application to fractionally charged solitons. *Physical Review B*, 26(8):4269–4277, October 1982.

[94] Pratik Sathe and Rahul Roy. Topological Triviality of Flat Hamiltonians, September 2023.

[95] K. v. Klitzing, G. Dorda, and M. Pepper. New method for high-accuracy determination of the fine-structure constant based on quantized hall resistance. *Physical Review Letters*, 45(6):494–497, August 1980.

[96] D. C. Tsui, H. L. Stormer, and A. C. Gossard. Two-dimensional magnetotransport in the extreme quantum limit. *Physical Review Letters*, 48(22):1559–1562, May 1982.

[97] M. Z. Hasan and C. L. Kane. Colloquium: Topological insulators. *Reviews of Modern Physics*, 82(4):3045–3067, November 2010.

[98] Xiao-Gang Wen. Colloquium: Zoo of quantum-topological phases of matter. *Reviews of Modern Physics*, 89(4):041004, December 2017.

[99] David J Thouless, M Kohmoto, M Nightingale, and M Den Nijs. Quantized Hall Conductance in a Two-Dimensional Periodic Potential. *Physical Review Letters*, 49(6):405–408, August 1982.

[100] Qian Niu, D. J. Thouless, and Yong-Shi Wu. Quantized Hall conductance as a topological invariant. *Physical Review B*, 31(6):3372–3377, March 1985.

[101] Joseph E. Avron and Ruedi Seiler. Quantization of the hall conductance for general, multiparticle schrödinger hamiltonians. *Physical Review Letters*, 54(4):259–262, January 1985.

[102] Yonglong Xie, Andrew T. Pierce, Jeong Min Park, Daniel E. Parker, Eslam Khalaf, Patrick Ledwith, Yuan Cao, Seung Hwan Lee, Shaowen Chen, Patrick R. Forrester, Kenji Watanabe, Takashi Taniguchi, Ashvin Vishwanath, Pablo Jarillo-Herrero, and Amir Yacoby. Fractional Chern insulators in magic-angle twisted bilayer graphene. *Nature*, 600(7889):439–443, December 2021.

[103] Zhao Liu and Emil J. Bergholtz. Recent developments in fractional Chern insulators. In *Reference Module in Materials Science and Materials Engineering*. Elsevier, 2023-01-01, 2023.

[104] Sebastiano Peotta and Päivi Törmä. Superfluidity in topologically nontrivial flat bands. *Nature Communications*, 6(1):8944, November 2015.

[105] Fang Xie, Zhida Song, Biao Lian, and B. Andrei Bernevig. Topology-Bounded Superfluid Weight in Twisted Bilayer Graphene. *Physical Review Letters*, 124(16):167002, April 2020.

[106] Hal Tasaki. From Nagaoka's Ferromagnetism to Flat-Band Ferromagnetism and Beyond: An Introduction to Ferromagnetism in the Hubbard Model. *Progress of Theoretical Physics*, 99(4):489–548, April 1998.

[107] Carlo Danieli, Alexei Andreanov, and Sergej Flach. Many-body flatband localization. *Physical Review B*, 102(4):041116, July 2020.

[108] Yoshihito Kuno, Takahiro Orito, and Ikuo Ichinose. Flat-band many-body localization and ergodicity breaking in the Creutz ladder. *New Journal of Physics*, 22(1):013032, January 2020.

[109] Goran Gligorić, Petra P. Beličev, Daniel Leykam, and Aleksandra Maluckov. Nonlinear symmetry breaking of Aharonov-Bohm cages. *Physical Review A*, 99(1):013826, January 2019.

[110] Murad Tovmasyan, Sebastiano Peotta, Long Liang, Päivi Törmä, and Sebastian D. Huber. Preformed pairs in flat Bloch bands. *Physical Review B*, 98(13):134513, October 2018.

[111] G. Pelegrí, A. M. Marques, V. Ahufinger, J. Mompart, and R. G. Dias. Interaction-induced topological properties of two bosons in flat-band systems. *Physical Review Research*, 2(3):033267, August 2020.

[112] Titus Neupert, Luiz Santos, Claudio Chamon, and Christopher Mudry. Fractional Quantum Hall States at Zero Magnetic Field. *Physical Review Letters*, 106(23):236804, June 2011.

[113] Kai Sun, Zhengcheng Gu, Hosho Katsura, and S. Das Sarma. Nearly Flatbands with Nontrivial Topology. *Physical Review Letters*, 106(23):236803, June 2011.

[114] Evelyn Tang, Jia-Wei Mei, and Xiao-Gang Wen. High-Temperature Fractional Quantum Hall States. *Physical Review Letters*, 106(23):236802, June 2011.

[115] Fa Wang and Ying Ran. Nearly flat band with Chern number $C=2$ on the dice lattice. *Physical Review B*, 84(24):241103, December 2011.

[116] Thomas Scaffidi and Steven H. Simon. Exact solutions of fractional Chern insulators: Interacting particles in the Hofstadter model at finite size. *Physical Review B*, 90(11):115132, September 2014.

[117] Matthew B. Hastings and Spyridon Michalakis. Quantization of Hall Conductance for Interacting Electrons on a Torus. *Communications in Mathematical Physics*, 334(1):433–471, February 2015.

[118] Koji Kudo, Haruki Watanabe, Toshikaze Kariyado, and Yasuhiro Hatsugai. Many-Body Chern Number without Integration. *Physical Review Letters*, 122(14):146601, April 2019.

[119] Elihu Abrahams, editor. *50 Years of Anderson Localization*. Number v. 24, no. 12 & 13, pt. 1-2 in International Journal of Modern Physics : B, Condensed Matter Physics, Statistical Physics, Applied Physics. World Scientific, Singapore ; London, 2010.

[120] E. Abrahams, P. W. Anderson, D. C. Licciardello, and T. V. Ramakrishnan. Scaling Theory of Localization: Absence of Quantum Diffusion in Two Dimensions. *Physical Review Letters*, 42(10):673–676, March 1979.

[121] Bodo Huckestein. Scaling theory of the integer quantum Hall effect. *Reviews of Modern Physics*, 67(2):357–396, April 1995.

[122] Fenner Harper, Rahul Roy, Mark S. Rudner, and S.L. Sondhi. Topology and Broken Symmetry in Floquet Systems. *Annual Review of Condensed Matter Physics*, 11(1):345–368, March 2020.

[123] Alexei Kitaev. Periodic table for topological insulators and superconductors. *AIP Conference Proceedings*, 1134(1):22–30, May 2009.

[124] Alexander Altland and Martin R. Zirnbauer. Nonstandard symmetry classes in mesoscopic normal-superconducting hybrid structures. *Physical Review B*, 55(2):1142–1161, January 1997.

[125] Rahul Roy and Fenner Harper. Periodic table for Floquet topological insulators. *Physical Review B*, 96(15):155118, October 2017.

[126] Albert Brown. *Geometric Current Response in Chern Systems and Topological Delocalization in Floquet Class AIII Systems*. PhD thesis, UCLA, 2019.

[127] Xu Liu, Fenner Harper, and Rahul Roy. Chiral flow in one-dimensional Floquet topological insulators. *Physical Review B*, 98(16):165116, October 2018.

[128] Alexei Kitaev. Anyons in an exactly solved model and beyond. *Annals of Physics*, 321(1):2–111, January 2006.

[129] Y. V. Fyodorov and H. J. Sommers. Spectra of random contractions and scattering theory for discrete-time systems. *Journal of Experimental and Theoretical Physics Letters*, 72(8):422–426, October 2000.

[130] Cord A. Müller and Dominique Delande. Disorder and interference: Localization phenomena. *arXiv:1005.0915 [cond-mat, physics:quant-ph]*, May 2010.

[131] Adrian B. Culver, Pratik Sathe, and Rahul Roy. Scattering Expansion for Localization in One Dimension, February 2023.

[132] Adrian B. Culver, Pratik Sathe, and Rahul Roy. Scattering Expansion for Localization in One Dimension: From Disordered Wires to Quantum Walks, February 2023.

[133] Tilen Čadež, Yeongjun Kim, Alexei Andreanov, and Sergej Flach. Metal-insulator transition in infinitesimally weakly disordered flat bands. *Physical Review B*, 104(18):L180201, November 2021.

[134] Stephen D. Clow and Bruce R. Johnson. Wavelet-basis calculation of Wannier functions. *Physical Review B*, 68(23):235107, December 2003.

[135] Horia D Cornean, A Nenciu, and Gheorghe Nenciu. Optimally localized Wannier functions for quasi one-dimensional nonperiodic insulators. *Journal of Physics A: Mathematical and Theoretical*, 41(12):125202, 2008.

[136] Ingrid Daubechies. *Ten Lectures on Wavelets*. SIAM, 1992.

[137] Clyde Edmiston and Klaus Ruedenberg. Localized atomic and molecular orbitals. *Reviews of Modern Physics*, 35(3):457–464, July 1963.

[138] Patrick Fischer and Mireille Defranceschi. Numerical solution of the Schrödinger equation in a wavelet basis for hydrogen-like atoms. *SIAM journal on numerical analysis*, 35(1):1–12, 1998.

[139] Patrick Fischer. Numerical solution of eigenvalue problems by means of a wavelet-based Lanczos decomposition. *International Journal of Quantum Chemistry*, 77(2):552–562, 2000.

[140] Sergej Flach, Daniel Leykam, Joshua D Bodyfelt, Peter Matthies, and Anton S Desyatnikov. Detangling flat bands into Fano lattices. *EPL (Europhysics Letters)*, 105(3):30001, 2014.

[141] F. D. M. Haldane. Model for a quantum hall effect without landau levels: Condensed-matter realization of the "Parity Anomaly". *Physical Review Letters*, 61(18):2015–2018, October 1988.

[142] Israel N Herstein. *Topics in Algebra*. John Wiley & Sons, second edition edition, 1975.

[143] K Kaneda and T Odagaki. Two-scale relations in one-dimensional crystals and wavelets. *Journal of Physics A: Mathematical and General*, 28(15):4389, 1995.

[144] Yeongjun Kim, Tilen Čadež, Alexei Andreanov, and Sergej Flach. Flat band induced metal-insulator transitions for weak magnetic flux and spin-orbit disorder. *Physical Review B*, 107(17):174202, May 2023.

[145] David Vanderbilt and R. D. King-Smith. Electric polarization as a bulk quantity and its relation to surface charge. *Physical Review B*, 48(7):4442–4455, August 1993.

[146] W. Kohn and J. R. Onffroy. Wannier functions in a simple nonperiodic system. *Physical Review B*, 8(6):2485–2495, September 1973.

[147] W. Kohn. Construction of wannier functions and applications to energy bands. *Physical Review B*, 7(10):4388–4398, May 1973.

[148] R. B. Laughlin. Quantized Hall conductivity in two dimensions. *Physical Review B*, 23(10):5632–5633, May 1981.

[149] P. Lecheminant, B. Bernu, C. Lhuillier, L. Pierre, and P. Sindzingre. Order versus disorder in the quantum Heisenberg antiferromagnet on the ***kagomé*** lattice using exact spectra analysis. *Physical Review B*, 56(5):2521–2529, August 1997.

[150] Ching Hua Lee, Daniel P Arovas, and Ronny Thomale. Band flatness optimization through complex analysis. *Physical Review B*, 93(15):155155, 2016.

[151] Sanghoon Lee, Alexei Andreanov, and Sergej Flach. Critical-to-insulator transitions and fractality edges in perturbed flat bands. *Physical Review B*, 107(1):014204, January 2023.

[152] Elliott H. Lieb. Two theorems on the Hubbard model. *Physical Review Letters*, 62(10):1201–1204, March 1989.

[153] Wulayimu Maimaiti, Alexei Andreanov, and Sergej Flach. Flat-band generator in two dimensions. *Physical Review B*, 103(16):165116, April 2021.

[154] Stéphane Mallat. *A Wavelet Tour of Signal Processing*. Elsevier, 1999.

[155] A Maloney, James L Kinsey, and Bruce R Johnson. Wavelets in curvilinear coordinate quantum calculations: H 2+ electronic states. *The Journal of chemical physics*, 117(8):3548–3557, 2002.

[156] Paul A. McClarty, Masudul Haque, Arnab Sen, and Johannes Richter. Disorder-free localization and many-body quantum scars from magnetic frustration. *Physical Review B*, 102(22):224303, December 2020.

[157] Andreas Mielke. Ferromagnetic ground states for the Hubbard model on line graphs. *Journal of Physics A: Mathematical and General*, 24(2):L73, 1991.

[158] A Mielke. Ferromagnetism in the Hubbard model on line graphs and further considerations. *Journal of Physics A: Mathematical and General*, 24(14):3311, 1991.

[159] S Miyahara, S Kusuta, and N Furukawa. BCS theory on a flat band lattice. *Physica C: Superconductivity*, 460:1145–1146, 2007.

[160] Alexandrina Nenciu and G. Nenciu. Existence of exponentially localized Wannier functions for nonperiodic systems. *Physical Review B*, 47(16):10112–10115, April 1993.

[161] Eulàlia Nicolau, Anselmo M. Marques, Ricardo G. Dias, and Verònica Ahufinger. Flat-band induced local Hilbert space fragmentation, June 2023.

[162] Eulàlia Nicolau, Anselmo M. Marques, Jordi Mompart, Verònica Ahufinger, and Ricardo G. Dias. Local Hilbert space fragmentation and weak thermalization in Bose-Hubbard diamond necklaces. *Physical Review B*, 107(9):094312, March 2023.

[163] Shinya Nishino, Masaki Goda, and Koichi Kusakabe. Flat bands of a tight-binding electronic system with hexagonal structure. *Journal of the Physical Society of Japan*, 72(8):2015–2023, 2003.

[164] Shinya Nishino and Masaki Goda. Three-dimensional flat-band models. *Journal of the Physical Society of Japan*, 74(1):393–400, 2005.

[165] Vidvuds Ozoliņš, Rongjie Lai, Russel Caflisch, and Stanley Osher. Compressed plane waves yield a compactly supported multiresolution basis for the Laplace operator. *Proceedings of the National Academy of Sciences*, 111(5):1691–1696, 2014.

[166] János Pipek and Paul G Mezey. A fast intrinsic localization procedure applicable for abinitio and semiempirical linear combination of atomic orbital wave functions. *The Journal of Chemical Physics*, 90(9):4916–4926, 1989.

[167] Qian Niu. Theory of quantized adaibatic particle transport. *Modern Physics Letters B*, 05(14n15):923–931, June 1991.

[168] Junfeng Qiao, Jiaqi Zhou, Zhe Yuan, and Weisheng Zhao. Calculation of intrinsic spin Hall conductivity by Wannier interpolation. *Physical Review B*, 98(21):214402, December 2018.

[169] Xiao-Liang Qi, Yong-Shi Wu, and Shou-Cheng Zhang. General theorem relating the bulk topological number to edge states in two-dimensional insulators. *Physical Review B*, 74(4):045125, July 2006.

[170] N. Regnault and B. Andrei Bernevig. Fractional Chern Insulator. *Physical Review X*, 1(2):021014, December 2011.

[171] J. J. Rehr and W. Kohn. Wannier functions in crystals with surfaces. *Physical Review B*, 10(2):448–455, July 1974.

[172] Raffaele Resta. Macroscopic polarization in crystalline dielectrics: The geometric phase approach. *Reviews of Modern Physics*, 66(3):899–915, July 1994.

[173] Raffaele Resta. Theory of the electric polarization in crystals. *Ferroelectrics*, 136(1):51–55, 1992.

[174] M Röntgen, CV Morfonios, and P Schmelcher. Compact localized states and flat bands from local symmetry partitioning. *Physical Review B*, 97(3):035161, 2018.

[175] Ken Shiozaki, Hassan Shapourian, Kiyonori Gomi, and Shinsei Ryu. Many-body topological invariants for fermionic short-range entangled topological phases protected by antiunitary symmetries. *Physical Review B*, 98(3):035151, July 2018.

[176] Gilbert Strang. *Linear Algebra and Its Applications*. Academic press, 2014.

[177] H Tasaki. Hubbard model and the origin of ferromagnetism. *The European Physical Journal B*, 64(3-4):365–372, 2008.

[178] DJ Thouless. Quantization of particle transport. *Physical Review B*, 27(10):6083, 1983.

[179] Stepan S. Tsirkin. High performance Wannier interpolation of Berry curvature and related quantities with WannierBerri code. *npj Computational Materials*, 7(1):1–9, February 2021.

[180] Christopher N. Varney, Kai Sun, Marcos Rigol, and Victor Galitski. Topological phase transitions for interacting finite systems. *Physical Review B*, 84(24):241105, December 2011.

[181] W Von Niessen. Density localization of atomic and molecular orbitals. *Theoretica chimica acta*, 27(1):9–23, 1972.

[182] Thorsten B Wahl, H-H Tu, Norbert Schuch, and J Ignacio Cirac. Projected entangled-pair states can describe chiral topological states. *Physical review letters*, 111(23):236805, 2013.

[183] Chong Wang, Xiaoyu Liu, Lei Kang, Bing-Lin Gu, Yong Xu, and Wenhui Duan. First-principles calculation of nonlinear optical responses by Wannier interpolation. *Physical Review B*, 96(11):115147, September 2017.

[184] Xinjie Wang, Jonathan R. Yates, Ivo Souza, and David Vanderbilt. *Ab Initio* calculation of the anomalous Hall conductivity by Wannier interpolation. *Physical Review B*, 74(19):195118, November 2006.

[185] Gregory H Wannier. Dynamics of band electrons in electric and magnetic fields. *Reviews of Modern Physics*, 34(4):645, 1962.

[186] Congjun Wu, Doron Bergman, Leon Balents, and S Das Sarma. Flat bands and Wigner crystallization in the honeycomb optical lattice. *Physical review letters*, 99(7):070401, 2007.

[187] Congjun Wu and S Das Sarma. P x, y-orbital counterpart of graphene: Cold atoms in the honeycomb optical lattice. *Physical Review B*, 77(23):235107, 2008.

[188] Shaoyu Yin, Nigel R. Cooper, and Benjamin Béri. Strictly local tensor networks for short-range topological insulators. *Physical Review B*, 99(19):195125, May 2019.